uOttawa

L'Université canadienne
Canada's university

FACULTÉ DES ÉTUDES SUPÉRIEURES ET POSTOCTORALES

uOttawa

L'Université canadienne
Canada's university

FACULTY OF GRADUATE AND POSDOCTORAL STUDIES

Kyna Mensch

AUTEUR DE LA THÈSE / AUTHOR OF THESIS

M.Sc. (Biochemistry)

GRADE / DEGREE

Department of Chemistry, Microbiology and Immunology

FACULTÉ, ÉCOLE, DÉPARTEMENT / FACULTY, SCHOOL, DEPARTMENT

A study of V(D)J recombination and DNA-damage response factors

TITRE DE LA THÈSE / TITLE OF THESIS

Robert Haché

DIRECTEUR (DIRECTRICE) DE LA THÈSE / THESIS SUPERVISOR

CO-DIRECTEUR (CO-DIRECTRICE) DE LA THÈSE / THESIS CO-SUPERVISOR

EXAMINATEURS (EXAMINATRICES) DE LA THÈSE / THESIS EXAMINERS

Jocelyn Coté

Martin Pelchat

Gary W. Slater

Le Doyen de la Faculté des études supérieures et postdoctorales / Dean of the Faculty of Graduate and Postdoctoral Studies

A study of V(D)J recombination and DNA-damage response factors

Kyna Mensch

Thesis submitted to the Faculty Biochemistry, Microbiology and Immunology
in partial fulfillment of the requirements of an M.Sc. degree in biochemistry
with specialization in human and molecular genetics

University of Ottawa
Ottawa, Canada, 2008

Your file Votre référence
ISBN: 978-0-494-46489-2
Our file Notre référence
ISBN: 978-0-494-46489-2

Abstract

DNA double-stranded breaks (DSBs) represent a significant threat to genomic integrity, as failure to repair, or the incorrect repair of these lesions can lead to tumour formation and carcinogenesis. These breaks are not only caused by external factors, but are also generated within cells during regulated physiological processes, such as V(D)J recombination. This process is essential for lymphocyte development and involves the activity of factors involved in the non-homologous end-joining (NHEJ) repair pathway. A tri-partite study of V(D)J recombination and DNA damage response factors was conducted in order to gain insight into these overlapping pathways. The factors examined include Rag-1 (a component of the recombinase complex that initiates V(D)J recombination); Ku70 (a subunit of the Ku heterodimer involved in NHEJ and V(D)J recombination); Artemis (a nuclease involved in NHEJ and V(D)J recombination); and the Octamer-binding transcription factor-1 (which contributes to cellular survival post-DNA damage). The three facets of this study include (i) defining the Ku70 binding region of Rag-1 through the use of association assays, (ii) examining the regulation of ectopic Artemis expression in non-permissive cells, and (iii) identifying Oct-1 interacting factors with the use tandem affinity purification.

Acknowledgements

I would like to thank Dr. Robert Haché for providing me with the opportunity to work in such a positive laboratory environment, with such caring and helpful lab mates. I would also like to thank Dr. Sebastien Soubeyrand for his extensive assistance and guidance over the course of my studies, and Rahin Farzadfar and Houssein Salem Abdou for their friendship and kindness. Lastly, I would like to thank Danny Caminiti for encouraging and supporting me during this entire process…I cannot thank you enough.

Abbreviations

53BP1 (p53 binding protein 1)

Ab (antibody)

ATM (ataxia-telangiectasia mutated)

ATR (ATM- and Rad3-related)

BRCA1 (breast cancer 1, early onset)

ChIP (chromatin immunoprecipitation)

Chk-1 and -2 (checkpoint kinases -1 and -2)

Cy2 (cyanine)

ddH20 (deionized distilled water)

DMEM (Dulbecco's Modified Eagle Medium)

DNA (deoxyribonucleic acid)

DNA-PKcs (DNA-dependent protein kinase catalytic subunit)

dNTP (deoxynucleoside triphosphate)

DSB (double-stranded break)

DTT (dithiothreitol)

E.coli (Escherichia coli)

EDTA (ethylene diamine tetraacetic acid)

EGFP (enhanced green fluorescent protein)

FBS (fetal bovine serum)

Hc (heavy chain)

HEPES (N-(2-hydroxyethyl)piperazine-N'-(2-ethanesulfonic acid))

His (histidine)

HMG (high mobility group)

hMOF (human chromatin modifying factor)

MG132 (N-benzoyloxycarbonyl (Z)-Leu-Leu-leucinal)

mTOR (mammalian target of rapamycin)

HR (homologous recombination)

Ig (immunoglobulin)

IMAC (immobilized metal affinity chromatography)

IPTG (isopropyl-β-D-thiogalactopyranoside)

IR (ionizing radiation)

IRES (internal ribosomal entry site)

IRR (irradiation)

Lc (light chain)

LTR (long terminal repeat)

MBP (maltose binding protein)

MDC1 (mediator of DNA damage checkpoint 1)

MEF (mouse embryonic fibroblast)

MEM (minimum essential medium)

MHC (Major Histocompatability Complex)

MMLV (Maloney murine leukemia virus)

MRN (MRE11-NBS1-RAD50)

NHEJ (non-homologous end-joining)

Oct-1 (Octamer-binding transcription factor-1)

PCR (polymerase chain reaction)

PBS (phosphate buffered saline)

PIKK (phosphoinositide 3-kinase-related kinase)

TCR (T-cell receptor)

TRRAP (transformation/transcription domain-associated protein)

RAG (recombination activating gene)

Rb (retinoblastoma)

RNA (ribonucleic acid)

RPM (rotations per minute)

RSS (recombination signal sequence)

RT (reverse transcriptase)

RT-PCR (reverse transcription polymerase chain reaction)

SCID (severe combined immunodeficiency)

TAP (tandem affinity purification)

TBS-T (tris-buffered saline with 0.1% tween-20 detergent)

TCR (T-cell receptor)

TRIS (tris(hydroxymethyl)aminomethane)

UTR (untranslated region)

XRCC4 (x-ray repair cross complementing factor 4)

XLF (XRCC4-like factor)

Table of Contents

Table of Figures

Introduction

Cellular responses to DNA double-strand breaks

DNA double-stranded breaks (DSBs) represent a particularly genotoxic type of DNA damage encountered within a cell; if left unrepaired, these lesions can lead to cell cycle arrest and eventually cell death. If incorrectly repaired, loss of genomic information, chromosomal translocations, and genomic instability can lead to tumour formation and carcinogenesis (1, 2). The cellular response to DNA DSBs is determined by numerous factors, but is primarily governed by the nature of the DNA damage itself. For example, although DSBs can be caused both by ionizing radiation (IR) and the radiomimetic drug bleomycin, the nature of the break, and therefore the subsequent response, appears to be different (3-5). Regardless of the source of damage, key biological events, including changes in gene expression, induction of cell cycle arrest checkpoints, DNA repair and/or apoptosis are known to occur subsequent to the exposure of DNA to damaging agents (6).

The DNA damage signal transduction cascade

The link between extracellular stress and an intracellular response often involves the coordination and convergence of signal transduction cascades. Typically, these events involve the synchronization of sensors, transducers and effectors. This sequence of events is well established for many stress stimuli, including serum starvation and heat shock, with the induction of signal transduction cascades such as the Ras/Raf-MAPK (mitogen-activated protein kinase) pathway (7-9). The transduction of DNA damage, however, is not as well understood.

Sensing DNA DSBs was primarily thought to occur through the PIKK (phosphoinositide 3-kinase-related kinase) family of protein kinases, including ATM (ataxia-telangiectasia mutated), ATR (ATM- and Rad3-related) and DNA-PKcs (DNA-dependent protein kinase catalytic subunit). Consensus was that upon DNA association, the kinases would convey chromatin aberrations by undergoing conformational changes thus initiating a signalling cascade (10-12). Newer models, however, support the idea that PIKKs, on their own, cannot function as DNA DSB sensors (13). Instead, the kinases are likely recruited to sites of DNA damage through interactions with upstream factors (13, 14). It is hypothesized that these sensors are most likely components of repair complexes, such as the MRN (MRE11-NBS1-RAD50) complex, Ku70/80, 53BP1 (p53 binding protein 1), and members of the Rad family of proteins (15-17). As additional factors are recruited to the sites of damage, nuclear foci emerge and expand (18, 19). This recruitment and assembly of factors at the sites of DNA damage was demonstrated by Lukas *et al* (20) who used DSB-generating microlasers coupled to laser-scanning confocal microscopy to describe the sequential binding of DNA damage sensors and adaptor proteins following the induction of DNA DSBs. This system has been shown to induce approximately 90-300 DSB sites per diploid cell (21). In this model Lukas' group showed the initial binding of sensor and adaptor proteins such as MRN, 53BP1, and MDC1 (mediator of DNA damage checkpoint 1) in a γ-H2AX-dependent manner. H2AX is a variant form of the core histone protein H2AX, and is known to be phosphorylated by members of the PIKK family of kinases following the induction of DNA DSBs. Phosphorylation of H2AX (γ-H2AX) occurs rapidly *in vivo* (within minutes of the induction of DNA DSBs) and it is one of the earliest events to occur within the DNA damage response pathway (22). This model does not address additional known factors such as BRCA1 (breast cancer 1, early onset), hMOF (human chromatin modifying factor), or

Ku70/80, to name a few, but instead illustrates the role of sensor proteins upstream of the PIKKs. A conundrum within this model exists in the absence of early ATM recruitment to the site of DNA damage despite the requirement of this kinase in phosphorylating histone H2AX- an event which appears to be required for foci emergence. This may reflect a non-linear signal transduction cascade, where the cyclical involvement of factors assists in signal amplification (23).

Regardless of the hierarchy of the signalling cascade, it is generally agreed that members of the PIKK family of kinases mediate the signal transduction phase of the DNA damage response (24). These serine/threonine kinases recognize the same consensus sequence (S/T, Q), and therefore may share common substrates *in vivo* as well as be involved in overlapping DNA-damage response pathways. For example, whereas both ATM and DNA-PKcs are activated in response to IR, only ATR responds to stalled replication forks (25, 26). Conversely, it has been demonstrated that ATR overexpression can rescue many of the phenotypes of ATM deficiency (27). Additionally, significant cross-talk between these kinases has been observed, such as in the ATR-dependent phosphorylation and activation of ATM in response to ultra-violet (UV) radiation (28, 29).

PIKKs are known to relay DNA damage signals by phosphorylating downstream factors, including those involved in DNA damage repair pathways. Before repair, however, PIKKs first initiate cell cycle arrest checkpoints by phosphorylating factors involved in cell cycle progression, namely the checkpoint kinases Chk-1 and -2. This provides the damaged cell with sufficient time to repair the DNA lesions, or if the damage is too extensive, initiate the apoptosis pathway (Figure 1) (30, 31).

Figure 1. The detection and signalling of DNA double-strand breaks. The signal transduction of DNA double-strand break repair involves the activity and coordination of adapter, signalling and effector proteins. The cellular consequences of these breaks is often dependent on the nature of the break itself, but key events including apoptosis, altered gene expression, cell-cycle arrest, and/or repair of the damage are known to occur. Adapted from Bradury, J.M. *et al* (31).

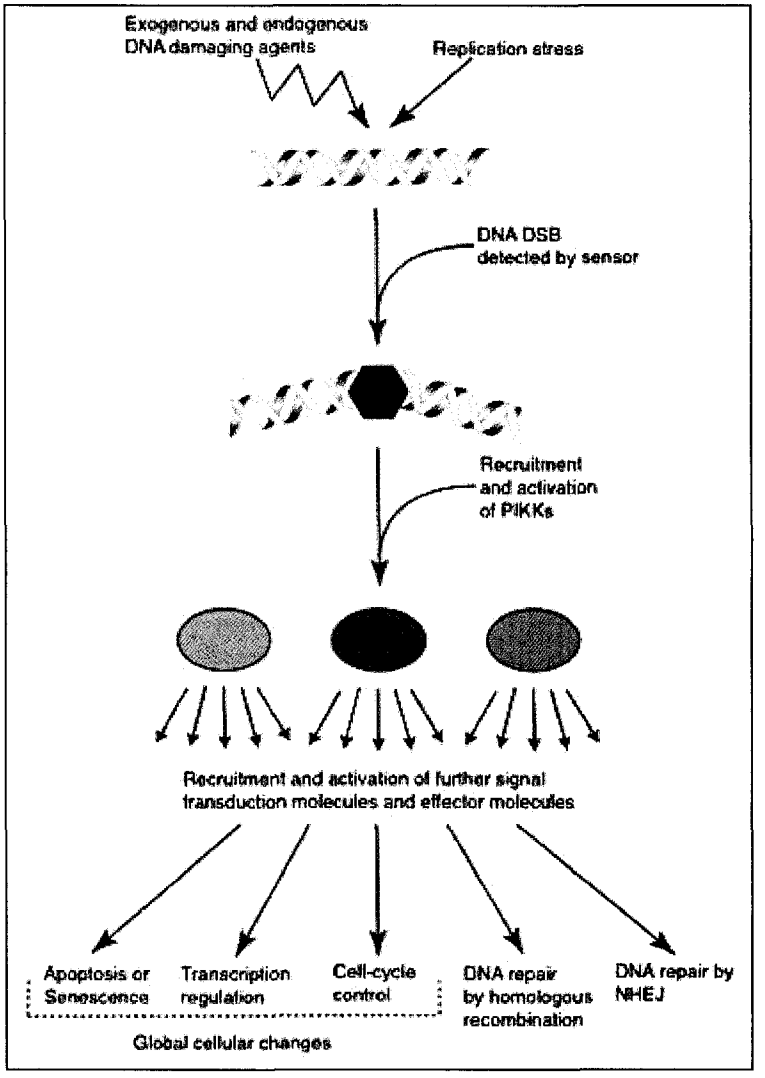
Exogenous and endogenous
DNA damaging agents
Replication stress
DNA DSB
detected by sensor
Recruitment
and activation
of PIKKs
Recruitment and activation of further signal
transduction molecules and effector molecules
Apoptosis or
Senescence
Transcription
regulation
Cell-cycle
control
DNA repair
by homologous
recombination
DNA repair by
NHEJ
Global cellular changes

Consequences of DNA damage

Cell-cycle arrest

The activation of cell cycle checkpoints results in the transient stalling of cell cycle progression until (i) the damaged DNA is repaired, or (ii) the cell undergoes apoptosis. DNA damage-induced cell cycle checkpoints occur at both the G1/S and G2/M transitions, and are necessary to prevent the transmission of damaged genetic material to daughter cells. The tumor suppressor protein p53 is a key regulator of cell-cycle progression, and is known to function primarily during the G1/S checkpoint. Subsequent to DNA damage, p53 experiences marked stabilization and activation. In addition to acetylation and methylation of p53, extensive phosphorylation is known to occur following DNA damage (31b). This event requires ATM, ATR, and potentially DNA-PKcs (32-34). This activation can occur both directly, (via direct phosphorylation of p53), or indirectly (via phosphorylation of Chk1, which in turn, phosphorylates p53) (35). Upon stabilization, p53 activates the expression of numerous effector proteins, including p21 (cyclin-dependent kinase inhibitor 1A). The expression of p21 inhibits the kinase activity the cyclinE/Cdk2 complex, which in turn, blocks the phosphorylation of Rb (retinoblastoma), which is necessary for the transition from G1 to S phase (36). The G2/M checkpoint is initiated by the phosphorylation of the checkpoint kinases Chk-1 and -2 by members of the PIKK family of kinases. Phosphorylation and activation of these kinases allows them to phosphorylate Cdk1, thus inactivating the cyclinB/Cdk1 complex, and blocking G2-to-M phase transition (37, 38).

Differential gene expression

Cells exposed to DNA damaging agents exhibit profoundly altered gene expression profiles (39-42). These transcriptional differences link the physiological phenotype of a cell under genotoxic stress to the source of the stress, in the sense that the cellular response to the stimuli will be dictated by the up- or down-regulation of key stress response factors. Numerous transcription factors have been described in the regulation of stress-inducible genes, including c-Myc, c-fos, c-jun, p53, and the octamer-binding transcription factor-1 (Oct-1) (43, 44). The differential regulation of transcription factors in response to DNA damage is primarily achieved at the level of post-translational modification. In the case of DNA DSBs, phosphorylation of transcription factors by ATM, ATR and DNA-PKcs is well established (19, 45).

Octamer-binding transcription factor-1

Oct-1 is member of the POU (Pit-1, Oct1/2, and Unc-86) sub-family of homeodomain transcription factors, and was initially identified by its ability to bind a conserved octamer motif (ATGCAAAT) present in the enhancer region of the immunoglobulin heavy chain (IgH) gene (46). Ubiquitously expressed, Oct-1 is involved in the expression of numerous housekeeping (histone H2B, U2/U6 snRNAs) and tissue-specific (Ig heavy and light chains, GnRH) genes, as well as in the transcription of viral protein products, and in viral DNA replication (herpes simplex virus, adenovirus) (47-55). Oct-1 can also repress the expression of certain genes, including the von Willebrand factor, and virus-induced interferon-A (56, 57).

Oct-1 is comprised of three domains; the glutamine-rich transactivation domain (aa1-280), the POU domain (aa281-438), and the C-terminal domain (aa439-743) (Figure 2). Most N-terminal, the glutamine-rich transactivation domain is involved in mediating protein-protein interactions with transcription factors, co-activators, and repressors. Additionally thirteen DNA-PKcs-dependent phosphorylation sites have been mapped to this domain *in vitro*, and are believed to be phosphorylated in response to IR (58). In this sense, the glutamine-rich transactivation domain may provide a regulatory role in the differential activity of Oct-1, providing a direct link between the transduction of a DNA damage signal and altered gene expression. Adjacent to the transactivation domain is the POU domain, which is comprised of a POU- specific (POUs) and a POU homeodomain (POUhd) motif. This bipartite domain possesses a capacity for DNA binding, with the POUs motif conferring low affinity for DNA, but high sequence specificity, and the POUhd exhibiting low specificity and high affinity (59). These two motifs are separated by a hypervariable linker segment (24aa in humans). Crystallographic analysis reveals that the POUs motif makes direct contacts with the first four residues (ATGC) of the octamer motif, whereas the POUhd contacts the remaining portion (AAAT) (60-62). Additionally, although these two motifs bind the same DNA sequence, no physical protein-protein interactions exist between them. Instead, an α-helix (α3) within both motif makes contact with the major groove on opposite sites of the DNA helix (60).

Oct-1 is an essential transcription factor, as Oct-1 deficiency is embryonic lethal (63). Immortalized Oct-$1^{-/-}$ mouse embryonic fibroblasts (MEFs) show an increased sensitivity to DNA damaging agents resulting in DSBs, evident in their reduced survival post-irradiation (58). In wild-type cells however, Oct-1 demonstrates increased phosphorylation and

Figure 2. Structure of octamer-binding transcription factor-1. Modular depiction outlining the three domains of Oct-1. Numbers shown mark the amino acid position of the domain borders. Most N-terminal, the glutamine-rich transactivation domain contains multiple DNA-PKcs phosphorylation sites. Adjacent, the bi-partite POU domain is comprised of the POU-specific (POUs) and the POU-homeodomain (POUhd) motifs. Lastly, is the hydrophobic C-terminal domain.


1
280
438
743
O
O
POU

stabilization post-DNA damage (43, 64). *In vitro* analyses have identified DNA-PKcs as the kinase responsible for phosphorylating Oct-1 post DNA damage (58). Paradoxically, co-incident with the stabilization and phosphorylation of Oct-1 is a decrease in its ability to enhance the transcription of target genes (ex: H2B, U2/6 snRNA). ChIP analysis reveals that subsequent to DNA damage, Oct-1 nonetheless occupies the promoters of these genes (58). Additionally, phosphorylation of Oct-1 by DNA-PKcs appears required for the contribution of Oct-1 to cell survival, as disrupting target phosphorylation sites results in an increased sensitivity to IR (58). In line with these observations, Oct-1 has recently been described as a stress sensor (65). Microarray data show differential activation of genes regulated by Oct-1 in $Oct1^{-/-}$ MEFs versus wild type cells following treatment with DNA damaging agents. Many of these genes are known factors in cellular stress response pathways (*Gpx3;* glutathione peroxidase 3, *Prdx2*; peroxiredoxin 2, and *Cdo1*; cysteine dioxygenase 1, to name a few). Interestingly, however, many of the affected genes do not possess any known octamer motifs within their promoter, and may suggest a less-conventional role of Oct-1 in regulating their expression. Oct-1 primarily functions via direct DNA binding, where it recruits the transcriptional pre-initiation complex to the promoter region of target genes. Unconventional Oct-1 activity has been described in the transcription of genes such as cyclin D1, as well as those under the regulation of RXR (retinoid X receptor) containing a TRE (thyroid-responsive element) within their promoter. In these instances, Oct-1 affects gene expression via protein-protein interactions, and not protein-DNA binding (66, 67).

DNA repair pathways

In mammalian cells, there are two primary pathways used to resolve DNA double-stranded breaks; homologous recombination (HR) and non-homologous end-joining (NHEJ) (Figure 3) (68-71). HR is a relatively error-free repair process used to address DNA DSB encountered during certain phases of the cell cycle, and is commonly used to repair DSBs generated as a result of stalled replication forks (72). In this pathway, key factors include the MRN complex, ATM, and members of the RAD52 epistasis family of proteins (73). Subsequent to the recognition of the DNA lesion, repair ensues with the use of an intact sister chromatid (or a homologous chromosome) as a template. This pathway appears limited to the S and G2 phases of the cell cycle. NHEJ, however, is a template independent process which occurs throughout the cell cycle. Core NHEJ factors include the Ku70/80 heterodimer, which is responsible for the initial binding and protection of free DNA ends, the catalytic subunit of the DNA-dependent kinase (DNA-PKcs) which, together with the Ku70/80 heterodimer, forms the DNA-PK holoenzyme responsible for phosphorylating target proteins in response to DNA damage; the ligase IV/XRCC4 complex, responsible for ligating the two DNA ends together; polλ and polμ, which are responsible for filling-in gaps in the nucleotide sequence; the Artemis nuclease, which possesses both exo- and endonuclease activity required for DNA-end processing, and the newly identified XLF (XRCC4-like factor; Cernunnos), which may be involved in stimulating the activity of the ligase IV/XRCC4 complex (74-78).

The Ku autoantigen

The Ku autoantigen (or Ku) is a heterodimer comprised of two structurally similar

Figure 3. The non-homologous end-joining (NHEJ) pathway of DNA double-strand break repair. Core NHEJ factors include the Ku70/80 heterodimer, the catalytic subunit of the DNA-dependent kinase (DNA-PKcs), the ligase IV/XRCC4 complex, the Artemis nuclease, and the newly identified XLF (XRCC4-like factor; Cernunnos). Adapted from Weterings and Chen (72b).

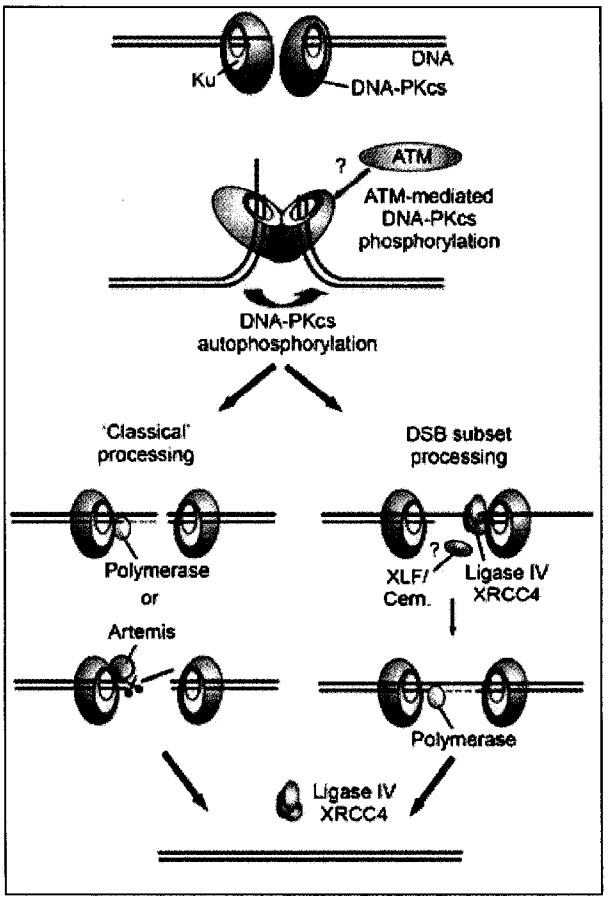
DNA
Ku
DNA-PKcs
?
ATM
ATM-mediated
DNA-PKcs
phosphorylation
DNA-PKcs
autophosphorylation
'Classical'
processing
DSB subset
processing
Polymerase
or
Artemis
?
XLF/
Cern.
Ligase IV
XRCC4
Polymerase
Ligase IV
XRCC4

and evolutionarily related subunits; Ku70 and Ku80. Both subunits are comprised of three domains; an N-terminal α/β domain, a central β-barrel domain, and a helical C-terminal arm (79, 80). Unlike the N-terminal and central domains, the C-terminal domains of Ku70 and 80 are not homologous, despite their high degree of conservation in mammalian cells (81, 82). Crystallographic studies of Ku, both DNA-bound and free, reveal that the two subunits come together to form a ring-shaped dimer, through which a free DNA end can be inserted (Figure 4). In accordance with its high affinity for duplex DNA, Ku is responsible for recruiting DNA-PKcs to free DNA ends via the C-terminal arm of Ku80 (80, 83, 84). As well as binding DNA-PKcs, numerous factors are also thought to interact with Ku, including Rag-1, hTERT (human telomerase reverse transcriptase), the pro-apoptotic protein Bax, Werner syndrome protein, and the octamer-binding transcription factor-1 (Oct-1) to name a few (85-91).

In addition to its role in NHEJ, Ku has been implicated in maintaining telomere integrity (92-94). Mice that are deficient in Ku are immunodeficient, and display increased sensitivity to ionizing radiation (95-97). Additionally, both human and mouse cells deficient in Ku appear to contain chromosomal rearrangements, have shortened telomeres, and undergo premature senescence (95, 98, 99).

DNA-PKcs

DNA-PK is a large protein kinase comprised of two subunits; the 460kDa catalytic subunit (DNA-PKcs) and the Ku heterodimer. DNA-PKcs is a member of the PIKK family of serine/threonine protein kinases, including ATM, ATR, mTOR (mammalian target of rapamycin), and TRRAP (transformation/transcription domain-associated protein) (19).

Figure 4. Structure of the Ku70/80 heterodimer. **(A)** Ribbon diagram of the Ku70/80 heterodimer crystallized in the absence of DNA. Ku70 is shown in red and Ku80 in grey. The C-terminus of Ku70 is drawn in dark red. The dotted line indicates a disordered linker region between residues 539–558. **(B)** Ribbon diagram of DNA-bound Ku70/80. The figure on the left is viewed down the DNA helix. The figure on the right is rotated by 90°. Ku70 is coloured red and Ku80 is orange. The DNA sugar-phosphate backbone is shown in light gray, whereas the bases are shown in dark grey. Adapted from Walker *et al* (100).

A

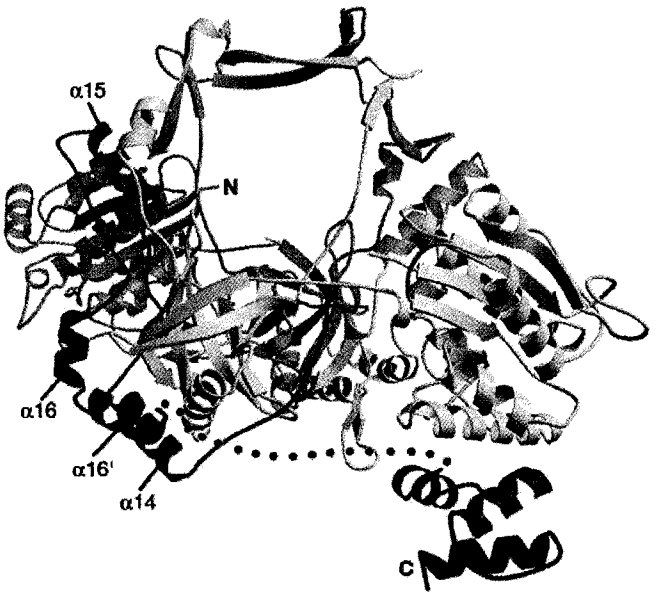

I

B

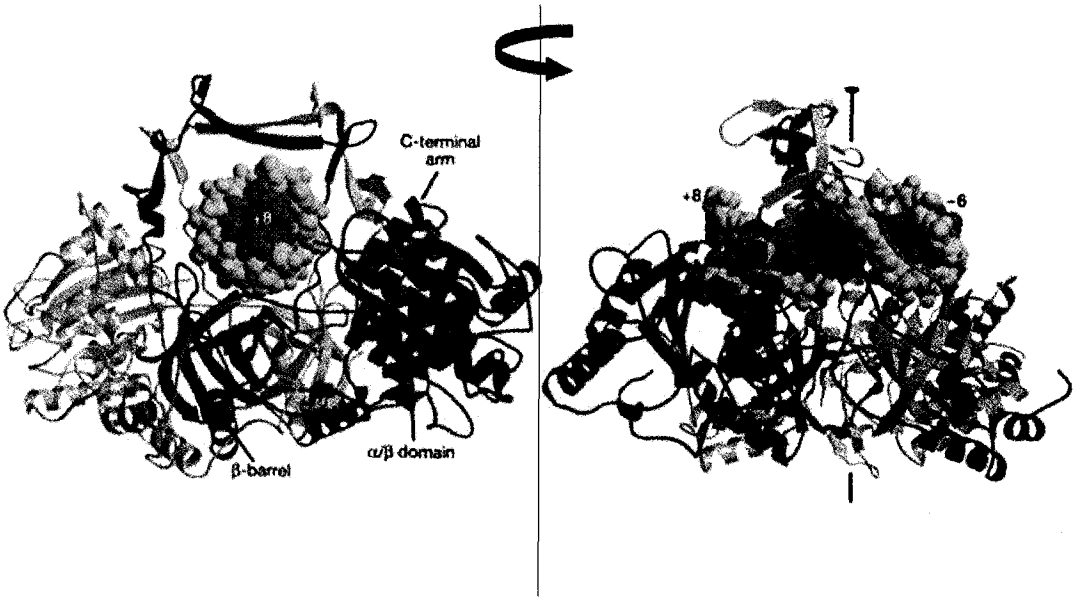

With the exception of TRRAP (a component of histone acetyltransferase complexes) all members possess kinase activity, and, with the exception of TRRAP and mTOR, all are known to phosphorylate target proteins in response to DNA damage.

In addition to its role in NHEJ, DNA-PK is thought to be involved in numerous cellular events, including the regulation of gene expression, induction of apoptosis, retroviral DNA integration, and cell cycle progression (14, 101, 102). Mutations in DNA- PKcs lead to immunodeficiency, increased sensitivity to DNA damaging agents, chromosomal aberrations, and a predisposition to cancer (103, 104).

Ligase IV, XRCC4, and Cernunnos-XLF

Mammalian cells possess three genes encoding DNA ligases; LIG1, LIG3 and LIG4. DNA ligases I and III are involved in Okazaki fragment processing and general DNA repair, respectively (105). DNA ligase IV is the only DNA ligase involved in the repair of DNA DSBs. Although null mutations in LIG4 are embryonic lethal, hypomorphic mutations in DNA ligase IV have been described (106, 107). The resulting Lig4 syndrome is characterized by immunodeficiency and developmental/growth delay (108-110).

XRCC4 (x-ray repair cross complementing factor 4) was initially identified as deficient in the XR-1 Chinese hamster ovary cell line, which displays impaired DNA DSB repair, resulting in increased sensitivity to ionizing radiation (111, 112). *In vivo,* XRCC4 exists in a tight protein complex with DNA ligase IV. Together, the ligase IV/XRCC4 complex catalyzes the ligation step during NHEJ. Through direct contacts between DNA-PKcs and XRCC4, the ligase IV/XRCC4 complex is recruited to free DNA ends, where its activity is modified via phosphorylation by the kinase (113, 114).

Cernunnos-XLF (XRCC4-like factor) is the most recently identified NHEJ factor, and was initially characterized by two independent groups in 2006 (115, 116). The identification of Cernunnos-XLF as an essential NHEJ factor arose from studies of a cell line derived from a severely immunocompromised child (117). This cell line displayed defects in DSB repair and V(D)J recombination that could not be complemented by any of the known NHEJ factors (118). Although little is known concerning the role of Cernunnos-XLF in NHEJ, it appears to associate as a homodimer with the ligase IV/XRCC4 complex where it stimulates ligase activity (119-121). Recent *in vivo* studies have shown that the Ku heterodimer is essential for the recruitment of Cernunnos-XLF to DSBs, and that XRCC4 is dispensable for this recruitment. It appears, however, that XRCC4 stabilizes the recruited XLF at the DSBs (122, 123).

Artemis

Artemis/Snm1C is a member of the metallo-ß-lactamase (ß-Lact) superfamily of enzymes that process nucleic acids, and is involved in the V(D)J recombination pathway as a NHEJ factor (124-129). Artemis is a 692aa long nuclear phosphoprotein that is organized into three domains (Figure 5). Most N-terminal, the β- lactamase homology domain (aa1-155) is highly conserved among members of this protein family. Comprised of five conserved motifs, the β-lactamase domain often constitutes the catalytic core of proteins within the β-Lact superfamily. In Artemis, however, only motifs I-IV are present within this domain, whereas the last (motif V) is located within the adjacent β-CASP domain (aa156-385) (132). This second domain of Artemis is conserved between a sub-group of proteins within the β-lactamase superfamily (metallo-β-lactamases-associated CPSF, Artemis, Snm1,

Figure 5. The Artemis nuclease. (A) Cartoon representation of the Artemis protein. The numbers shown correspond to the amino acid number of the border of adjacent domains. DNA-PK phosphorylation sites are depicted within the C-terminal domain. Below is depicted the hypothetical model for the structure of the catalytic site of Artemis (based on structures 1BC2 and 1SML (PDB codes) from *B. cereus* and *S. maltophilia*, respectively). Gray and red spheres indicate the position of zinc and water oxygen atoms, respectively. Shaded areas correspond to the two Zn(II)-binding domains. Adapted from Poinsingon *et al* (130). **(B)** Structural alignment of the metallo-*b*-lactamase domain of ***B. cereus***, *B. fragilis*, *P. aeruginosa,* and *C. meningosepticum* (subclass B1 enzymes), and of ***S. maltophilia*** and Fluoribacter gormanii (subclass B3). Adapted from Heinz and Adolf (132).

A

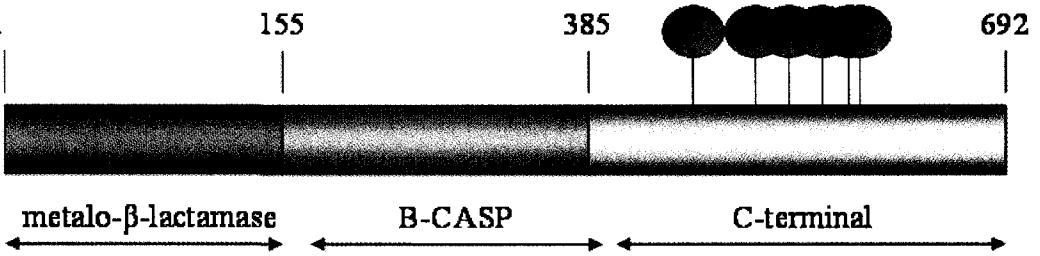

B

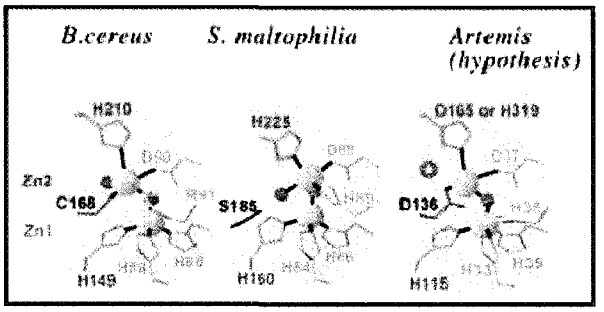

DNA-PK phosphorylation sites: S516, S531, S537, S541, S545 and S646

Pso2), and together with the β-lactamase domain, comprises the catalytic core of Artemis (132). Lastly, the C-terminal domain (aa386-692) is non-conserved between members of the Snm1 family of proteins. Importantly, though, it has been proposed that the C-terminal domain provides a regulatory function in Artemis activity. This domain contains three basal phosphorylation sites, as well as numerous other sites that are phosphorylated in response to DNA damage by members of the PIKK family of kinases (133-135).

On its own, Artemis possesses intrinsic 5' to 3' exonuclease activity with specificity for single-stranded DNA. However, upon interaction with and phosphorylation by DNA-PKcs, the activity of Artemis shifts to endonucleolytic, allowing Artemis to act on DNA substrates with 5' and 3' overhangs, as well as on areas of DNA with secondary structures and single-to-double-strand transitions (Figure 6) (136-143). This shift in activity allows Artemis to act on a subset of double-stranded breaks (DSBs) repaired via the NHEJ pathway (144, 145), and also allows Artemis to resolve the hairpin-coding end structures generated by the Rag-1/2 complex during V(D)J recombination (see below) (125, 146-148). Mutations in Artemis result in the accumulation of these hairpin intermediates, and are implicated in immunodeficiency disorders including Omenn Syndrome and RS-SCID (radiosensitive severe combined immunodeficiency disorder) (149-153).

NHEJ and V(D)J recombination

DNA DSBs not only arise from exposure of the cell to exogenous sources, but are also generated during normal physiological processes, such as those generated during meiosis, Ig class switching, and as a result of the formation of reactive oxygen species during cellular metabolism (154-156). Consequently, the integration of DSB repair pathways into

Figure 6. DNA substrates of the Artemis endonuclease. Artemis tends to cleave at sites located immediately 3' of a stretch of 4nt of single-strandedness adjacent to the double-stranded region. Adapted from Ma *et a*l (135).

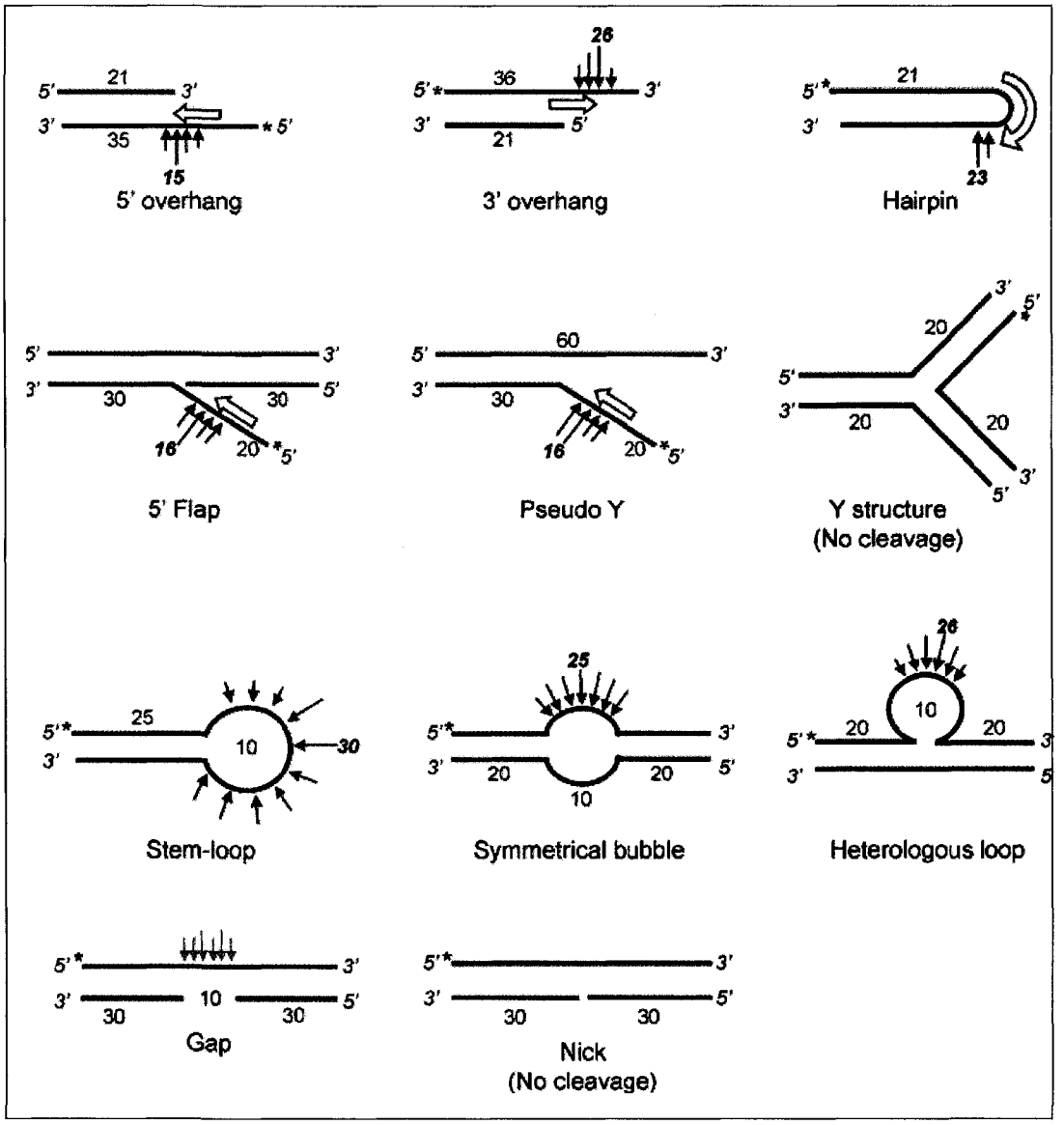
5' overhang
3' overhang
Hairpin
5' Flap
Pseudo Y
Y structure
(No cleavage)
Stem-loop
Symmetrical bubble
Heterologous loop
Gap
Nick
(No cleavage)

normal cellular metabolism, and even during immune system development is required. For example, the NHEJ repair pathway is employed to resolve DSBs generated during somatic hypermutation and V(D)J recombination (154, 157-161). V(D)J recombination is the site-specific, somatic recombination event that is ultimately responsible for generating the vast repertoire of the vertebrate adaptive immune system (162). This process occurs exclusively in developing lymphocytes, and involves processing the genes encoding the variable region of T-cell receptors (TCRs) and immunoglobulins (Igs) at the DNA level (Figure 7). As the production of TCRs and Igs is essential for the development of T- and B-cells, respectively, V(D)J recombination constitutes an extremely important process in the adaptive immunity of an organism.

The adaptive immune system

The adaptive immune system, also known as acquired immunity, is exclusive to jawed vertebrates, and is comprised of two parts; cell-mediated and humoral immunity (163-165). Cell-mediated immunity involves non-antibody producing T-cell lymphocytes and is mediated by T-cell receptors (TCRs) expressed on the surface of these cells. Humoral immunity involves B-cell lymphocytes, and is mediated by the generation of antibodies/immunoglobulins (Igs), which are either presented on the surface of the B cells, or secreted into the surrounding environment. Although important differences exist between these two types of immunities, parallels can be observed in many aspects, especially concerning the gene organization, expression and structure of TCRs and Igs.

Figure 7. V(D)J recombination. Schematic representation of V(D)J recombination. Dashed-line indicates the involvement of the NHEJ factors. Adapted from Schlissel, M.S (146).

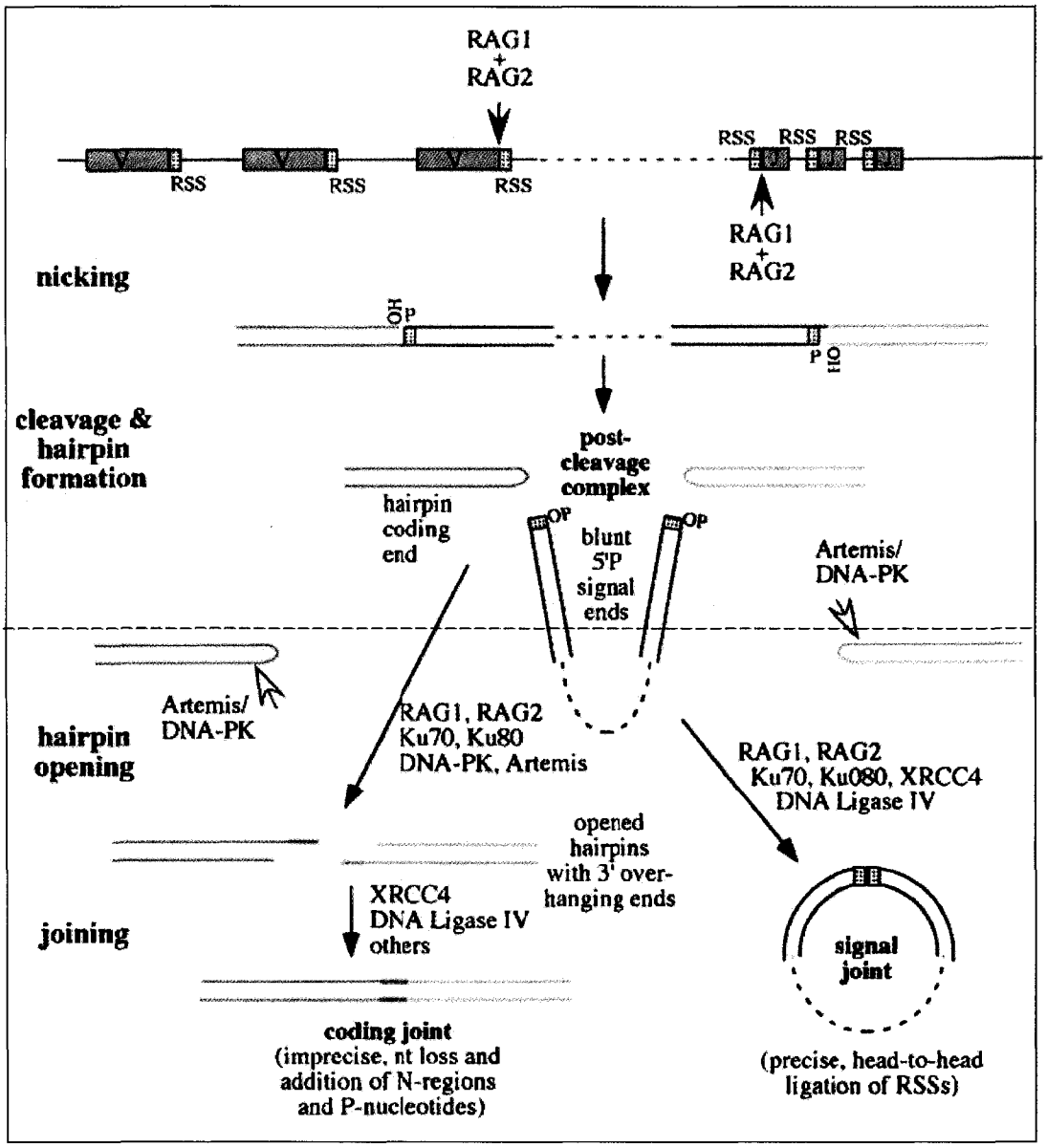
RAG1
+
RAG2
RSS
RSS
RSS
RSS
RSS
RSS
RAG1
+
RAG2
nicking
OH
P
P
HO
cleavage &
hairpin
formation
post-
cleavage
complex
hairpin
coding
end
OP
OP
blunt
5'P
signal
ends
Artemis/
DNA-PK
Artemis/
DNA-PK
hairpin
opening
RAG1, RAG2
Ku70, Ku80
DNA-PK, Artemis
RAG1, RAG2
Ku70, Ku080, XRCC4
DNA Ligase IV
opened
hairpins
with 3' over-
hanging ends
XRCC4
DNA Ligase IV
others
joining
signal
joint
coding joint
(imprecise, nt loss and
addition of N-regions
and P-nucleotides)
(precise, head-to-head
ligation of RSSs)

TCRs and Igs

Immunoglobulins are comprised of four polypeptide chains; two identical heavy chains (Hc) and two identical light chains (Lc), each of which are joined via disulfide bonds (166-167). Each polypeptide chain contains a variable N-terminal region and a constant C-terminal region. Together, the variable regions of the heavy and light chains provide antigen-binding surfaces, whereas their constant regions confer additional variation, as well as structural support. The constant region of light chain peptides falls into two functionally comparable classes, kappa (κ) and lambda (λ), whereas the constant region of the heavy chain peptide confers Ig isotype (α, δ, ε, γ, μ) as well as the tissue expression and distribution of the Ig.

TCRs differ from Igs, in that they are comprised of two polypeptide chains. TCRs exist as either α/δ chain or β/γ chain dipeptides which are joined together through disulfide linkages. Each chain within the TCR contains an Ig-like variable region at the N-terminus which binds both a specific antigen, as well as a Major Histocompatability Complex (MHC) type I or type II molecule (168-170). The constant region at the C-terminus contains a hydrophobic transmembrane domain necessary for anchoring the receptor to the surface of the cell (166).

Gene organization and processing of TCRs and Igs

The genes encoding the variable regions of Igs and TCRs are organized as clusters of V (variable), D (diversity) and J (joining) gene segments. The individual V, D and J gene segments must be isolated from within their respective gene clusters, and recombined in

order to generate a continuous variable gene with a single copy of each gene segment. The variable region of the Hc (Igs) and the β/δ (TCRs) chains are comprised of a V-D- and J-gene segment, whereas the variable region of the Lc (Igs) and the α/γ (TCRs) chains are comprised of only a V- and J- gene segment (171-172). The cellular process responsible for assembling the individual gene segments is appropriately termed V(D)J recombination.

Initiation of V(D)J recombination

At the 3' end of each V, D and J gene segment is a recombination signal sequence (RSS) comprised of a conserved heptamer (CACAGTG) and nonamer (ACAAAAACC) motif separated by a non-conserved 12 or 23 bp spacer sequence (173-174). The RSS is recognized by a lymphocyte-specific recombination complex comprised of the recombination activating gene (RAG) products Rag-1 and Rag-2, as well as either HMG (high mobility group protein) -1 or -2 (175-182).

Using water as a nucleophile, the RAG complex introduces a single-stranded nick in the DNA, 5' to the heptamer sequence, where the RSS borders the gene segment (183-186). This results in the generation of a free 3'OH in the DNA backbone, which is subsequently used in the nucleophilic attack of the phosphodiester backbone of the complementary strand of DNA. This process results in the generation of a covalently-sealed hairpin structure containing the gene segment (coding end), as well as a blunt 5' phosphorylated structure containing the RSS (signal end) (187-191). Efficient recombination will only occur between an RSS containing a 12bp spacer (12-RSS) and one containing a 23bp spacer (23-RSS), a condition known as the 12/23 rule (192-197).

Rag-1 and -2

The role of Rag-1 and -2 in V(D)J recombination was unequivocally demonstrated by their ability to confer V(D)J recombinase activity to non-lymphoid cell lines (198). The expression of Rag-1 and- 2 is limited to the early developmental stages of B and T lymphocytes, wherein they are responsible for the generation of Igs and TCRs, respectively. Since an inability to generate these biomolecules blocks lymphocyte development, mutations in either Rag-1 or -2 result in severe combined immunodeficiency (SCID) or Omenn Syndrome.

Murine Rag-1 consists of 1040 residues (1043 in humans), whereas both the murine and human homologues of Rag-2 are comprised of 527 residues. Both Rag-1 and -2 contain a minimum core region required for efficient RSS cleavage. Core-Rag-1 spans residues 384-1008, whereas core-Rag-2 is comprised of residues 1-387.

Although both proteins are required during V(D)J recombination, the catalytic residues are found solely within Rag-1. These residues, aspartate-600, aspartate-708, and glutamate-962, form a catalytic triad termed the DDE motif, and are necessary for coordinating the divalent cations required for RAG activity (199-201). Additionally, the nonamer-binding region is also found within Rag-1. Beyond the core regions of these proteins, both Rag-1 (Figure 8) and -2 are comprised of numerous distinct domains (201-208).

NHEJ in V(D)J recombination

The second phase of V(D)J recombination involves the factors of the NHEJ pathway. In 2002, Artemis was identified as the nuclease responsible for opening the hairpin

Figure 8. Rag-1 protein. **(A)** Modular organization of Rag-1. Relative positions of domains I-IX, as well as the catalytic residues (D_{600}, D_{708}, E_{962}) are depicted. **(B)** Amino acid position/span of domains I-IX.

A

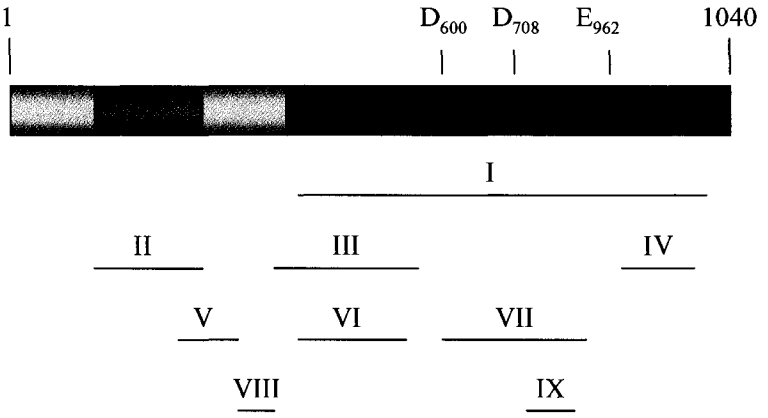

B

Domain number	Domain name	Amino acid span
I	Core Rag-1	384-1008
II	Ring zinc finger	288-330
III	Nonamer binding domain	384-454
IV	C-terminal binding domain	889-974
V	Homodimerization helices	340-351
VI	Homeodomain-like motif	389-446
VII	Central domain	528-760
VIII	Zinc finger A	353-374
IX	Zinc finger B	727-750

intermediates generated during this process, thus allowing the individual gene segments to be joined together (124, 125, 146-148, 209, 210). Following hairpin resolution, Ku70/80, DNA-PKcs, ligase IV/XRCC4, and XLF each perform their respective roles in processing the DNA ends, as per generic NHEJ repair (211). Two additional processes also occur, and are each responsible for increasing the variability of the antigen binding domain of TCRs and Igs. Firstly, the addition of nucleotides following the asymmetric opening of the hairpin intermediate, a process termed P-nucleotide addition, often occurs. It is named such, as the nucleotides added generate a palindrome in the DNA sequence (212-214). The second process involves the random insertion of nucleotides at the coding joint. This process is called N-nucleotide addition (non-templated), and is catalyzed by terminal deoxynucleotidyl transferase (TdT), which is expressed solely in developing lymphocytes (214-216). Additionally, the random deletion of nucleotides at the coding joint may also occur, further increasing diversity. The result of these processes is the formation of an imperfect coding end, and an extra-chromosomal circular DNA structure containing the signal joint.

Rationale and objectives

Although DNA double-strand breaks represent a significant threat to mammalian cells, they are also an intrinsic part of the development of adaptive immunity. A tri-partite study of V(D)J recombination and DNA damage response factors was conducted in order to gain insight into three facets of these two overlapping, yet independent pathways.

(i) Defining the Ku70 binding region of Rag-1.

The roles of both Rag-1 and Ku70 have been described in the processes of V(D)J recombination and non-homologous end joining (NHEJ), respectively. Previous coimmunoprecipitation binding experiments performed within our laboratory have demonstrated that the binding of Ku70 to Rag-1 is a specific and DNA-independent event (Schild-Poulter, unpublished data). However, it remains unclear as to how these two proteins behave in concert, and what effect this interaction has on the process of V(D)J recombination. The direct binding of Rag-1 and Ku may indicate an upstream role for Ku in V(D)J recombination, independent of its function with DNA-PKcs in NHEJ. Additional association assays with Rag-1 peptides further indicated that the region of Rag-1 responsible for binding Ku70 is present within its catalytically active moiety (coreRag-1) (216b). In order to observe the contribution of Ku70-Rag-1 binding within the context of V(D)J recombination, it is necessary to delimit the residue(s) responsible for this interaction, so that the selective disruption of the interaction could be initiated, without compromising the recombinase activity of Rag-1. By generating deletion constructs of a MBP-core Rag1 fusion protein, and performing association assays, the Ku70-interacting domain of Rag-1 can be determined. Further refinement of this domain to a few amino acids, or ideally, to a signal amino acid, can be achieved, and subsequently disrupted through the use of site-directed mutagenesis. By defining the Ku70-binding domain of Rag-1, as well as the specific residues responsible for this interaction, the impact of Rag-1-Ku70 complex formation can be measured through a V(D)J recombination assay. In this context, the use of Ku70-binding defective variants of Rag-1, and wild type Rag-1 proteins can provide new information

concerning the contributions of Ku70-Rag-1 binding to this very important biological process.

(ii) Examining the regulation of ectopic Artemis expression.

Artemis is a recently identified member of the NHEJ repair factors (217). Consequently, little is known concerning its regulation, activity, and contribution to the repair of different types of DNA damage. Attempts within our laboratory to observe the contribution of Artemis within *in vivo* NHEJ and V(D)J systems were stunted, as we observed a limitation in the ectopic expression of Artemis. Interestingly, although endogenous Artemis is a ubiquitously expressed NHEJ factor, the ectopic expression of Artemis protein can only be detected within a restricted repertoire of cell lines. Previous groups have also described difficulty ectopically expressing Artemis, as well as an extreme sensitivity of endogenous Artemis to nucleotide and/or amino acid changes. Both Moshous and Evans were unable to derive stable transfectants of wild-type or mutant Artemis for use in complementation studies (152, 217). Furthermore, Li and Ege both describe single nucleotide/amino acid substitutions in hypomorphic Artemis cell lines that almost completely eliminate Artemis expression at either the RNA or protein levels (150, 151). Additionally, cellular toxicity has been observed following the overexpression of other members of the Snm1 family of proteins; a characteristic consistent with the extremely low endogenous expression level of these factors (217). We rationalized that the tight regulation of Artemis expression was limiting its ectopic expression. By manipulating and observing conditions that would allow for Artemis expression in a non-permissive cell line, information concerning the level(s) at which Artemis is regulated, and possibly the factors involved in

eliciting this regulation, may be identified. Once the ectopic Artemis expression is achieved, the contributions of Artemis on V(D)J recombination and NHEJ can be further studied.

(iii) Identification of Oct-1 interacting factors.

Oct-1 is an essential transcription factor that is involved in the cellular survival response subsequent to DNA DSBs (58, 63). This involvement requires the DNA-PKcs-dependent phosphorylation of Oct-1 within its glutamine-rich transactivation domain; a domain known to mediate protein-protein interactions and influence the expression of a number of genes (47-55, 58, 66, 67). Disruption of these phosphorylation sites by site-directed mutagenesis eliminates the contribution of Oct-1 to cellular survival post-DNA damage (58). By utilizing the TAP (tandem affinity purification) method, the interaction of Oct-1 with binding partners can be explored. The differential interactions between wild-type Oct-1 and phosphorylation defective Oct-1 mutants with cellular factors both in the presence and absence of DNA damage may identify interactors with potential regulatory significance.

Material and Methods

Cell Culture

Cos-7 (ATCC CRL-1651), CV-1 (ATCC CCL-70), NIH-3T3 (ATCC CRL-1658), HEK-293T (ATCC CRL-11268), Phoenix-293T Ampho (ATCC SD-3443), primary 3T3 immortalized mouse embryonic fibroblasts (MEFs), and HeLa (ATCC CCL-2) cells were maintained in high glucose DMEM (Dulbecco's Modified Eagle Medium; Gibco-BRL) supplemented with 10% FBS (fetal bovine serum; JRH Bioscience), non-essential amino acids (2 mM), sodium pyruvate (2 mM), and 0.1% penicillin/streptomycin. HEK-293T cells were also supplemented with 0.1% G418. Human Jurkat T cells (ATCC CRL-1990) were maintained in RPMI-1640 (Gibco-BRL) supplemented with 2 mM L-glutamine, 0.1% penicillin/streptomycin, and 10% FBS. MCF-7 (ATCC HTB-22) cells were maintained in MEM (minimum essential medium) supplemented with L-glutamine (2 mM), non-essential amino acids (1 mM), sodium pyruvate (1 mM), 10% FBS, and insulin (0.01 mg/ml; company). HCT116 (ATCC CCL-247) cells were maintained in McCoy's 5a medium (Gibco-BRL), supplemented with non-essential amino acids (2 mM), 0.1% penicillin/streptomycin, and 10% FBS. All cells were maintained at 37°C and 5% CO_2.

Plasmid constructs

MBP-coreRag-1 deletion constructs

Inverse PCR (polymerase chain reaction) was used to generate the appropriate deletions within pET-MBP-coreRag-1 (pET-30b(+) vector from Novagen). Primers sequences are listed in Appendix I. pET-MBP-coreRag-1(Δ528-763) was produced with

primers I and II, pET-MBP-coreRag1(Δ528-720) with primers II and III, and pET-MBP-coreRag-1(Δ721-763) with primers I and IV. PCR reactions (20 mM Tris-HCl (pH 8.8), 2 mM $MgSO_4$, 10 mM KCl, 10 mM $(NH_4)_2SO_4$, 0.1% Triton X-100, 0.1 mg/ml BSA (bovine serum albumin), 15 ng of each primer, 15 ng template DNA, 500 μM dNTPs (deoxynucleotides), and 2 units of PFU Turbo polymerase) were carried out in a volume of 50 μl. The following program was used in a PTC-200 thermocycler: (i) 90 seconds at 95°C, (ii) 30 seconds at 95°C, (iii) 1 minute at 57°C, (iv) 10.5 minutes at 68°C, (v) repeat from step (ii) 25 times.

Artemis bicistronic construct

pIRES2-EGFP-Artemis is a bicistronic vector which allows the expression of EGFP (enhanced green fluorescent protein) from an internal ribosomal entry site (IRES), and myc-tagged Artemis from a CMV promoter. The following steps were used to generate a construct in which Artemis is expressed from the IRES, and EGFP from the CMV promoter:

(i) The EGFP coding sequence was removed from the pIRES2-EGFP backbone via restriction digest with flanking restriction sites BstXI (5') and NotI (3').

(ii) A second multiple cloning site (MCS) was generated (see Appendix I for oligonucleotide sequences), and ligated into the linearized vector in lieu of the EGFP sequence.

(iii) This new vector, pIRES(-EGFP), was digested with NheI and SacII (which cut within the original MCS), and an EGFP sequence generated via PCR (see below) was ligated within these sites.

(iv) The Artemis nucleotide sequence (including a myc tag) was removed from a donor plasmid (pTREtight-Artemis) via restriction digest with BamHI (5') and SalI (3'). The product generated in (iii) was digested with BglII and SalI (which cuts within the second MCS) and the Artemis amplicon generated in (iv) was ligated within these sites.

EGFP PCR

The PCR reaction (20 mM Tris-HCl (pH 8.8), 2 mM $MgSO_4$, 10 mM KCl, 10 mM $(NH_4)_2SO_4$, 0.1% Triton X-100, 0.1 mg/ml BSA, 15 ng of each primer, 15 ng template DNA, 100 μM dNTPs, and 1 unit of PFU Turbo DNA polymerase) was carried out in a total volume of 50 μl. The following program was used in a PTC-200 thermocycler: (i) 1 minute at 95°C, (ii) 30 seconds at 95°C, (iii) 1 minute at 55°C, (iv) 90 seconds at 68°C, (v) repeat from step (ii) 25 times. The primers used (EGFP forward, EGFP reverse) are listed in Appendix I.

Generation of pCeMM-NTAP-Oct1

The pCeMM-NTAP(GS) backbone was a generous gift from Dr. Tilmann Bürckstümmer. The Oct-1 nucleotide sequence was amplified from pMSCV-puro-Oct1 (wt) within a 50 μl PCR reaction (20 mM Tris-HCl (pH8.8), 10 mM $(NH_4)_2SO_4$, 10 mM KCl, 2 mM $MgSO_4$, 0.1% TritonX-100, 200 μM dNTPs, 15 ng template DNA, 30 ng each primer, and 0.5 units of VentR DNA polymerase) under the following conditions: (i) 90 seconds at 95°C, (ii) 30 seconds at 95°C, (iii) 1 minute at 57°C, (iv) 2.5 minutes at 75°C, (v) repeat

from step (ii) 29 times. The resulting amplicon, as well as the pCeMM backbone, were digested with NdeI and XhoI, after which, they were ligated together.

Generation of pBABE-NTAP-Oct1

The NTAP-Oct1 cassette was amplified from the pCeMM-NTAP-Oct1 backbone (see above for PCR reaction conditions), after which, along with the pBABE vector, was digested with BamHI and SalI. The digested insert and vector were ligated together as per standard protocol.

RT-PCR and Northern analysis of Artemis

Total RNA was extracted from HEK-293T and HCT116 cells using the RNeasy Mini Kit from Qiagen. RT-PCR was performed on RNA extracted from HEK-293T and HCT116 cells transiently transfected with pIRES-EGFP-Artemis or pIRES-EGFP expression plasmids. First strand cDNA synthesis was performed in duplicate using SSII reverse transcriptase (RT) (Gibco), and Artemis- and EGFP- specific antisense oligonucleotides (see Appendix I). Amplification of the cDNA products via nested PCR resulted in a 500bp Artemis product, and a 450bp EGFP product. 30 PCR cycles were used to generate appropriate signals, which, incidentally, was sufficient to detect endogenous Artemis transcripts in both cell lines.

Northern analysis was performed from total RNA extracted from HEK-293T and HCT116 cells transiently transfected with pIRES-EGFP-Artemis or pIRES-EGFP. Ten micrograms of total RNA per sample (in duplicate) was electrophoresed on a 1% agarose-

formaldehyde gel. 28S and 18S rRNA was visualized via SYBR Gold staining (Molecular Probes). Samples were transferred to a nitrocellulose membrane overnight via standard downward capillary method. The membrane was then incubated with a ^{32}P-labeled α-Artemis or α-EGFP antisense probe (see Appendix I). Phosphorimages were captured with the Typhoon imaging system (Amersham Biosciences).

Preparation of cell extracts

Jurkat T cell nuclear extracts

Jurkat T cell nuclear extracts were used as a source of Ku70/80 for association assays with TALON^{TM}-bound MBP-coreRag-1 proteins. Cells were harvested via scraping in PBS (phosphate buffered saline), and pelleted via centrifugation at 2000 rpm for 5 minutes. The pellet was washed twice with cold PBS, and resuspended in 400 µl of cold Buffer A (10 mM HEPES (pH 7.9), 10 mM KCl, 1.5 mM $MgCl_2$, 0.5 mM DTT (dithiothreitol), and 0.2 mM PMSF (phenylmethylsulphonyl fluoride)). The cell suspension was incubated on ice for 10 minutes, then vortexed for 10 seconds. Lysates were centrifuged for 15 minutes at 13000 rmp at 4°C. The resulting supernatant represents the cytosolic fraction. The pelleted nuclei were re-suspended in 100 µl of cold Buffer C (20 mM HEPES (pH7.9), 1.5 mM $MgCl_2$, 420 mM $NaCl_2$, 25% glycerol, and 0.2 mM PMSF). EDTA and DTT were omitted from buffer C, as they interfere with the binding of the MBP-coreRag-1 proteins to the TALON^{TM} resin. Cells were incubated on ice for 20 minutes, followed by centrifuged at 13000 rpm for 20 minutes at 4°C. The supernatant (representing the nuclear extract) was collected and dialyzed against binding buffer (15 mM HEPES (pH7.9), 60 mM KCl, 12% glycerol, and 0.2 mM

PMSF) for 6 hours with 3 buffer changes. The dialyzed nuclear extracts were quantified via the Bradford Assay (Bio-Rad Laboratories Inc.), and stored in aliquots at -80°C.

Whole cells extracts (for Rag-1/Ku and Artemis lysates)

Cells were harvested via scraping in PBS and pelleted via centrifugation for 5 minutes at 2000 rpm. Pelleted cells were washed twice in cold PBS, and resuspended in an appropriate volume of cold lysis buffer (50 mM Tris-HCl (pH 8), 125 mM NaCl, 5% glycerol, 0.2% NP-40, and 1.5 mM $MgCl_2$ supplemented with Complete Mini Protease Inhibitor Cocktail Tablets (Roche)). Cells were allowed to swell on ice for 15 minutes, followed by a 3 x 20 second sonication, with 30 second incubations on ice between rounds. Sonication was performed on a Branson Sonifier 450 at a constant duty cycle (output control = 1). Lysates were cleared via centrifugation at 13000 rpm for 20 minutes. Protein concentration was determined via the Bradford Assay, and aliquots were frozen at -80°C or used as required.

Whole cell extracts (for Oct-1 TAP lysates)

Media was aspirated from adherent HCT116 cells, and cells were washed twice with 2-4 ml of cold PBS. Cells were scraped in ice cold lysis/binding buffer (50 mM Tris-HCl (pH 8.0) 125 mM NaCl, 5% glycerol, 0.2 NP-40, and 1.5 mM $MgCl_2$ supplemented with Complete Mini Protease Inhibitor Cocktail Tablets (Roche) and Phosphatise Inhibitor Cocktails 1 and 2 (Sigma)). The cells were collected and allowed to swell on ice for 15

minutes, after which the lysates were cleared via centrifugation at 13000 rpm for 15 minutes. Protein concentration was determined as above.

Bacterial expression of coreRag-1 deletion constructs

His-tagged recombinant MBP-coreRag-1 (wild-type and deletion constructs) and MBP alone were expressed in bacteria using the pET30 System (Novagen). BL21(DE3) *E.coli* bacteria were transformed via electroporation with the appropriate pET-MBP-coreRag-1 plasmids (Bio-Rad E. coli pulser), plated on LB-agar with kanamycin, and allowed to grow overnight at 37°C. The following day, 3 ml of LB^{kan} was inoculated with a single colony picked from the plates described above, and allowed to grow overnight in a shaking incubator at 37°C and 250 rpm. The starter culture was used the following morning to inoculate 30 ml of LB^{kan}. Bacteria were allowed to grow at 37°C in a shaking incubator until an OD_{600} of 0.4-0.8 was reached. Expression of the recombinant protein was induced overnight at 4°C on a rocking platform via the addition of IPTG (isopropyl-β-D-thiogalactopyranoside) at a final concentration of 0.1 mM.

Preparation of recombinant protein bacterial lysates

Following protein induction, cells were harvested via centrifugation at 5000 rpm for 15 minutes at 4°C. Pelleted cells were resuspended in extraction buffer (50 mM $NaPO_4$, 300 mM NaCl, pH8.0), and sonicated 3 x 20 second, with 30 second incubations on ice between rounds. The lysate was cleared via centrifugation at 13000 rpm for 5 minutes at 4°C, after which the supernatant was collected and stored at -80°C.

Purification of recombinant proteins using the TALON™ resin

MBP-coreRag-1 proteins were purified from bacterial lysates with the TALON™ system (Clontech) via a C-terminal His-tag. For each sample, 60 µl of TALON™ resin (50% w/v) was aliquoted into a microcentrifuge tube and centrifuged for 2 minutes at 2000 rpm. The supernatant was removed, and the resin was washed twice with 10 bed volumes of ice-cold extraction buffer. 200 µl of bacterial lysate and 200 µl of cold wash/extraction buffer (50 mM $NaPO_4$, 300 mM NaCl, pH 7.0) was added to the resin, and incubated for 2 hours at 4°C on a rotating wheel. Following binding, samples were centrifuged for 5 minutes at 2000 rpm. The supernatant was removed, and the resin was washed 3 x 10 minutes with cold wash/extraction buffer at 4°C on the rotating wheel. Resin-bound protein samples were either (i) used directly for association assays (ii) stored at 4°C for up to 2 weeks, or (iii) proteins were eluted from the resin via incubation with elution buffer (50 mM $NaPO_4$, 300 mM NaCl, 150 mM imidazole, pH 7.0) and stored at -80°C with 30% glycerol. Protein quality and yield was determined via SDS-PAGE, followed by Coomassie blue staining.

MBP-coreRag-1 / Ku association assays

Association assay with TALON™ -bound MBP-coreRag-1 proteins

Equal amounts of TALON™-bound MBP-coreRag-1 proteins were incubated with either 60 µg Jurkat T cell nuclear extract or 75 µg HeLa cell nuclear extract. Binding was allowed to proceed for 2 hours at 4°C on a rotating wheel. To ensure DNA-independent binding, the binding buffer (15 mM HEPES (pH 7.4), 12% glycerol, 0.12 mM PMSF, 60 mM, 160 mM or 360 mM KCl, and 0.1 or 0.2% NP-40) was supplemented with 200 µg/ml

ethidium bromide. TALON™-bound proteins were collected via centrifugation at 2000 rpm at 4°C, and washed 3 x 500 µl binding buffer.

Association assay with TALON™ -eluted MBP-coreRag-1 proteins

Elution of purified proteins from the TALON™ resin via imidazole elution (as per company protocol) was verified via SDS-PAGE, followed by Coomassie blue staining. Equal amounts of eluted proteins were incubated with immunoprecipitated Ku70/80 under the conditions shown above.

Immunoprecipitation of Ku70/80 from Jurkat T cell nuclear extracts

Jurkat T cell nuclear extracts (60 µg per pulldown) were pre-cleared with protein G sepharose beads (30 µl 50% w/v slurry per pulldown) for 30 minutes at 4°C on a rotating wheel. The cleared lysate was collected via centrifugation and incubated with (i) 2 µg α-Ku70 primary antibody (Ab4) for 1 hour, followed by (ii) protein G sepharose beads (30 µl 50% w/v slurry per pulldown) for an additional hour at 4°C on the rotating wheel. The immunoprecipitated Ku heterodimer was washed 3 x 10 bed volumes IP buffer (15 mM HEPES (pH 7.4), 12% glycerol, 0.12 mM PMSF, 400 mM KCl, and 0.3% NP-40), and collected via centrifugation.

SDS-PAGE and western analysis

Electrophoretic separation of protein samples was accomplished via sodium dodecyl sulfate polyacrylamide gel electrophoresis (SDS-PAGE). The acrylamide percentage of the

gels used was determined by the size of the protein(s) of interest; 10% acrylamide gels were used when analyzing Ku/Rag-1 proteins, two-tier 8/12.5% acrylamide gels were used when analyzing Artemis/EGFP proteins, 6 or 8% acrylamide gels were used to analyze Oct-1 proteins, and 4-15% commercially prepared gradient gels (BioRad) were used when analyzing TAP-tagged Oct-1 interactors.

Subsequent to electrophoresis, proteins were transferred to a PVDF (polyvinylidene fluoride) membrane for 1hr at 100V or overnight at 30V. The membrane was blocked in 5% (w/v) powdered milk in TBS-T (Tris-buffered saline, 0.1% TWEEN-20) for 30 minutes at room temperature on a rocking platform. Incubation with the primary antibody was performed for 2 hours at room temperature on the rocking platform, or overnight at 4°C on the rotating wheel. The membrane was washed 3 x 10 minutes with TBS-T, followed by incubation with a horseradish peroxidase (HRP) -conjugated secondary antibody for 1 hour at room temperature on the rocking platform. Detection of the protein/antibody complexes was accomplished via ECL (enhanced chemiluminescence), using Enhanced Luminol Reagent (Western Lightening™, NEN PerkinElmer Life Sciences) as per company protocol. Chemiluminescence was captured by using the GeneSnap image acquisition system (Syngene).

Transient transfection

At approximately 50-60% confluency, cells were transiently transfected with 3 μg of expression vector plasmid using 18 μl FuGENE 6 transfection reagent (Roche Diagnostics), as per company protocol. Cells were harvested 48 hours post-transfection, and lysates were

quantified via the Bradford assay. Samples were either aliquoted and stored at -80°C for future use, or SDS-PAGE/western analysis was performed.

Indirect immunofluorescence

24 hours prior to transient transfection, cells were seeded at an appropriate density (~50-60% confluency) on 22 x 22 mm glass coverslips in 6-well culture dishes. Cells were transfected as per standard protocol. 24 or 48 hours post-transfection, wells were washed twice with 2 ml PBS, and then fixed with 2 ml of 4% paraformaldehyde for 10 minutes at room temperature with gentle rocking. Cells were next permeabilized with 0.1% Triton X-100 in TBS-T, then blocked with 5% goat serum (both for 10 minutes at room temperature). Primary antibody solutions were added to the coverslips at a dilution of 1:200-1:750, depending on the nature of the antibody used, and allowed to incubate for 1 hour at room temperature with gentle rocking. Following 3 x 5 minute washes with TBS-T, coverslips were incubated with the appropriate secondary antibody at a dilution of 1:500. This incubation was performed in the dark for 30 minutes at room temperature with gentle rocking. Fluorescence images were captured via standard microscopy (Eclipse Microscope, Model TE300; Nikon 2001).

Inhibition of proteasomal- and lysosomal- mediated protein degradation

24 hours post-transfection, HEK-293T, and MCF-7 cells were treated with the proteasome inhibitor MG132 (Calbiochem). Briefly, media containing 1 μM MG132 dissolved in DMSO, or DMSO alone, was added directly to the media covering the cells.

Cells were harvested 24 hours after treatment. In the same manner, MCF-7 cells were treated with the lysosomal pathway inhibitor chloroquine (Sigma Aldrich) dissolved in PBS (phosphate buffered saline), or PBS alone, at a concentration of 100 μM.

Oct-1 DNA damage response

Treatment of cells with DNA damaging drugs

HEK-293T, HCT116, MCF7 and HeLa cells were incubated for 2 hours at 37°C with media containing bleomycin (25 μg/ml), zeocin (100 μg/ml), etoposide (25 mM), or vehicle alone (PBS or DMSO). Following incubation, cells were either harvested immediately, or replaced with fresh media and harvested at different recovery times. 30-50 μg of lysate was loaded on a 10% acrylamide gel, and Oct-1 was detected via western protocol. Ponceau staining was used to normalize the fold increase of Oct-1 protein levels.

Irradiation of cells

24 hours pre-irradiation, cells were seeded onto 60 mm dishes at ~50-60% confluency. The following day, cells were exposed to 6 Gy of γ-irradiation (Pantak irradiator; dose rate = 1.68 Gy/min). Cells were returned to the 37°C incubator, and harvested at indicated recovery times. Lysates were analyzed as above.

TAP-tagged Oct-1 stable cell lines

24 hours pre-transfection, 2.5 x 10^6 293T-Phoenix cells were seeded on a 60 mm dish. Using a standard $CaCl_2$ transfection protocol, phoenix cells were transiently transfected

with 10 μg DNA. Immediately prior to the addition of the transfection cocktail, phoenix cell media was changed to contain 25 μM chloroquine. Ten hours post-transfection, the media was replaced with 6 ml fresh media. Twenty-four hours post-transfection, the media was changed again (6 ml), and 48 hours post-transfection, the viral supernatant was collected with an 18-guage needle, and passed through a 0.4 μm syringe filter. Viral supernatant was stored at -80°C, or immediately used for infection.

At ~60-70% confluency, HCT116 cells plated on a 60 mm dish were infected with 2 ml of viral supernatant. Briefly, HCT116 media was replaced with 4 ml fresh media, 2 ml viral supernatant, and 6 μl of polybrene (1000X). Cells were passaged as per usual, and the expression of the TAP-tagged Oct-1 protein was monitored over time via indirect immunofluorescence and western analysis.

Tandem affinity purification (TAP)

HCT116 cells transiently transfected with pCeMM-NTAP-Oct-1 were harvested (as above) in ice cold lysis/binding buffer (50 mM Tris-HCL (pH 8.0) 125 mM NaCl, 5% glycerol, 0.2 NP-40, and 1.5 mM $MgCl_2$ supplemented with Complete Mini Protease Inhibitor Cocktail Tablets (Roche) and Phosphatise Inhibitor Cocktails 1 and 2 (Sigma)). 10 mg whole cell lysate was incubated for 2 hours at 4°C on a rotating wheel with 800 μl (50% w/v) rabbit IgG agarose resin (Sigma). The volume of the binding reaction was brought up to 5 ml with cold binding buffer. The resin was collected via centrifugation at 1000 rpm and washed three times with binding buffer, and twice with AcTEV protease cleavage buffer (50 mM Tris-HCl (pH8.0), and 0.5 mM EDTA). The resin was then incubated with 400 units AcTEV protease (Invitrogen) in a final volume of 1200 μl cleavage buffer overnight at 4°C

or for 1 hour at 30°C. Following cleavage, the resin was pelleted via centrifugation for 2 minutes at 1000 rpm, and the supernatant was collected. The supernatant was then incubated with 500 µl (50% w/v) UltlraLink Immobilized Streptavidin Plus (Pierce), in a final volume of 2250 µl binding buffer (100 mM Tris-HCL (pH8.0), 150 mM NaCl, and 1 mM EDTA) for 2 hours at 4°C on a rotating wheel. The resin was collected via centrifugation (as above) and washed three times in binding buffer. TAP-tagged protein complexes were eluted from the streptavidin resin in 1250 µl of biotin elution buffer (2.5 mM biotin, 100 mM Tris-Cl (pH7.4), 1 mM EDTA). The final elution was allowed to proceed at 4°C for 2 hours or overnight.

Silver staining

Following standard SDS-PAGE, the acrylamide gel was incubated with fixation solution (5% acetic acid, 30% ddH_2O) for 30 minutes with gentle rocking. The gel was then washed 4 x 5 minutes with ddH_2O, followed by a 1 minute incubation with sensitization solution (0.02% sodium thiosulfate pentahydrate). After a second wash with ddH_2O (2 x 1 minute), the gel was incubated with a silver stain solution (0.2% silver nitrate) for 30-120 minutes with gentle rocking. The gel was again washed 2 x 1 minute with ddH_2O, followed by a 15 minute incubation with developing solution (4% potassium carbonate, 0.025% (v/v) formalin). The reaction was stopped by incubating the gel with stopping solution (4% Tris, 2% acetic acid) for 30 minutes at room temperature.

Antibodies

Rabbit α-Ku70 Ab4 (NH3H10; Neomarkers, Fremont, CA); rabbit α-Ku80 Ab2 (111; Neomarkers); rabbit α-MBP (C18; Santa Cruz Biotechnology Inc.); rabbit α-Oct1 (C-21; Santa Cruz Biotechnology Inc.); mouse α-c-myc (9E10; Santa Cruz Biotechnology Inc.); Living Colors® Full-length A.v. Polyclonal Antibody (Clontech); BD Living Colors™ A.v. Monoclonal Antibody (JL-8; Clontech); donkey α-rabbit IgG (H+L) Alexa Fluor 594 (Molecular Probes); donkey α-mouse IgG (H+L) Alexa Fluor 488 (Molecular Probes).

Results

Section I: MBP-CoreRag-1 / Ku binding

Previous coimmunoprecipitation binding experiments performed within our laboratory have demonstrated that the binding of Ku70 to Rag-1 is a specific and DNA-independent event (Schildt-Poulter). With the use of MBP-fusion peptides, a minimal region of coreRag-1 capable of binding Ku70 was identified (Zheng, Appendix II). This peptide corresponds to amino acids 660-763 of Rag-1. In order to further refine the Ku70 binding domain of Rag-1, deletion constructs were generated.

Generation of CoreRag-1 deletion constructs

Spanning amino acids 660-763 are two overlapping coreRag-1 domains; the central domain (aa528-760) and zinc finger B (ZFB; aa727-750). (Refer to Figure 8 for Rag-1 domain details). Zinc fingers are classically known to function as DNA-binding motifs; however, these domains have also been described in mediating protein-protein interactions (218). Therefore, in generating subsequent coreRag-1 deletions within aa660-763, the structural integrity of zinc finger B was maintained. Figure 9 outlines the following deletion constructs generated: MBP-coreRag-1 (Δ660-763), MBP-coreRag-1 (Δ660-720), and MBP-coreRag-1 (Δ721-763).

Expression and purification of MBP-coreRag-1 deletion constructs

Protein expression was achieved using the pET-vector / BL21(DE3) bacterial expression systems. Core-Rag-1 constructs were generated as MBP fusion peptides, as MBP

Figure 9. Rag-1 protein constructs. Outline of deletion constructs within the context of full-length, wild-type Rag-1. For use in binding assays, deletions were generated as MBP-coreRag-1 fusion proteins.

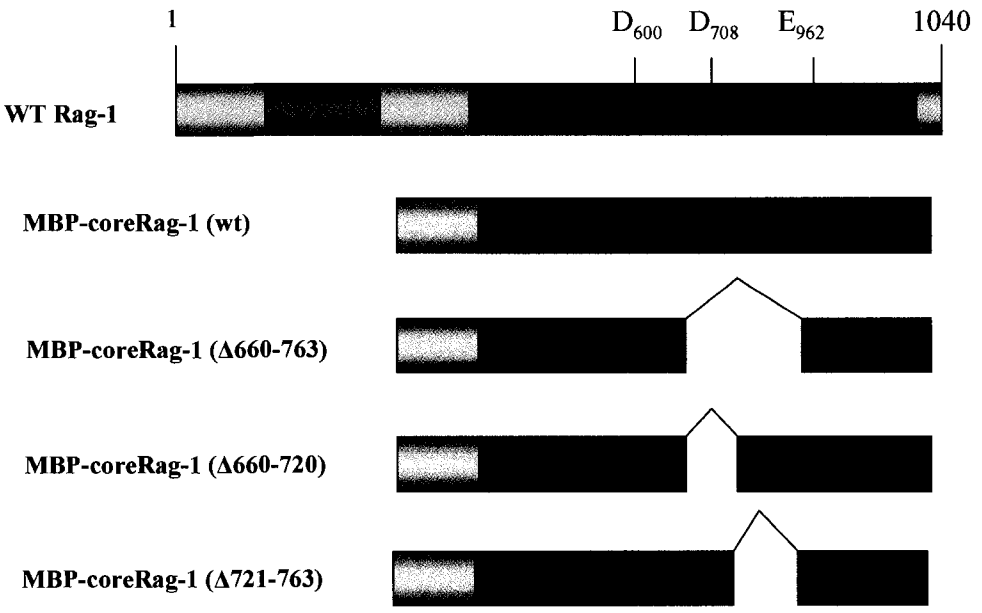
1
D600
D708
E962
1040
WT Rag-1
MBP-coreRag-1 (wt)
MBP-coreRag-1 (Δ660-763)
MBP-coreRag-1 (Δ660-720)
MBP-coreRag-1 (Δ721-763)

(maltose-binding peptide) has been shown to increase the solubility and stability of proteins expressed in bacteria. This reduces the chance of the expressed proteins forming insoluble aggregates within the bacteria (218b). MBP-coreRag-1 (wt and deletions), and MBP protein expression was induced in BL21(DE3) *E. coli* transformed with the appropriate plasmid construct (pET30-MBP-coreRag-1 wt and deletions, and pET30-MBP). To minimize the sequestration of the recombinant proteins within inclusion bodies, protein induction was performed with a low dose of IPTG (0.1 μM) overnight at 4°C. Taking advantage of a C-terminal 6 x His-tag, MBP-coreRag-1 proteins and MBP were purified from bacterial lysates using the TALON^{TM} resin. This cobalt-based form of IMAC (immobilized metal affinity chromatography) binds His-tagged proteins with an enhanced selectivity over nickel-based resins (219). Bacterial lysates were incubated with the TALON^{TM} resin for 2 hours at 4°C on a rotating wheel. The expression and purification of the recombinant MBP-coreRag-1 (wt and deletions), as well as MBP, alone was verified via SDS-PAGE, followed by Coomassie staining (Figure 10).

MBP-coreRag-1 (wt and deletions), as well as MBP alone bind Ku70 from Jurkat T cell nuclear extracts

Following the purification of MBP-coreRag-1 constructs from bacterial lysates, equal amounts of TALON^{TM}-bound proteins were incubated with Jurkat T cell nuclear extracts; which provide an abundant source of Ku70/80. As the purification efficiencies of wild-type MBP-coreRag-1, MBP alone, and the MBP-coreRag-1 deletion constructs each differed from one another (Figure 10), the volume of each TALON^{TM}-bound protein was corrected such that the quantitative amount of each protein used in the association assays were

Figure 10. Purification of MBP-coreRag-1 constructs with TALON™ resin. Following IPTG induction and lysate preparation, MBP-coreRag-1 constructs and MBP alone were purified via a C-terminal His tag. The TALON™ resin uses IMAC (immobilized metal affinity chromatography) via Co^{2+} chelation to preferentially bind a 6 x His tag present at the C-terminus of all recombinant proteins. The overall binding efficiency can be determined by comparing the amount of TALON™-bound proteins to those remaining in the supernatant post-binding.

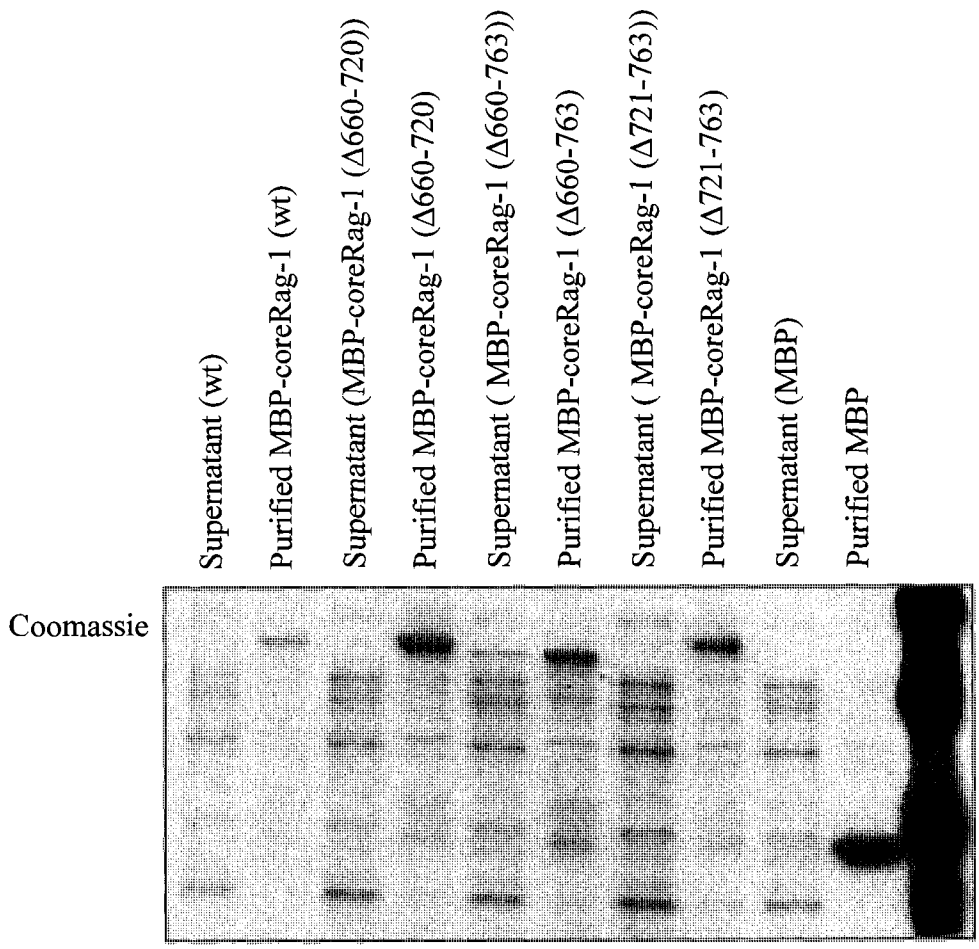
Coomassie
Supernatant (wt)
Purified MBP-coreRag-1 (wt)
Supernatant (MBP-coreRag-1 (Δ660-720))
Purified MBP-coreRag-1 (Δ660-720)
Supernatant (MBP-coreRag-1 (Δ660-763))
Purified MBP-coreRag-1 (Δ660-763)
Supernatant (MBP-coreRag-1 (Δ721-763))
Purified MBP-coreRag-1 (Δ721-763)
Supernatant (MBP)
Purified MBP

equivalent. In order to ensure that binding was DNA-independent, 200 μg/ml of ethidium bromide was included in all reactions (219b-d). Binding was allowed to occur at 4°C for 2 hours, following which, the TALON^{TM} resin was collected via centrifugation and washed with binding buffer. As a positive and negative control, binding with wt MBP-coreRag-1 and MBP, respectively, was also performed. Under these conditions (160 mM salt, 0.1% NP-40), the binding of Ku with all MBP- coreRag-1 derivatives, as well as with MBP alone, was observed (Figure 11). The Ku heterodimer is known to interact with numerous cellular factors (85-91). It is reasonable to propose that under the binding conditions used, Ku may be non-specifically interacting with MBP, or with a factor within the cell lysate that is capable of binding MBP. In an attempt to reduce the non-specific interaction between Ku and MBP, the stringency of the binding buffer was increased (360 mM salt, 0.2% NP-40), and the association experiment was repeated. TALON^{TM}-bound proteins were allowed to incubate with HeLa cell nuclear extracts, as previously described. Subsequent immunoblot analysis revealed the binding of MBP-coreRag-1 derivatives, as well as MBP, with Ku70 (Figure 12).

Although the binding conditions employed in these association assays were at least as stringent as those previously used to identify Rag-1 / Ku70 binding, non-specific interactions were nonetheless observed. It was hypothesized that the Ku heterodimer may be non-specifically binding the TALON^{TM} resin itself. To circumvent this potential obstacle, as well as obtain a "cleaner" source of Ku, the Ku heterodimer was immunoprecipitated from Jurkat T cell nuclear extracts under conditions more stringent than those used in the previous association assays (400 mM NaCl; 0.3% NP-40). Prior to immunoprecipitation, the nuclear extracts were pre-cleared for half an hour with protein-G sepharose beads. The cleared lysate was then incubated with an α-Ku70 antibody (Ab4) for 1 hour, followed by a 60

Figure 11. TALON™-bound MBP-coreRag-1 (wt and deletions) and MBP alone bind Ku70 from Jurkat T cell nuclear extracts. Direct binding between MBP-coreRag-1 constructs (wt and deletions), as well as MBP with Jurkat T cell nuclear extracts (60 μg). Top panel is an immunoblot against MBP, which detects the MBP-coreRag-1 fusion proteins, as well as MBP alone. The bottom panel is an immunoblot against Ku70.

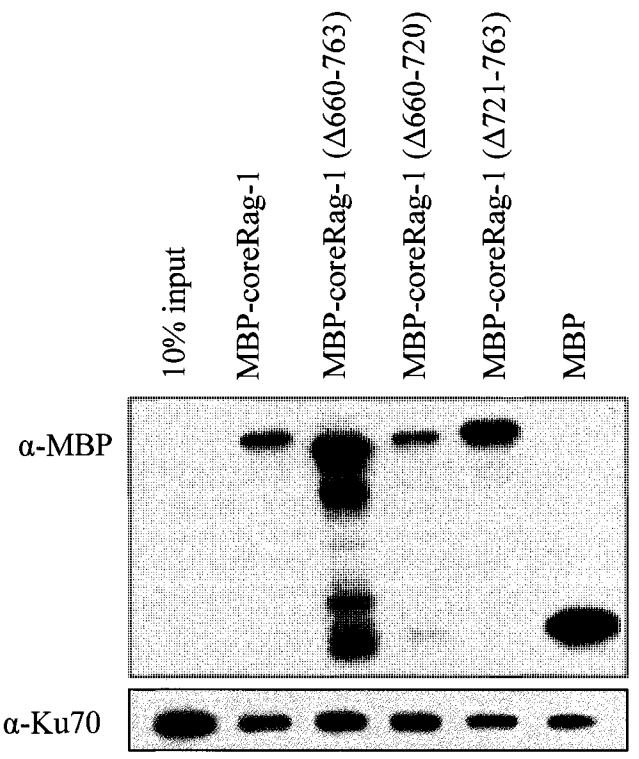
10% input
MBP-coreRag-1
MBP-coreRag-1 (Δ660-763)
MBP-coreRag-1 (Δ660-720)
MBP-coreRag-1 (Δ721-763)
MBP
α-MBP
α-Ku70

Figure 12. TALON^{TM}-bound MBP-coreRag-1 (wt and derivatives) and MBP alone bind Ku70 from HeLa cell nuclear extracts. Direct binding between MBP-coreRag-1 constructs (wt and deletions), as well as MBP, with HeLa cell nuclear extracts (75 μg). Top panel is an immunoblot against MBP, which detects the MBP-coreRag-1 fusion proteins, as well as MBP alone. The bottom panel is an immunoblot against Ku70.

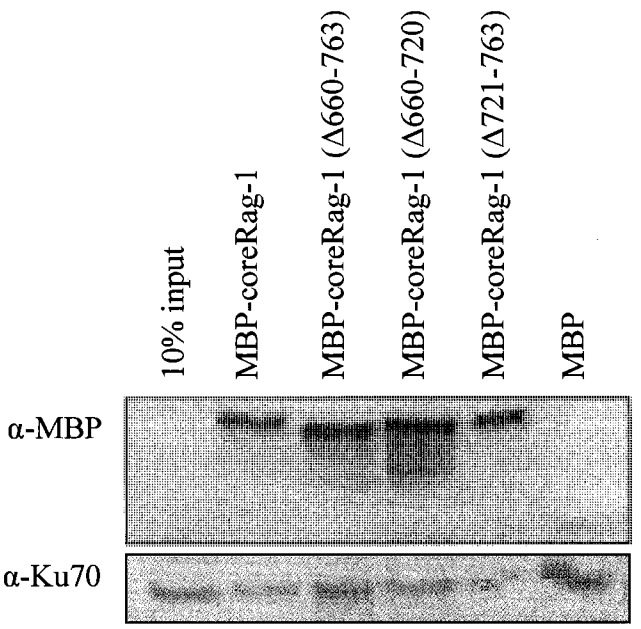
10% input
MBP-coreRag-1
MBP-coreRag-1 (Δ660-763)
MBP-coreRag-1 (Δ660-720)
MBP-coreRag-1 (Δ721-763)
MBP
α-MBP
α-Ku70

minute incubation with fresh protein-G sepharose beads. The immunoprecipitated Ku70/80 complex was thoroughly washed with immunoprecipitation buffer. As the Ku heterodimer was resin-bound, the ensuing association assays required MBP-coreRag-1 proteins to be eluted from the TALON™ resin. Imidazole elution of the MBP-coreRag-1 proteins was verified via SDS-PAGE, followed by Coomassie blue staining. The eluted proteins were incubated with immunoprecipitated resin-bound Ku70/80 for 2 hours at 4°C. Despite this attempt to disrupt non-specific specific interactions, binding between Ku70 and MBP was still observed. Additionally, all MBP-coreRag-1 derivatives bound Ku70 as well (Figure 13).

MBP-coreRag-1 (wt and deletions), but not MBP, bind Baculo-Ku

In the subsequent set of association assays, a commercially expressed and purified source of Ku70/80 from baculovirus-infected Sf9 insect cells (Baculo-Ku) was obtained for use. As the non-specific interactions observed in the previous association assays do not appear to be the result of Ku binding the TALON™ resin, the interaction between Ku70 and MBP may be attributed to the presence of cellular factors associated with Ku70 that are capable of binding MBP. If this theory is true, the use of Baculo-Ku in subsequent association assays should circumvent this problem, as it is guaranteed to be greater than 90% pure (220). Equal amounts of TALON™-bound MBP-coreRag-1 constructs (wt and deletions), as well as MBP alone, were incubated with 21 ng Baculo-Ku for 2 hours at 4°C. The samples were collected via centrifugation and washed thoroughly with binding buffer. Figure 14A shows the binding of Ku70 to all MBP-coreRag-1 derivatives (wt and deletions), but not with MBP alone. This observation led to the conclusion that the region of coreRag-1

Figure 13. TALON^{TM}-eluted MBP-coreRag-1 (wt and deletions) and MBP alone bind Ku70 immunoprecipitated from Jurkat T cell nuclear extracts. Ku70 was immunoprecipitated from Jurkat T cell nuclear extracts, and incubated with MBP-coreRag-1 (wt and deletions), and MBP alone. The latter proteins were eluted from the TALON^{TM} resin via immidazole elution. Top panel is an immunoblot against MBP, which detects the MBP-coreRag-1 fusion proteins, as well as MBP alone. The bottom panel is an immunoblot against Ku70.

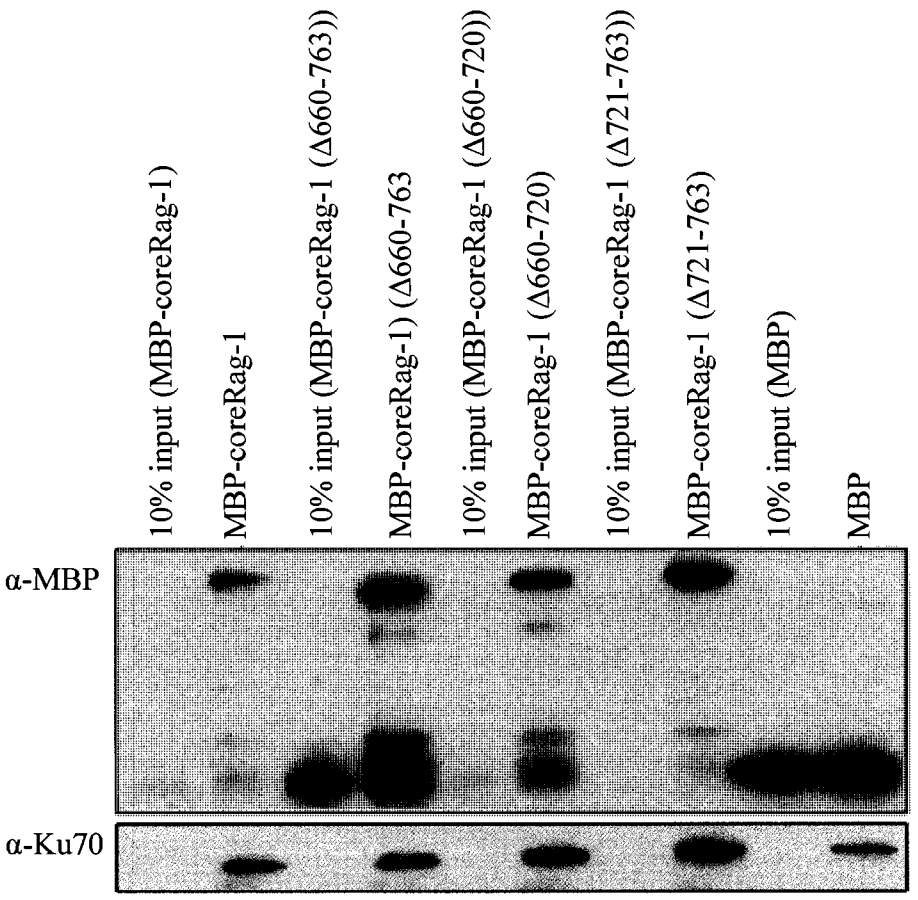
10% input (MBP-coreRag-1)
MBP-coreRag-1
10% input (MBP-coreRag-1 (Δ660-763))
MBP-coreRag-1) (Δ660-763
10% input (MBP-coreRag-1 (Δ660-720))
MBP-coreRag-1 (Δ660-720)
10% input (MBP-coreRag-1 (Δ721-763))
MBP-coreRag-1 (Δ721-763)
10% input (MBP)
MBP
α-MBP
α-Ku70

Figure 14. TALON™-bound MBP-coreRag-1 (wt and deletions), but not MBP alone, bind Baculo-Ku. Direct binding between MBP-coreRag-1 derivatives and MBP alone with commercially purchased Baculo-Ku. Baculo-Ku binding is observed between all MBP-coreRag-1 derivatives, but not between MBP.

A

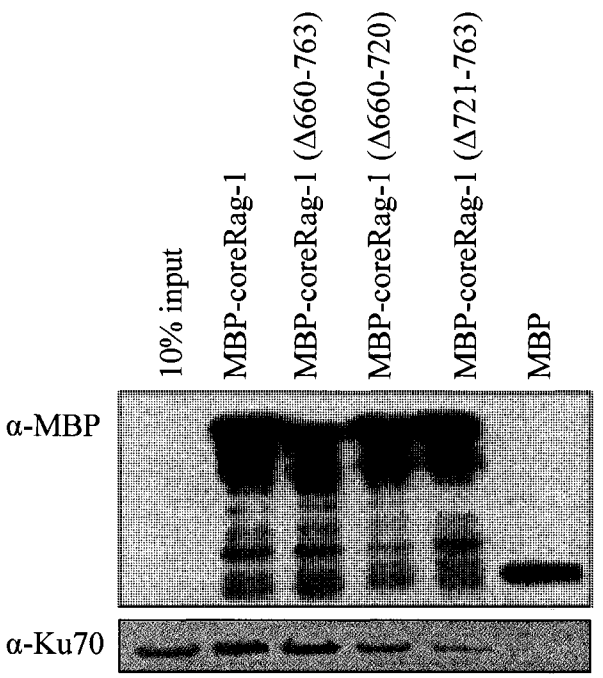
10% input
MBP-coreRag-1
MBP-coreRag-1 (Δ660-763)
MBP-coreRag-1 (Δ660-720)
MBP-coreRag-1 (Δ721-763)
MBP
α-MBP
α-Ku70

B

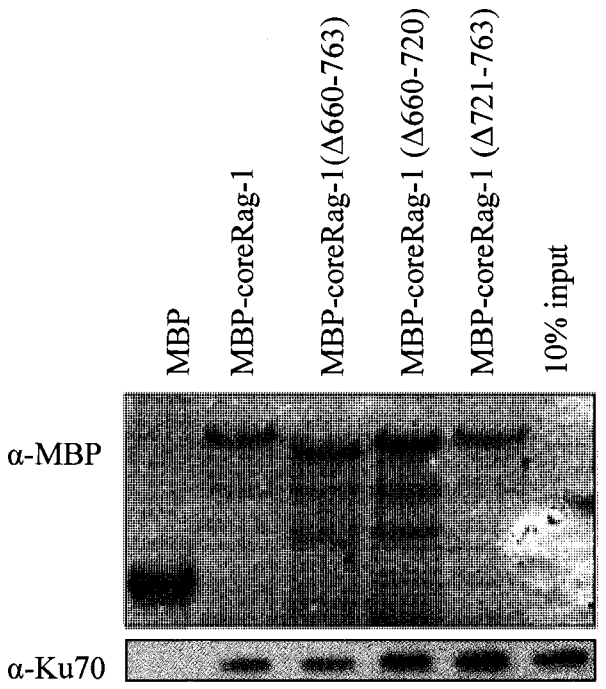
MBP
MBP-coreRag-1
MBP-coreRag-1(Δ660-763)
MBP-coreRag-1 (Δ660-720)
MBP-coreRag-1 (Δ721-763)
10% input
α-MBP
α-Ku70

spanning amino acids 660-763 is sufficient, but not required for Ku70 binding.

As all deletions still bound Ku70, a new set a deletion constructs removing a larger region of coreRag-1 were generated. These deletions, MBP-coreRag-1(Δ528-763) and MBP-coreRag-1(Δ528-720) were used in association assays along with the previously generated MBP-coreRag-1(Δ721-763), MBP-coreRag-1(WT) and MBP. MBP-coreRag-1(Δ528-763) was chosen as it completely removes the Rag-1 central domain, (aa528-760). However, despite the removal of this region of coreRag-1, binding was still observed between all deletion mutants, but not MBP alone, and baculo-Ku (Figure 14B). Since the removal of increasingly larger regions of coreRag-1 may interfere with proper protein folding, and the deletion of secondary regions of coreRag-1 requires the re-implementation of peptide mapping experiments, it was decided that further steps to identify the Ku70 binding domain of Rag-1 would not be taken. Instead, a novel study examining the ectopic expression of an integral V(D)J recombination/NHEJ factor (Artemis) would be pursued.

Section II: Examining the regulation of ectopic Artemis expression

Within our laboratory, we have observed a limitation in the ectopic expression of Artemis. We rationalized that the tight regulation of Artemis expression was limiting its ectopic expression. By manipulating and observing conditions that would allow for Artemis expression in a non-permissive cell line, information concerning the level(s) at which Artemis is regulated, and possibly the factors involved in eliciting this regulation, may be identified. Once the ectopic Artemis expression is achieved, the contributions of Artemis on V(D)J recombination and NHEJ can be further studied.

Artemis/EGFP bicistronic expression system

The use of a bicistronic Artemis/EGFP expression vector (pIRES-EGFP) was a useful tool in monitoring the expression of Artemis, as it allows for the expression of two separate proteins from a single bicistronic transcript under the control of a single promoter. In this system, the first protein (myc-Artemis, hereafter referred to as Artemis) is translated from the mRNA in a canonical cap-dependent manner, whereas the second protein (EGFP) is translated in a cap-independent manner from an internal ribosomal entry site (IRES) situated between the coding sequences of these two peptides (Figure 15). The expression of EGFP serves as a powerful control in two senses. Firstly, the expression of EGFP confirms the transcription of Artemis, as both sequences are present on the same transcript. Secondly, changes in Artemis expression can be normalized to EGFP expression levels, and expressed as Artemis:EGFP ratios. This allows for the comparison of Artemis expression under different experimental conditions.

Identification of Artemis permissive and non-permissive cell lines

In order to identify cells that were either permissive or non-permissive to the ectopic expression of Artemis, a variety of different cell lines were transiently transfected with equal amounts of the Artemis/EGFP bicistronic expression vector. Whereas EGFP expression could be detected in all cell lines, only two cell lines, HEK-293T and Cos-7, showed both Artemis and EGFP expression (Figure 16A). Due to the similarity in growth times, ease of transfection, and similar levels of EGFP expression, HEK-293T and HCT116 were chosen as the representative permissive and non-permissive cell lines, respectively (Figure 16B).

Figure 15. Artemis / EGFP bicistronic constructs. (A) Schematic representation of the pIRES-EGFP vector, into which Artemis was cloned. **(B)** Cartoon depicting the translation of two separate peptides from a single bicistronic mRNA under the control of (i) a single promoter at the level of transcription, and (ii) two independent promoters at the level of translation.

A

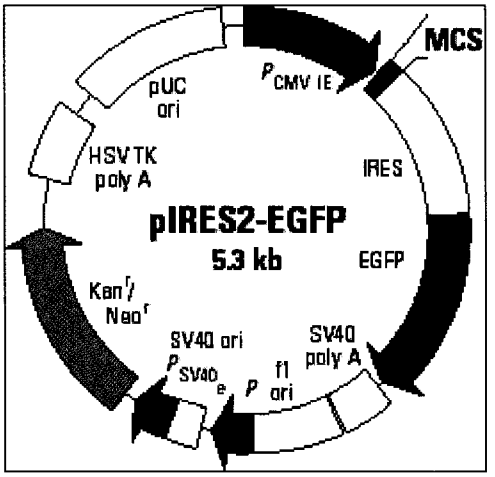
MCS
pUC ori
P CMV IE
HSV TK poly A
IRES
pIRES2-EGFP
5.3 kb
EGFP
Kan r/ Neo r
SV40 ori
SV40 poly A
P SV40 e
P
f1 ori

B

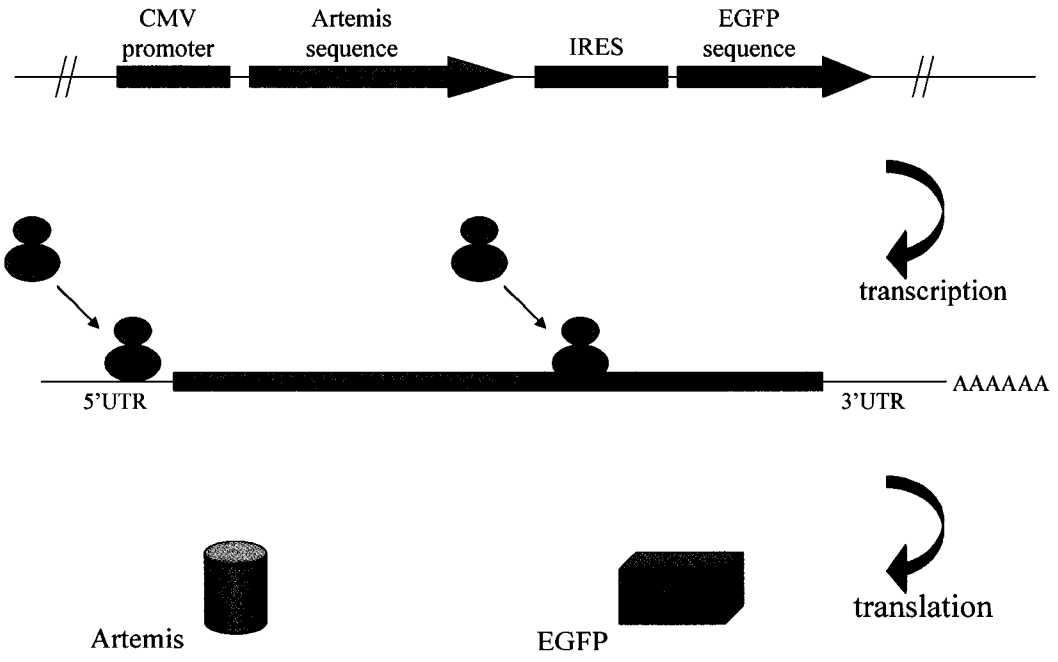
CMV promoter
Artemis sequence
IRES
EGFP sequence
transcription
5'UTR
3'UTR
AAAAAA
Artemis
EGFP
translation

Figure 16. The ectopic expression of Artemis is limited to a restricted repertoire of cell lines. (A) Western blot analysis shows a panel of cell lines transiently transfected with pIRES-EGFP-Artemis. The expression of EGFP is detected in all transfectants, whereas the expression of Artemis is limited to the HEK-293T and Cos7 cell lines. **(B)** Indirect immunofluorescence shows EGFP in both cell lines, as well as the nuclear subcellular localization of Artemis in (i) HEK-293T but not in (ii) HCT116 cells transiently transfected with pIRES-EGFP-Artemis. Panel (iii) shows a subpopulation of HCT116 cells (~2-5%) that are able to express Artemis.

A

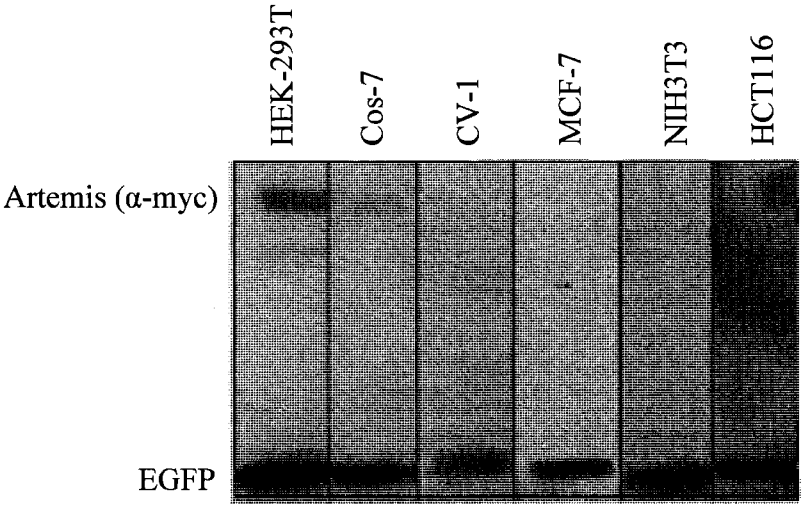
HEK-293T
Cos-7
CV-1
MCF-7
NIH3T3
HCT116
Artemis (α-myc)
EGFP

B

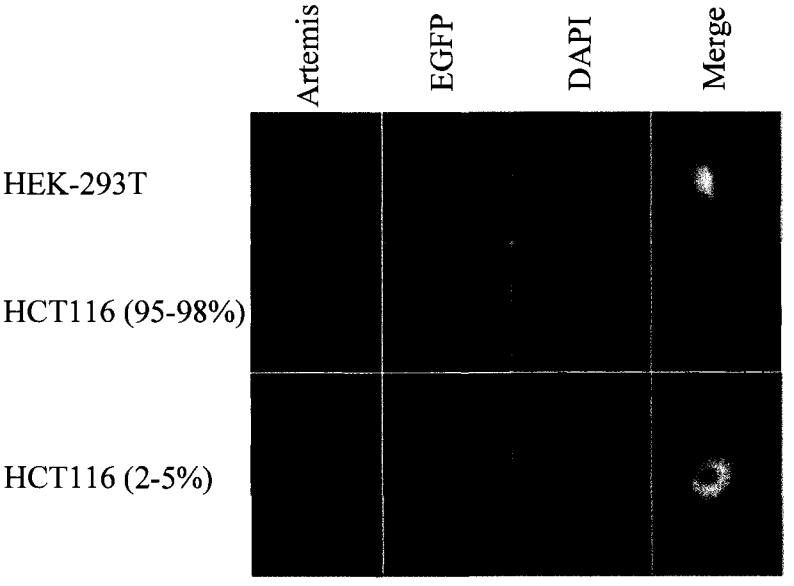
Artemis
EGFP
DAPI
Merge
HEK-293T
HCT116 (95-98%)
HCT116 (2-5%)

Transcriptional / post-transcriptional regulation

Since (1) EGFP and Artemis are transcribed on the same mRNA, and (2) EGFP was being expressed, it was rationalized that the ectopic expression of Artemis was not being regulated at the level of transcription. However, to rule out the possibility of mRNA processing that would selectively disrupt the Artemis coding sequence, Northern analysis was performed on total RNA extracted from HEK-293T and HCT116 cells transiently transfected with the Artemis/EGFP bicistronic construct. Figure 17A shows duplicate Northern blots hybridized with either a ^{32}P-labeled anti-Artemis or ^{32}P-labeled anti-EGFP probe. In this experiment, both probes recognized the Artemis/EGFP transcript in the HEK-293T, but not the HCT116, cell line. Furthermore, the ^{32}P-labeled anti-EGFP probe recognized the EGFP transcript in the HEK-293T cell line, yet failed to recognize it in the HCT116 cell line. This observation was contradictory to immunofluorescence analysis, where an EGFP signal was visible in both cell lines. To clarify the conflicting EGFP result obtained via Northern analysis, RT-(reverse transcriptase) PCR was employed. Both transcripts (Artemis/EGFP and EGFP) were found to be present in the HEK-293T and HCT116 cell lines at similar levels (Figure 17C). Additionally, this method was sensitive enough to detect endogenous Artemis transcripts in both cell lines, albeit at significantly lower levels.

Post-translational degradation

To observe whether or not Artemis was being selectively targeted for post-translational degradation, non-permissive MCF-7 cells transiently transfected with either the Artemis/EGFP or EGFP alsone bicistronic constructs were treated with an inhibitor of

Figure 17. Northern and RT-PCR analyses of Artemis/EGFP and EGFP transcripts in permissive and non-permissive cell lines. HEK-293T and HCT116 cells were transiently transfected with pIRES-EGFP-Artemis or pIRES-EGFP (lanes 2 and 3, respectively; lane 1 represents non-transfected cells). **(A)** 10 μg total RNA was analyzed in duplicate. (i) Sybr-gold staining shows the quality of the RNA extracted. (ii) ^{32}P-labeld probes against Artemis (probe 1, left side of blot) and EGFP (probe 2, right side of blot) detect transcripts in the HEK-293T cell line only. **(B)** Schematic representation of the transcripts analyzed, and approximate positioning of the probes used. Orange represents Artemis sequence, blue represents the IRES, and green represents EGFP. **(C)** RT-PCR of RNA extracted from HEK-293T and HCT116 cells transiently transfected with pIRES-EGFP-Artemis and pIRES-EGFP expression constructs shows the transcription of Artemis/EGFP and EGFP alone in both cell lines. 1st strand cDNA synthesis was performed in duplicate using SSII reverse transcriptase (Gibco), and Artemis- and EGFP- specific antisense oligos. Amplification of the cDNA products via nested PCR resulted in a 500bp Artemis-specific product, and a 450bp EGFP-specific product. 30 PCR cycles were used to generate appropriate signals, which, incidentally, was sufficient to detect endogenous Artemis transcripts in both cell lines.

A

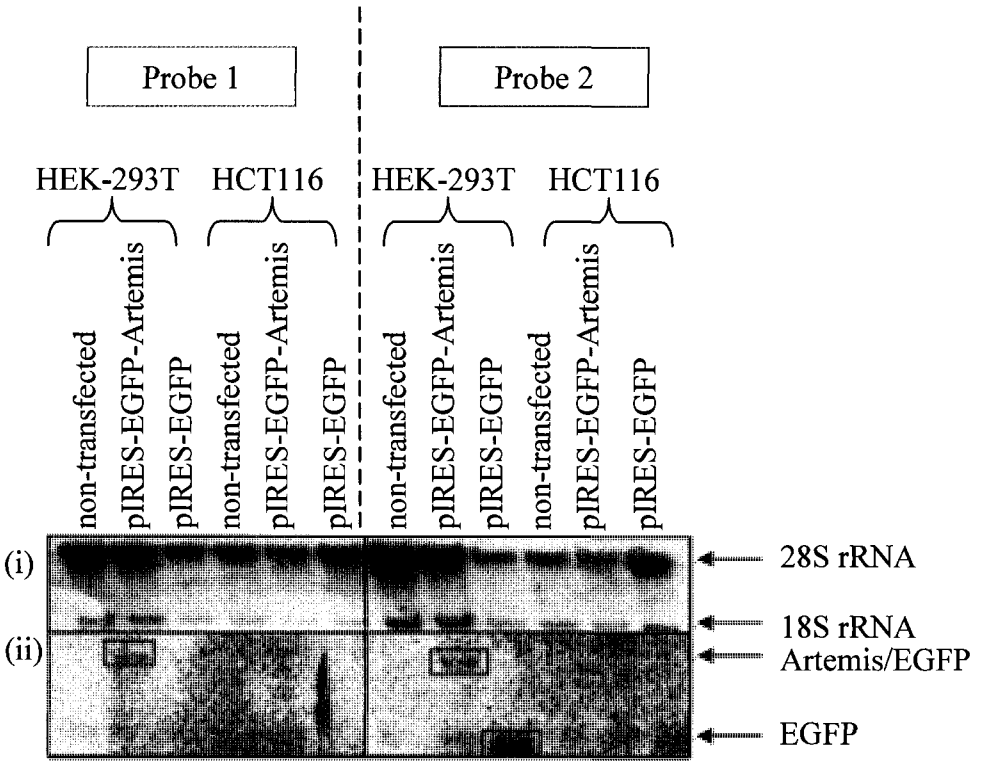
Probe 1
Probe 2
HEK-293T
HCT116
HEK-293T
HCT116
non-transfected
pIRES-EGFP-Artemis
pIRES-EGFP
non-transfected
pIRES-EGFP-Artemis
pIRES-EGFP
non-transfected
pIRES-EGFP-Artemis
pIRES-EGFP
non-transfected
pIRES-EGFP-Artemis
pIRES-EGFP
(i)
(ii)
28S rRNA
18S rRNA
Artemis/EGFP
EGFP

B


Artemis/EGFP
EGFP

C

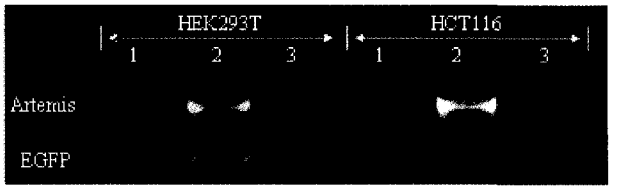
HEK293T
HCT116
1
2
3
1
2
3
Artemis
EGFP

proteasomal-mediated or lysosomal-mediated protein degradation (MG132 and chloroquine, respectively). MCF-7 cells were chosen as a non-permissive cell line, as these over-express the insulin-like growth factor receptor 1 (IGFR1), which is known to be targeted for lysosomal-mediate protein degradation (221). Treatment of MCF-7 cells with a neutralizing α-IGFR1 antibody prior to chloroquine treatment has been shown to partially block this degradation (221). Therefore, this system has an internal control for chloroquine treatment. Additionally, to control the efficacy of MG132 treatment, MCF-7 cells were transiently transfected with myc-GR (glucocorticoid receptor) which is sensitive to proteasomal-mediated protein degradation (222). Cells were treated with either agent for 20 hours, after which they were harvested and analyzed via immunoblotting against myc (Artemis) and EGFP. Figure 18 illustrates the efficacy of both drugs, as a stabilization of IGFR1 and myc-GR were both observed. Conversely, EGFP levels were unaffected by either treatment, and Artemis expression was not detected under any conditions. Therefore, the ectopic expression of Artemis was not being regulated via the post-translational proteasomal- or lysosomal-mediated degradation pathways.

Cap-dependent versus IRES-mediated translation

To investigate whether or not the mode of translation affected the ectopic expression of Artemis, a new Artemis/EGFP bicistronic construct was generated, in which EGFP would be translated form the CMV promoter (cap-dependent), and Artemis from the IRES (cap-independent) (Figure 19A). Immunoblot analysis of HEK-293T and HCT116 cells transiently transfected with either of the Artemis/EGFP bicistronic constructs identified that Artemis expression was enhanced through IRES-mediated translation (Figure 19B). In both

Figure 18. Inhibition of proteasomal- or lysosomal-mediated protein degradation does not result in the stabilization of Artemis in non-permissive MCF-7 cells. MCF-7 cells were transiently transfected with either pIRES-EGFP-Artemis or pIRES-EGFP and treated with 1 μM MG132 or 100 μM chloroquine for 20 hours. The activities of MG132 and chloroquine were verified by observing the stabilization of the glucocorticoid receptor (GR) and the insulin-like growth receptor I (IGFR-I), respectively.

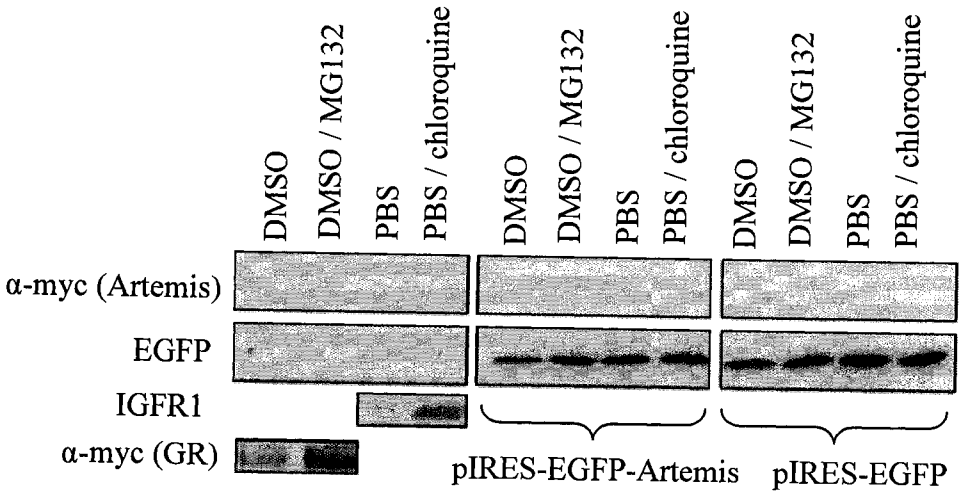
DMSO
DMSO / MG132
PBS
PBS / chloroquine
DMSO
DMSO / MG132
PBS
PBS / chloroquine
DMSO
DMSO / MG132
PBS
PBS / chloroquine
α-myc (Artemis)
EGFP
IGFR1
α-myc (GR)
pIRES-EGFP-Artemis
pIRES-EGFP

Figure 19. Cap-dependent versus IRES-mediated translation of Artemis. **(A)** Schematic representation of the Artemis/EGFP bicistronic expression constructs generated. Construct-1 results in the cap-dependent translation of Artemis (via a CMV promoter) and the IRES-mediated translation of EGFP. Construct-2 results in the cap-dependent translation of EGFP (CMV) and the IRES-mediated translation of Artemis.**(B)** Immunoblot showing the expression of Artemis and EGFP in HEK-293T and HCT116 cells transiently transfected with constructs -1 or -2. **(C)** Indirect immunofluorescence of Artemis in (i) HEK-293T and (ii-iii) HCT116 cells transiently transfected with construct-2.

A

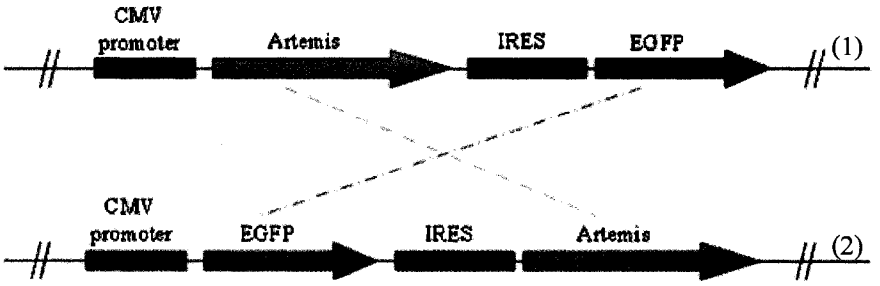
CMV promoter
Artemis
IRES
EGFP
(1)
CMV promoter
EGFP
IRES
Artemis
(2)

B

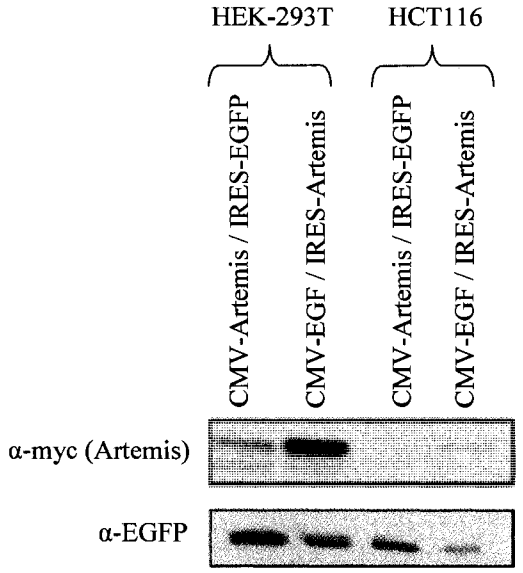
HEK-293T
HCT116
CMV-Artemis / IRES-EGFP
CMV-EGF / IRES-Artemis
CMV-Artemis / IRES-EGFP
CMV-EGF / IRES-Artemis
α-myc (Artemis)
α-EGFP

C

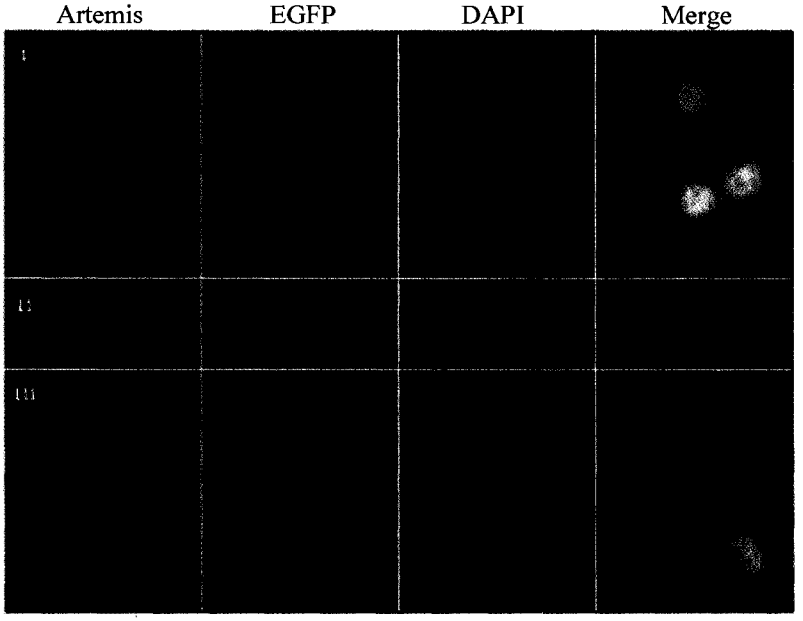
Artemis
EGFP
DAPI
Merge

cell lines, including the "non-permissive" HCT116 cells, Artemis expression was visible when translated in a non-cap-dependent manner. This effect, however, was not specific to Artemis, as EGFP protein levels were highest subsequent to IRES-mediated translation. Indirect immunofluorescence analysis of HEK-293T and HCT116 cells lines transiently transfected with this new bicistronic construct showed the unusual subcellular localization of Artemis in HCT116 cells, but not HEK-293T cells following IRES-mediated translation. Furthermore, within the same population of HCT116 cells, the observed mislocalization of Artemis was inconsistent; at times Artemis appeared to be excluded from the nucleus (Figure 19C; ii), where as in other instances protein distribution seem pan-cellular with slight nuclear enrichment (Figure 19C; iii). Additionally, none of the cells examined via indirect immunofluorescence had nuclear-only Artemis expression.

The results obtained thus far in examining the regulation of ectopic Artemis expression are difficult to draw definitive conclusions from, as many of these are negative in nature. At this point, it was decided that continued efforts to determine the regulation of ectopic Artemis expression would not be pursued. Instead, a new direction was followed, wherein a novel tandem affinity purification system would be established within our laboratory. This system would then be used to identify Oct-1 interacting factors with potential regulatory significance.

Section III: Identification of Octamer-binding transcription factor-1 interactors

The phosphorylation of Oct-1 by DNA-PKcs appears to be required for the contribution of Oct-1 to cell survival post-DNA damage (58). By utilizing a modified TAP (tandem affinity purification) method, the interaction of Oct-1 with binding partners can be

explored. The differential interactions between wild-type Oct-1 and phosphorylation defective Oct-1 mutants with cellular factors both in the presence and absence of DNA damage may identify interactors with potential regulatory significance.

Selecting a suitable cell line

Oct-1 is known to exhibit increased stabilization and hyperphosphorylation subsequent to DNA damage. In order to identify Oct-1 interactors with potential regulatory significance, a DNA damaging agent that results in the Oct-1 DNA damage phenotype must be identified. Of three cell lines examined (MCF-7, HeLa, and HCT116), HCT116 was chosen as these cells displayed the most consistent stabilization of Oct-1 protein following treatment with DNA damaging agents (Figure 20).

GS-TAP-tagged Oct-1 (NTAP-Oct-1)

Traditional TAP-tags consist of two copies of the IgG binding domain of protein A from *Staphylococcus aureus*, the cleavage recognition site of the tobacco etch virus (TEV), and a calmodulin-binding peptide (223, 224). A modified TAP-tag (GS-TAP) was used in this approach, as it has been shown to efficiently purify protein complexes at an order of magnitude higher than original TAP (225). The modified GS-TAP tag consists of two copies of the IgG binding domain of protein G from *Streptococcus sp.*, which displays a slightly higher affinity for a broader range of Igs from different subclass and species (225). This is followed by a TEV protease cleavage recognition site, and a streptavidin-binding peptide (SBP). SBP is used as it binds streptavidin with high affinity ($\sim 2 \times 10^{-9}$ M) and can be

Figure 20. Oct-1 is stabilized in HCT116 cells following treatment with DNA damaging agents that result in the accumulation of DNA-DSBs. HCT116 cells were treated with bleomycin (25 μg/ml), zeocin (100 μg/ml), or etoposide (25 mM) for 2 hours at 37°C. Cells were allowed to recover in fresh media for 2 hours post-damage, after which they were harvested. Lysates were resolved via SDS-PAGE, and probed for Oct-1 protein. **(A)** Oct-1 levels were first normalized to total protein (via Ponceau staining), then to undamaged Oct-1 (control). **(B)** Raw data generated by the GeneTools application (Syngene) for band quantification of Oct-1 levels. For each treatment, the average fold increase of Oct-1 levels (relative to undamaged Oct-1) and standard deviation of these changes are also shown.

A

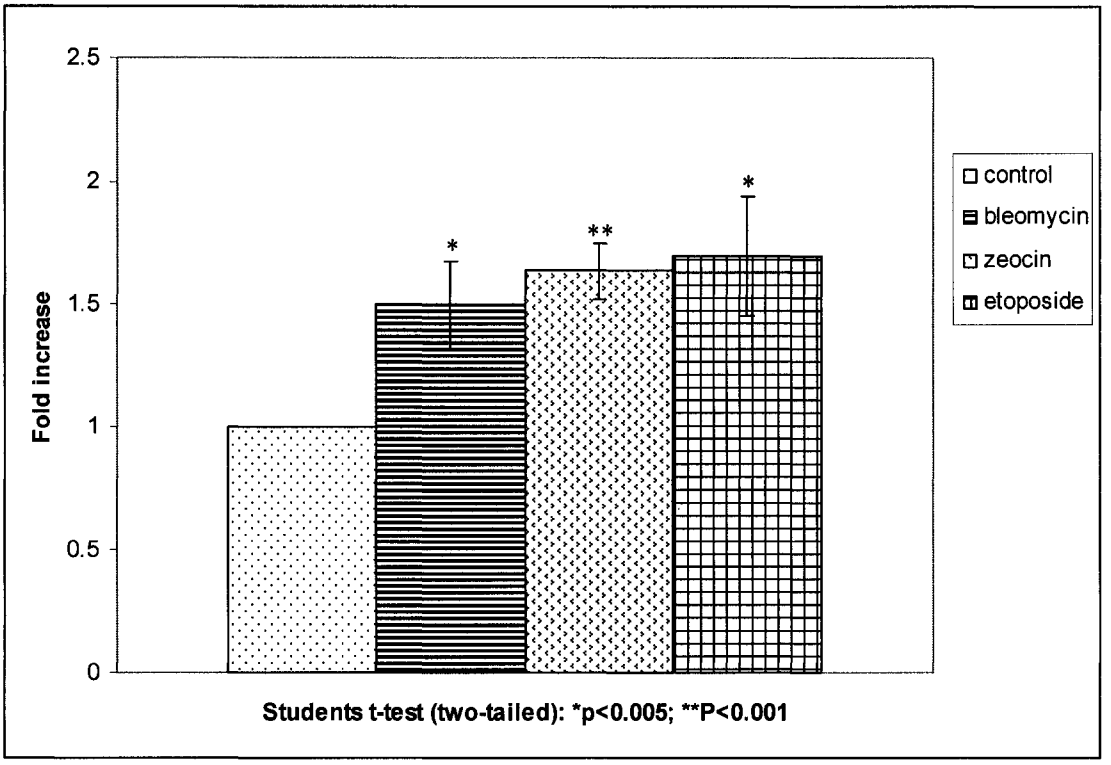

B

	Fold increase			Average	Standard deviation
	n = 1	n = 2	n = 3		
Control	1	1	1	1	0
Bleomycin	1.515738	1.660148	1.304732	1.493539	0.178745
Zeocin	1.672565	1.508924	1.731788	1.637759	0.115437
Etoposide	1.967334	1.635001	1.498752	1.700362	0.241032

specifically eluted by biotin (226). Additionally, the GS-TAP expression vector (pCeMM) is retrovirus-based, and can therefore be used to rapidly generate cell lines stably expressing the GS- TAP tagged protein. For Oct-1 TAP, the GS-TAP tag was generated as an N-terminal fusion protein (NTAP-Oct-1).

Stable expression of NTAP-Oct-1 in HCT116 cells (pCeMM)

Phoenix-293T cells transiently transfected with pCeMM-NTAP-Oct-1 retroviral vectors were used to generate viruses for the infection of HCT116 cells. As pCeMM does not contain an antibiotic resistance marker, selection of stably-expressing cells relies on the co-expression of EGFP from an IRES. Cells fluorescing green can be enriched from a mixed population via FACS (fluorescence activated cell sorting). Following infection, HCT116 cells were passaged for 1 week, after which green fluorescence was inspected via fluorescence microscopy. Unexpectedly, although green fluorescence was observed in the Phoenix-293T packaging cell line, it was not visible in the HCT116 cells. This may be attributed to variations in the cellular concentration of non-canonical translation factors, which are known to influence IRES activity in different cell lines (226b). As stably-expressing cells could not be selected from within the mixed population of HCT116 cells, western analysis and indirect immunofluorescence were used to verify the expression of NTAP-Oct-1 (Figure 21). Following staining with an α-Oct-1 primary antibody, low-level endogenous Oct-1 was visible in the nucleus of control and stable HCT116 cells. Conversely, HCT116 cells stably expressing NTAP-Oct-1 showed intense nuclear Oct-1 staining. Immunofluorescence identified approximately 20% of cells stably expressing

Figure 21. HCT116 cells stably expressing pCeMM-NTAP-Oct-1. (A) Indirect immunofluorescence against Oct-1 detects diffuse nuclear staining in all nuclei (endogenous Oct-1; upper and lower panels), and intense nuclear staining in the nuclei of the HCT116 stable cell line (over-expressed NTAP-Oct1; upper panels). **(B)** Western analysis showing the stable expression of NTAP-Oct1 in HCT116 cells (lane 1), and the endogenous expression of Oct-1 in stable and control HCT116 cells (lanes 1 and 2, respectively).

A

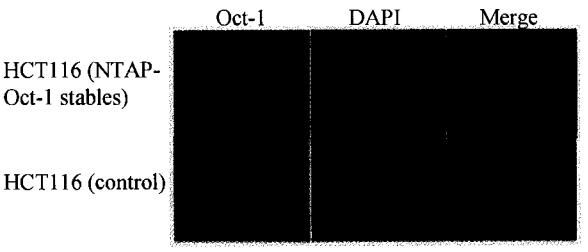
Oct-1
DAPI
Merge
HCT116 (NTAP-Oct-1 stables)
HCT116 (control)

B

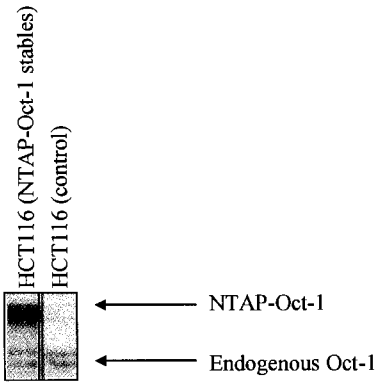
HCT116 (NTAP-Oct-1 stables)
HCT116 (control)
NTAP-Oct-1
Endogenous Oct-1

higher levels of Oct-1, presumably corresponding to NTAP-Oct-1. Western blot analysis of the mixed population indicated an approximate 5-fold overexpression of NTAP-Oct-1 levels over endogenous Oct-1. This suggests that the per-cell expression of NTAP-Oct-1 is in the range of 16-fold higher than the endogenous Oct-1 protein.

Stable expression of NTAP-Oct-1 in HCT116 cells (pBABE)

The stable expression of NTAP-Oct-1 in HCT116 cells is problematic in two senses. Firstly, the expression level of the bait protein (NTAP-Oct-1) is very high. This increases the chances of co-purifying non-specific interactors during the TAP method. More importantly, the overexpressed NTAP-Oct-1 proteins may not be sensitive to the levels of DNA damage initially defined for the observed endogenous Oct-1 damage phenotype. In addition, there is no selective pressure on the stably-expressing HCT116 cells therefore, NTAP-Oct-1 expression may be lost over time. To circumvent these problems, a new strategy was employed in which the entire GS-NTAP cassette (+/- Oct-1) would be transferred to a different retroviral backbone. The new vector, pBABE, was chosen because as it possesses a puromycin resistance gene suitable for selection of stably-expressing cells, and because the expression of NTAP-Oct-1 would be driven by a weaker promoter (the 5'LTR of the Maloney Murine Leukemia virus; MMLV), as opposed to the CMV promoter present in the pCeMM backbone.

Following the sub-cloning of NTAP-Oct-1 into the pBABE backbone, viruses encoding this new TAP vector were generated in the Phoenix-293T packaging cell line. Subsequent to infection, HCT116 cells stably expressing the TAP-tagged Oct-1 were selected via puromycin treatment. Non-infected, control HCT116 cells died after

approximately 3-4 days of puromycin treatment. As the resulting HCT116 cells represent a uniform population stably expressing NTAP-Oct-1, western blot analysis was used to detect the expression of the bait protein. Figure 22 shows the stable expression of both pBABE- and pCeMM- NTAP-Oct-1, as well as endogenous Oct-1 in HCT116. From this analysis, it is evident that although the expression of pBABE-NTAP-Oct-1 is significantly lower than that of pCeMM-NTAP-Oct-1 on a per cell basis, it is still several fold higher than the endogenous Oct-1.

Tandem affinity purification of NTAP-Oct-1 (pCeMM)

During the generation of the new NTAP-Oct-1 construct (pBABE), tandem affinity purification was used to purify NTAP-Oct-1 from HCT116 cells transiently transfected with pCeMM-NTAP-Oct-1. Before the entire TAP procedure was conducted, a one-step purification of NTAP-Oct-1 from the cell lysate was conducted in order to determine the efficiency of the TEV-cleavage reaction, and the recovery of the bait protein. In this experiment, cell lysates were incubated for 2 hours at 4°C with equal amounts of either the IgG resin or GST resin (control). Following incubation, both resins were collected via centrifugation and washed in binding buffer. The resins were then incubated with equal amounts of the AcTEV protease (Invitrogen) for 16 hours at 4°C. Following TEV cleavage the supernatants were collected and the resins were washed and boiled in SDS sample buffer. Figure 23 shows the efficient purification NTAP-Oct-1 from the cell lysate on the IgG, but not the GST resin. Additionally, although TEV cleavage of NTAP-Oct-1 from the IgG resin appears to be efficient, recovery of the cleavage product from the IgG resin appears incomplete. Although recovery of the bait protein was low following TEV cleavage, it was

Figure 22. Expression of TAP-tagged Oct-1 in HCT116 cells. Lane 1 contains whole cell extract from MEF Oct1$^{-/-}$ cells. Lanes 2, 3, and 4 contain lysates from HCT116 cells expressing pCeMM-NTAP-Oct1 (transiently transfection), pBABE-NTAP-Oct1 (transient transfection), and pBABE-NTAP-Oct1 (stable expression).

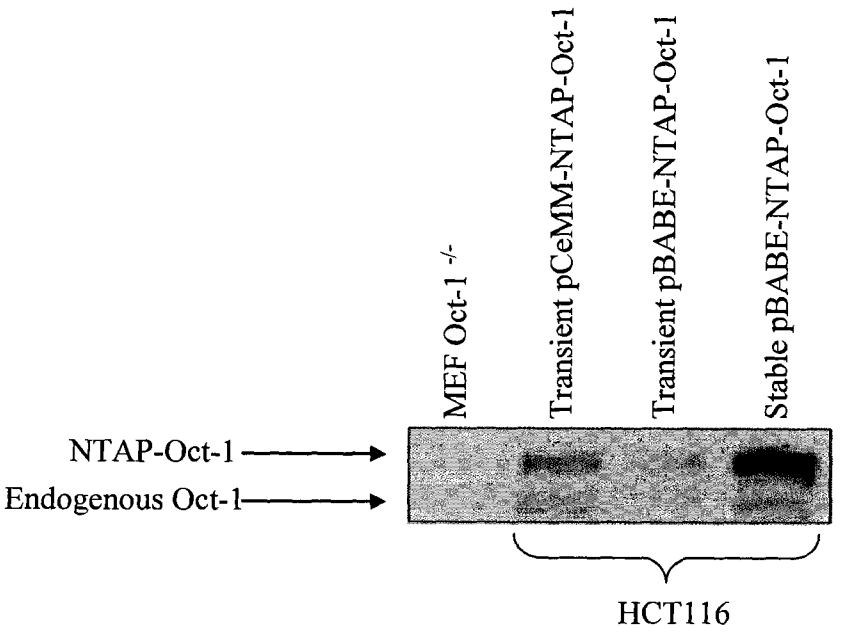
MEF Oct-1 -/-
Transient pCeMM-NTAP-Oct-1
Transient pBABE-NTAP-Oct-1
Stable pBABE-NTAP-Oct-1
NTAP-Oct-1
Endogenous Oct-1
HCT116

thought that if the amount of starting material was appropriately scaled up, a sufficient amount of the TEV-cleaved bait could be recovered for use in the two-step TAP procedure. TAP was conducted on cell lysates from HCT116 cells transiently transfected with pCeMM-NTAP-Oct-1 as well as control, non-transfected cells. Figure 24 shows the purification of an unknown factor specific to the NTAP-Oct-1 lysate (compare lane 5 to 10). This band, which appears to be approximately 55kDa was excised from the silver-stained gel and sent for identification via MALDI-TOF (matrix-assisted laser desorption time of flight) mass spectrometry (Figure 25). Subsequent analysis of the resulting mass spectrum revealed this factor to be human keratin.

Tandem affinity purification of NTAP-Oct-1 (pBABE)

A second round of TAP was employed with the newly generated pBABE-NTAP-Oct-1 stables. In addition to identifying basal Oct-1 interactors, TAP was used to identify factors specific to the DNA-damage response. HCT116 cells either (i) stably expressing NTAP-Oct-1 (pBABE), (ii) transiently expressing the GS-TAP tag alone, or (iii) uninfected were either mock treated (no damage) or treated for 1 hour with the DSB-inducing drug bleomycin. Following DNA damage, the media was replaced, and cells were allowed to recover for 2 hours. Following the 2 hour recovery, the cells were harvested and tandem affinity purification of NTAP-Oct-1 was conducted. Figure 26 shows the purification of four factors specific to the NTAP-Oct-1 (no damage) sample. These factors, which are approximately 100kDa, 95kDa, 65kDa, and 55kDa were excised from the silver-stained gel and sent for identification via MALDI-TOF mass spectrometry (Figure 27). Subsequent analysis of the resulting mass spectra revealed the

Figure 23. First-step purification and TEV-cleavage of NTAP-Oct-1 from HCT116 cells. Lysates from HCT116 cells transiently transfected with pCeMM-NTAP-Oct-1 were incubated with equal amounts of IgG or GST resin for 2 hours at 4°C. TEV-cleavage of NTAP-Oct-1 was allowed to proceed overnight at 4°C, after which the supernatants were collected and the resins boiled in SDS sample buffer. NTAP-Oct-1 and endogenous Oct-1 can both be detected in lane 1 (10% input). Lanes 2 and 3 show the relative amounts of NTAP-Oct-1 remaining unbound to the IgG and GST resins (respectively) following a 2 hour incubation with each resin (10% SN1 IgG or GST). Lane 4 shows the relative amount of full-length NTAP-Oct-1 remaining bound to the IgG resin post TEV-cleavage (efficiency of the cleavage reaction), as well as TEV-cleaved NTAP-Oct-1 remaining associated with the IgG resin post-cleavage (recovery). Although TEV cleavage of NTAP-Oct-1 appears to be efficient, the resulting cleavage product has a high affinity for the IgG resin, and thus reduces the recovery of the bait protein.

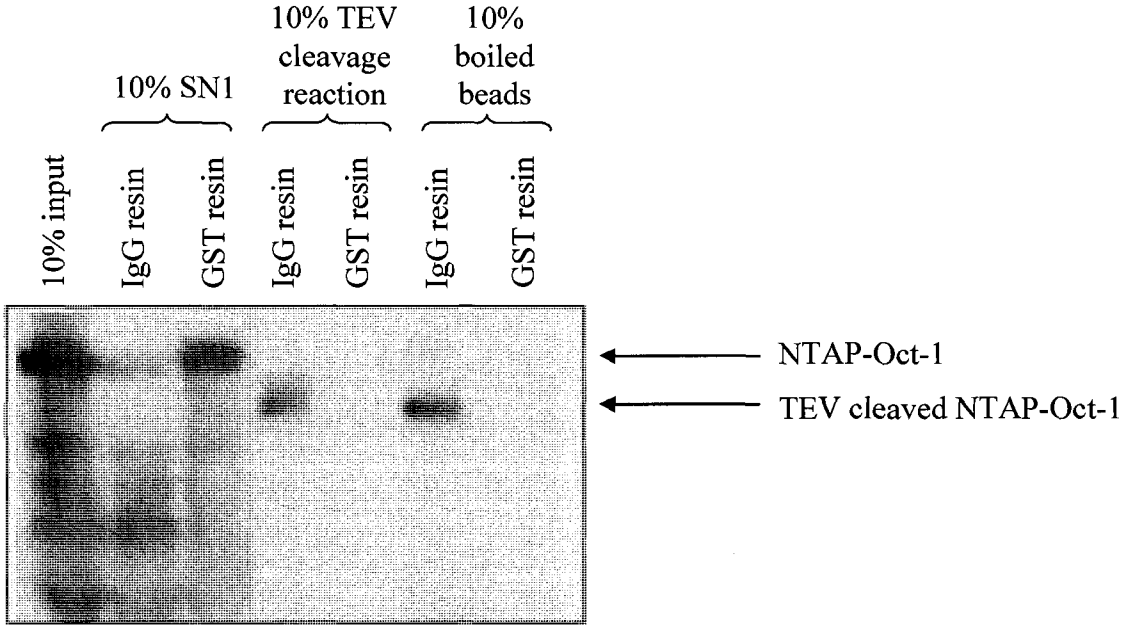
10% input
10% SN1
IgG resin
GST resin
10% TEV cleavage reaction
IgG resin
GST resin
10% boiled beads
IgG resin
GST resin
NTAP-Oct-1
TEV cleaved NTAP-Oct-1

Figure 24. Tandem affinity purification of transiently expressed NTAP-Oct-1 (pCeMM) from HCT116 cells. TAP analysis of lysates from HCT116 cells transiently expressing pCeMM-NTAP-Oct-1 (left side of gel/immunoblot) and control HCT116 cells (right side of gel/immunoblot). Silver stained gel shows an approximately 55kDa factor present in the NTAP-Oct-1 final eluate, yet absent from the control final eluate. The immunoblot below is against Oct-1, and shows the cleavage and recovery of NTAP-Oct-1 following an overnight TEV cleavage at 4°C.

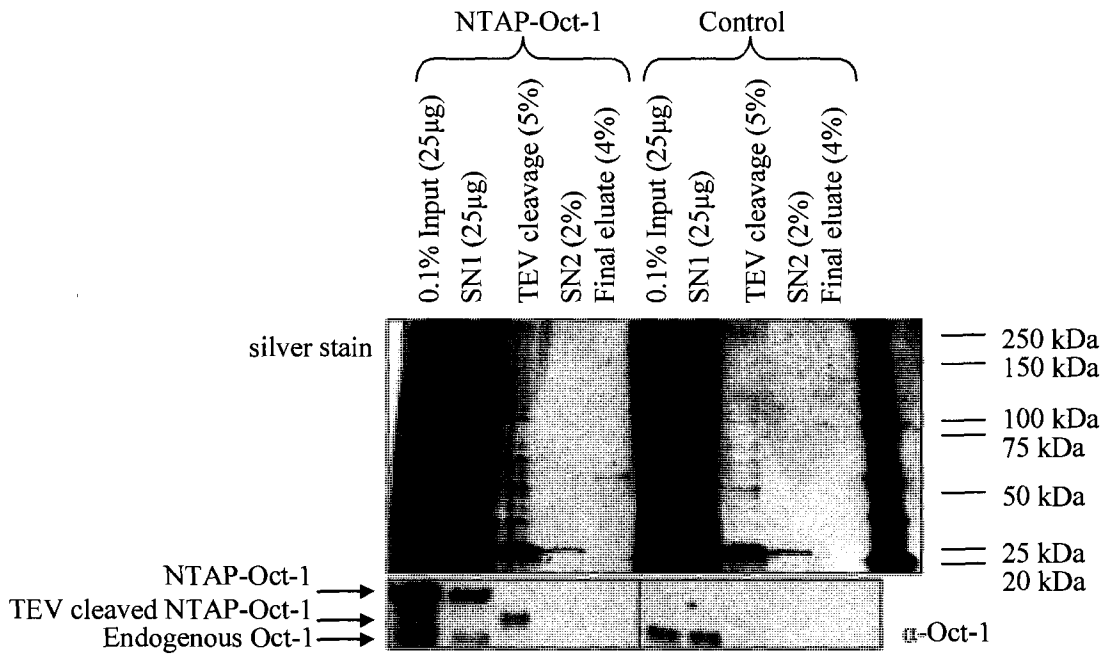
NTAP-Oct-1
Control
0.1% Input (25µg)
SN1 (25µg)
TEV cleavage (5%)
SN2 (2%)
Final eluate (4%)
0.1% Input (25µg)
SN1 (25µg)
TEV cleavage (5%)
SN2 (2%)
Final eluate (4%)
silver stain
250 kDa
150 kDa
100 kDa
75 kDa
50 kDa
25 kDa
20 kDa
NTAP-Oct-1
TEV cleaved NTAP-Oct-1
Endogenous Oct-1
-Oct-1

Figure 25. Mass spectrum of a potential NTAP-Oct-1 interactor. (A) An unknown factor migrating at approximately 55kDa was purified from lysates prepared from HCT116 cells transiently expressing pCeMM-NTAP-Oct-1 using the TAP method. **(B)** Parallel analysis of a control segment of SDS-PAGE gel excised at a migration distance corresponding to approximately 55kDa.

A

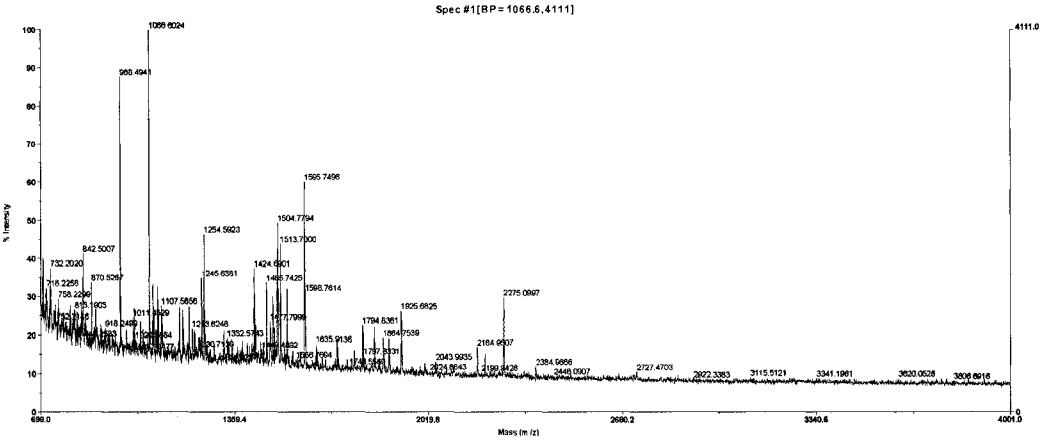
Spec #1[BP = 1066.6, 4111]
% Intensity
Mass (m/z)
698.0
1359.4
2019.8
2680.2
3340.6
4001.0
1066.6024
4111.0
966.4941
1595.7496
1504.7794
1513.7000
1254.5923
842.5007
732.2020
1424.6901
1245.6391
870.5267
1107.5856
1598.7614
1825.6825
2275.0897
1794.8361
1864.7538
1635.9136
2184.9507
2384.9866
2727.4703
2922.3383
3115.5121
3341.1961
3620.0528

B

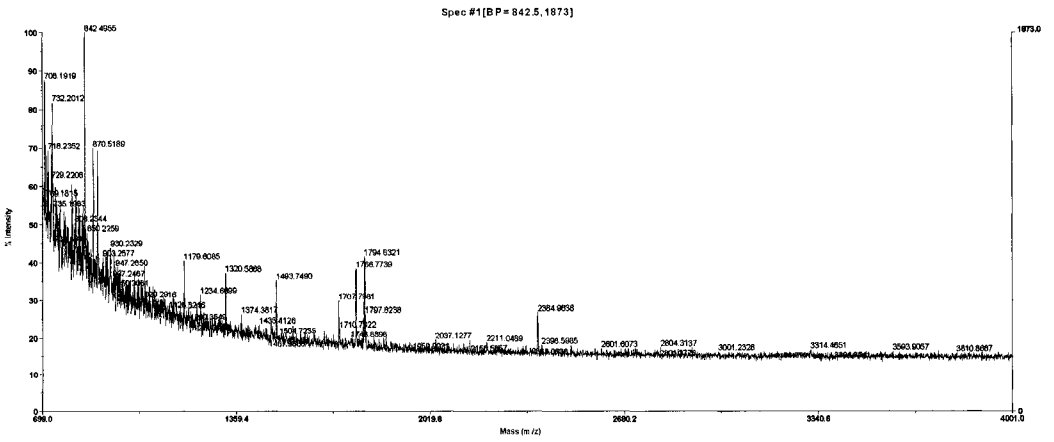
Spec #1[BP = 842.5, 1873]
% Intensity
Mass (m/z)
698.0
1359.4
2019.8
2680.2
3340.6
4001.0
842.4955
1873.0
708.1919
732.2012
718.2352
870.5189
1179.6085
1320.5868
1493.7490
1794.8321
1798.7739
1254.6899
1374.3817
1797.8238
2384.9858
2097.1277
2211.0499
2396.5995
2801.6073
2804.3137
3001.2328
3314.4651
3593.9057
3810.8867

Figure 26. Tandem affinity purification of stably expressed NTAP-Oct-1 (pBABE) from HCT116 cells (+/- DNA damage). TAP analysis of lysates from HCT116 cells **(A)** transiently expressing the NTAP-TAG, **(B)** uninfected/non-transfected control, and **(C)** stably expressing NTAP-Oct-1 (pBABE). Samples A, B and C were either mock treated or treated with 25μg/ml bleomycin for 1 hour at 37°C. Lysates were prepared at a recovery time of 2 hours post-treatment. Lane numbers are as follows: (1) 0.1% input, (2) 2.5% TEV cleavage, (3) 6.7% SN2, and (4) 8.3% final eluate. Gels are silver stained to detect the presences of potential interactors. Below each silver stained gel, an immunoblot against Oct-1 detects the presence of NTAP-Oct, TEV-cleaved NTAP-Oct-1 and endogenous Oct-1 in the samples. In Sample C, the silver stained gels shows the presence of four factors (100kDa, 97kDa, 65kDa, and 55kDa) present in the NTAP-Oct-1 final eluate (no DNA damage).

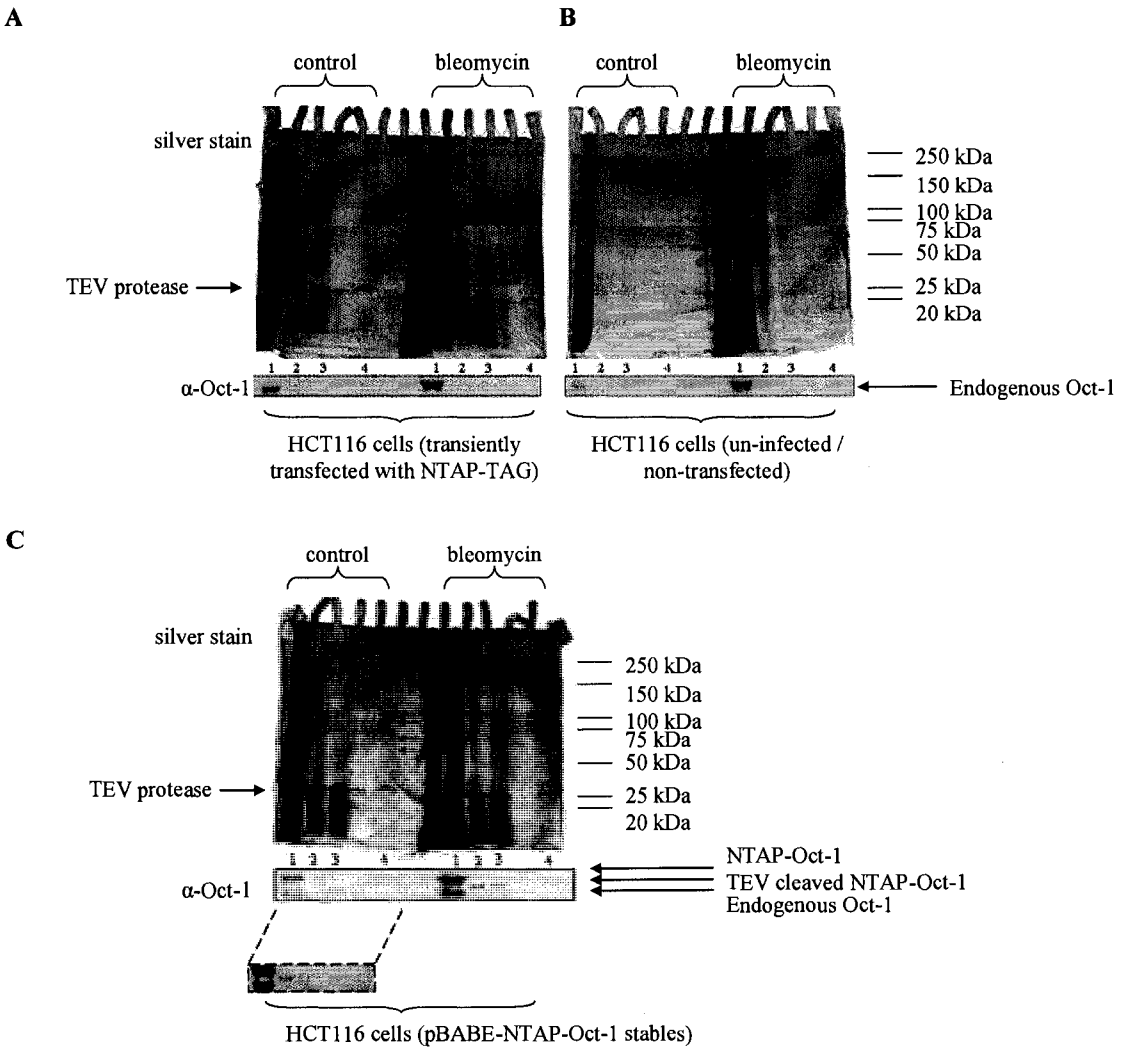
A
B
control
bleomycin
control
bleomycin
silver stain
TEV protease
250 kDa
150 kDa
100 kDa
75 kDa
50 kDa
25 kDa
20 kDa
1 2 3 4 1 2 3 4
1 2 3 4 1 2 3 4
α-Oct-1
Endogenous Oct-1
HCT116 cells (transiently transfected with NTAP-TAG)
HCT116 cells (un-infected / non-transfected)
C
control
bleomycin
silver stain
TEV protease
250 kDa
150 kDa
100 kDa
75 kDa
50 kDa
25 kDa
20 kDa
α-Oct-1
NTAP-Oct-1
TEV cleaved NTAP-Oct-1
Endogenous Oct-1
HCT116 cells (pBABE-NTAP-Oct-1 stables)

Figure 27. Mass spectra of four potential NTAP-Oct-1 interactors. Four factors were purified from HCT116 cells stably expressing pBABE-NTAP-Oct-1 using the TAP method. In-gel tryptic digest of each sample, followed by MALDI-TOF mass spectrometry yielded each spectrum. (i) Sample 1 is approximately 100kDa, (ii) sample 2 is approximately 97kDa, (iii) sample 3 is approximately 65kDa, and (iv) sample 4 is approximately 55kDa.

i

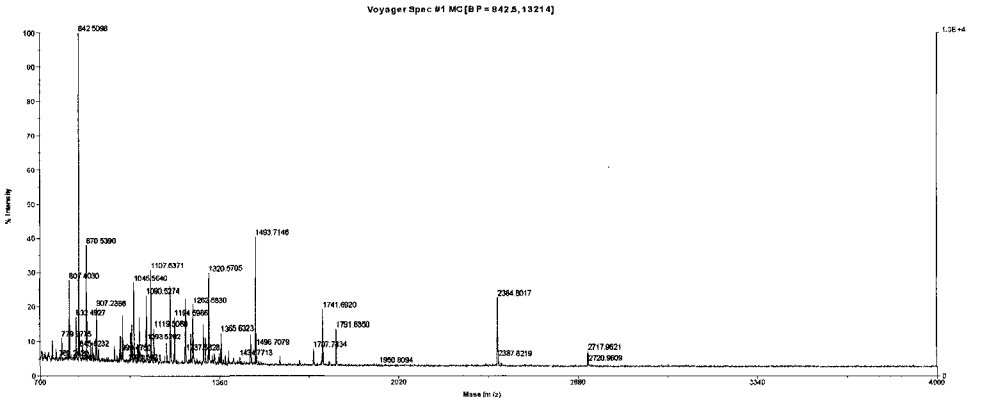
Voyager Spec #1 MC [BP = 842.5, 13214]
842.5098
670.5390
907.4030
1107.6371
1045.5640
1320.5705
1493.7146
1090.5374
1252.6830
907.2386
832.4527
1184.5998
1741.6920
1791.6950
1365.6323
1496.7079
1707.7934
1450.7713
2364.8017
2387.8219
2717.9621
2720.9609
1950.8094
% Intensity
Mass (m/z)

ii

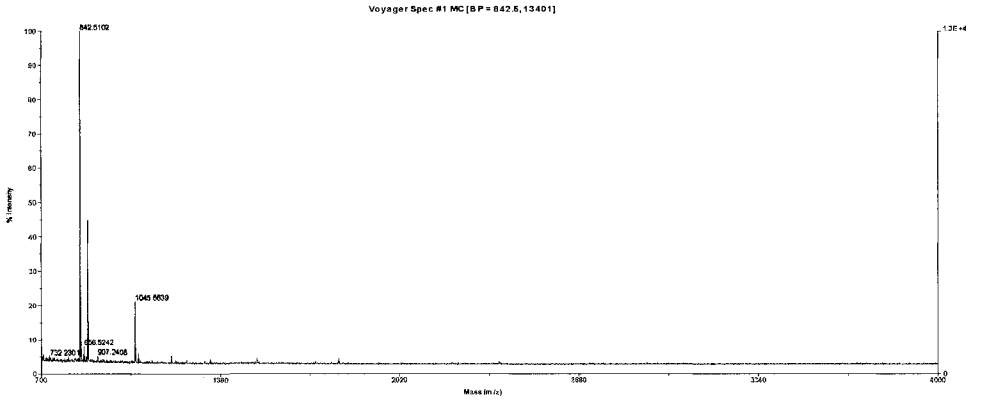
Voyager Spec #1 MC [BP = 842.5, 13401]
842.5102
1045.5639
856.5242
907.2408
732.2901
% Intensity
Mass (m/z)

iii

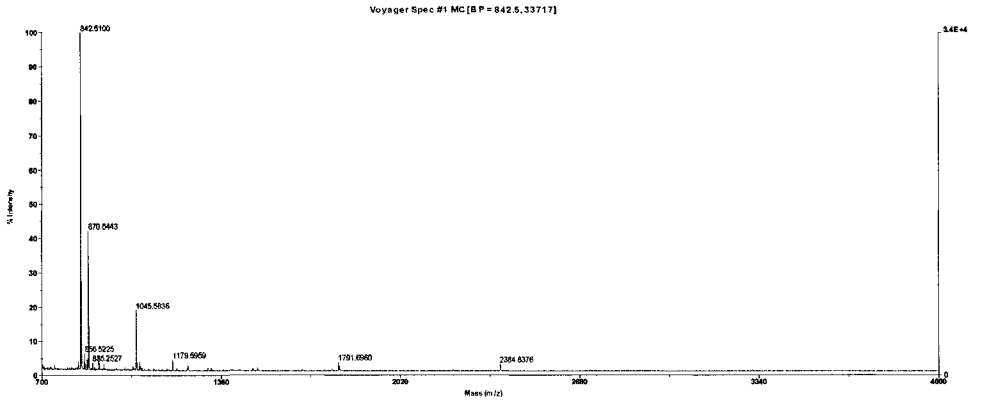
Voyager Spec #1 MC [BP = 842.5, 33717]
842.5100
870.5443
1045.5636
856.5225
885.2527
1179.5959
1791.6960
2364.8376
% Intensity
Mass (m/z)

iv

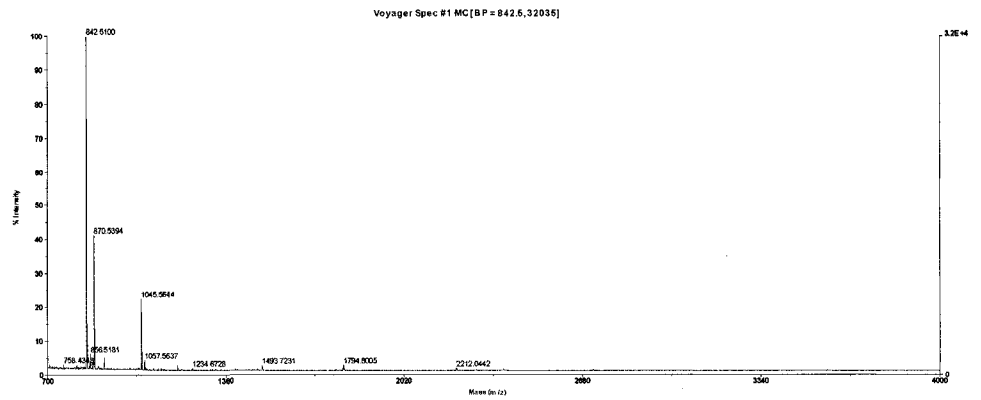
Voyager Spec #1 MC [BP = 842.5, 32035]
842.5100
870.5394
1045.5644
856.5181
1057.5637
1234.6728
1493.7231
1794.8005
2212.0442
% Intensity
Mass (m/z)

identity of the 100kDa unknown factor to be zinc finger protein 95. Unfortunately, the results of the remaining three spectra were inconclusive.

Discussion

Section I: MBP-CoreRag-1 / Ku binding

The independent roles of Rag-1 and Ku70 are well established within the process of V(D)J recombination, where Rag-1 is involved upstream of Ku70 as a DNA cleavage factor, and Ku70 is involved downstream as an NHEJ factor. The direct interaction between Rag-1 and Ku70 observed within our laboratory may be indicative of a novel upstream role for Ku70 within V(D)J recombination. Although literature does not provide evidence for the direct association of Ku70 with Rag-1, there is significant biochemical and genetic data that indirectly support the direct interaction of components of the NHEJ machinery with the Rag1/2 complex. For example, numerous laboratories have observed that the Rag-1/2 proteins are able to guide the repair of DNA DSBs generated during V(D)J recombination to the NHEJ pathway and away from alternative repair pathways (86, 227-230). Additionally, *in vitro* cleavage assays have been used to describe an increased fidelity of Rag-1/2 mediated cleavage with respect to the 12/23 rule in the presence of the Ku heterodimer and DNA-PKcs (231). Interestingly, Ku has been shown to associate with other recombinases active in vertebrate organisms, such as the *Sleeping Beauty* transposase (232). There is one physiological situation documented in which Rag-1 and Ku70 spatially colocalize, and that is within the post-synaptic complex (233). Studies have described the presence of Rag-1, Rag-2, DNA-PKcs, and Ku70/80

together within the post-synaptic complex generated subsequent to RSS cleavage (233, 234). It is tempting to conjecture that the specific binding of Rag-1 with Ku70 could be responsible for recruiting the NHEJ machinery to this complex, thus providing a physical link between the cleavage step of V(D)J recombination and the initiation of the subsequent NHEJ pathway. In accordance with this hypothesis, previous groups have described DNA-PKcs-independent roles of Ku within V(D)J recombination (235). In these cases, cells lacking DNA-PKcs fail to generate coding joints, whereas signal joints are generated at near normal levels (236). Conversely, Ku-defective cells display decreased levels and altered quality of both signal and coding joints (234, 237). It is speculated that this differential phenotype may be attributed to the ability of Ku to displace the Rag1/2 post-synaptic complex from the signal ends, thus allowing for the ligation of the two DNA ends (238). A recent study by Raval *et al* (86) has provided the first published biochemical evidence for an association between Rag-1 and Ku70/80. In this study, Raval's group showed the ability of antibodies against Rag-1 and Ku70 to supershift an RSS-containing protein complex in EMSA (electrophoretic mobility shift assay) experiments. This group found that the association of Ku70/80 with full-length Rag-1 (when co-expressed with coreRag-2), and with coreRag-1 (when co-expressed with full-length Rag-2). Additionally, based on this study, the interaction of the Ku heterodimer with coreRag-1/full-length Rag-2, but not full-length Rag1-/core Rag-2, appears to be DNA-dependent. The results observed by Raval's group are contradictory to those obtained within our laboratory, in the sense that, unlike Raval, we have consistently been able to show the direct, DNA-independent interaction between coreRag-1 and Ku70. By using EMSA, this work fails to show a direct interaction

between Rag-1 and the Ku heterodimer, and cannot rule out the possibility of an indirect interaction via co-purifying factors. Additionally, the examiners use Rag-1/2 heterodimers in their experiments, whereas our laboratory only uses MBP-coreRag-1 peptides in association experiments. Consequently, the physical interaction of the two Rag proteins may reveal a different epitope for Ku binding than the one presented on the surface of Rag-1 alone.

Before the consequences of Rag-1/Ku70 binding could be determined, the Ku70-binding domain of Rag-1 must first be defined and refined. As a cell-based V(D)J recombination assay would be employed to assess the contribution of Ku70/Rag-1 binding, and since the putative interaction domain is contained within the catalytic core of Rag-1, it was necessary to ensure that disruption of this interaction did not interfere with the recombinase activity of Rag-1. Three deletion constructs were generated in the initial refinement of the Ku70-binding domain (Figure 9). The first deletion construct generated removed the entire "Ku70 binding domain" previously identified (MBP-coreRag-1Δ660-763). The next two deletions further subdivided this region into two smaller deletions (MBP-coreRag-1Δ600-720 and Δ721-763). These deletions were chosen on the basis that an entire structural domain, zinc finger B (ZFB; aa727-750), is contained within aa660-763. Zinc fingers are classically known to mediate protein-DNA interactions (239-240), yet have also been described in bridging protein-protein interactions (218). Therefore, MBP-coreRag-1Δ660-720 was chosen to retain ZFB, whereas this domain is completely removed in MBP-coreRag-1Δ721-763. The expression and purification of these proteins was verified via SDS-PAGE followed by Coomassie blue staining (Figure 10).

Association assays were used to identify which MBP-coreRag-1 deletions were capable of binding Ku70. As both Rag-1 and Ku70 are known DNA-binding factors, ethidium bromide was included in all binding reactions to ensure DNA-independent interactions. Using a variety of salt and detergent concentrations, association assays revealed Ku70 binding between all MBP-coreRag-1 derivatives, wild-type MBP-coreRag-1, and MBP alone (Figures 11 and 12). As Ku70 binding was observed between the MBP negative control, it was clear that the interactions observed were non-specific. Many sources, including our laboratory, have established that the Ku heterodimer is a fairly "sticky" protein, in the sense that it can sustain non-specific interactions with cellular proteins and purification resins under reasonably stringent conditions (225, 241). To rule out the possibility that Ku was non-specifically interacting with the TALON^{TM} resin, association assays were performed with the Ku heterodimer immunoprecipitated from Jurkat nuclear T cell extracts, and TALON^{TM}-eluted MBP-coreRag-1 (wt and deletions) and MBP, alone. However, non-specific binding between Ku70 and all MBP-coreRag-1 derivatives, as well as MBP alone, were still observed (Figure 13).

As attempts to eliminate non-specific interactions proved insufficient, a commercially purified source of Ku70/80 was purchased for use in the subsequent association experiments. This route was chosen in lieu of further increasing the salt concentrations of the binding reactions, as it has been proposed that Rag1/2 protein interactions with Ku70 or Ku80 could be unstable in buffers that contain high concentrations of monovalent salt (86). Ku70/80 purified from Baculovirus-infected Sf9 insect cells (Baculo-Ku) is guaranteed to be greater than 90% pure, and is capable of complementing immunodepleted cell free DNA repair assays (220). Association assays

using Baculo-Ku proved sufficient to eliminate non-specific interactions, as binding with TALON^{TM}-bound MBP was not observed (Figure 14). Unfortunately, all TALON^{TM}-bound MBP-coreRag-1 derivatives were capable of binding Baculo-Ku. This observation led to the conclusion that the region of Rag-1 spanning amino acids 660-763 is sufficient, but not required for binding Ku70.

Stoichiometric analysis indicating the molecular ratio of Ku70 binding to Rag-1 would provide better insight into the nature of this interaction. The amount of Ku70 molecules associated with each Rag-1 molecule could provide clues as to why Ku70 binding is still observed in the absence of the previously-identified "Ku-binding domain" (aa660-763). In this sense, one would be able to differentiate between a single molecule of Rag-1 binding multiple molecules of Ku70 or a single molecule of Rag-1 binding a single molecule of Ku70. In the former scenario, multiple independent Ku70 binding sites would be present on Rag-1. Therefore, the removal of aa660-763 would eliminate the binding of only one Ku70 molecule to Rag-1, a phenotype masked by the additional Ku70 molecules remaining bound to Rag-1. Conversely, the latter scenario would suggest that within the context of a properly folded protein, multiple regions of Rag-1 cooperate to bind a single Ku70 molecule. This may indicate that the contribution of aa660-763 in this cooperative binding is minimal in the overall interaction of Rag-1 with Ku70. The stoichiometry of Rag-1/Ku70 binding might be difficult to determine, as Raval's group indicated that this interaction is not stoichiometric, and is likely due to the labile nature of their association.

Section II: Examining the regulation of ectopic Artemis expression

The Artemis nuclease was initially characterized in 2001 as molecularly deficient in individuals suffering from RS-SCID (radiosensitive severe-combined immunodeficiency) (217). Since its initial characterization, little information concerning the regulation of its expression or activity has been described. Endogenously, Artemis is ubiquitously expressed, although at considerably low levels (217). Endogenous Artemis expression also appears to be highly sensitive to nucleotide and/or amino acid changes. In 2002, Li *et al* characterized a founder mutation leading to A-SCID (Athabascan severe-combined immunodeficiency) resulting from a single-nucleotide substitution within exon 8 (150). This mutation (TAC→TAA) results in the substitution of a tyrosine residue with a premature stop codon. With this type of mutation, one may expect to observe decreased Artemis at the protein level, as the truncated, and possibly misfolded, protein may be targeted for degradation. Instead, nearly complete abrogation of Artemis at the mRNA level is observed (150). In another example, Ege *et al* described a hypomorphic Artemis allele within an individual suffering from Omenn Syndrome (151). Genetic analysis of the affected individual indicated an M1T mutation on one allele, resulting in a protein translated from the second AUG, and therefore missing the first seven amino acids, and a H35D on the other allele, resulting in a catalytically-dead nuclease. In this case, similar levels of Artemis transcript were described between the individual suffering from Omenn Syndrome and a healthy individual, whereas Artemis protein levels in the affected individual were significantly reduced. These two examples illustrate the heightened sensitivity of Artemis to changes within its primary sequence,

and show how relatively small mutations (single nucleotide or amino acid substitutions), can significantly reduce Artemis expression at both the mRNA and protein levels.

Within our laboratory, we have encountered extreme difficulty ectopically expressing Artemis, with the detection of the protein visible in only two cell lines (Figure 16). Previous studies have also described difficulties in ectopically expressing Artemis. Moshous *et al* observed that, although they were able to obtain high transient levels of Artemis expression, they were unsuccessful in deriving stable transfectants for use in IR complementation studies (217). They hypothesized that this may reflect a toxicity of long-term high level expression of Artemis in transfected fibroblasts; a characteristic previously observed upon the overexpression of other human and murine homologs of SNM1 (217). This phenotype may be a characteristic of this family of proteins, which appears to be in agreement with the physiological low level RNA expression of these genes (242). In accordance with this, Evans *et al* were unable to derive cells stably expressing Artemis protein (wt and mutant) (152). Hypothesizing that the tight regulation of Artemis was limiting its ectopic expression, a series of experiments were conducted to identify the level(s) at which Artemis was being regulated.

The transient transfection of a bicistronic pIRES-EGFP-Artemis construct into a range of different cell lines identified that Artemis could be ectopically expressed in only the HEK-293T and Cos-7 cell lines (Figure 16). EGFP expression was detected in all transfectants, indicating that the bicistronic Artemis/EGFP mRNA was being transcribed. The HEK-293T and HCT116 cell lines were chosen as the archetypal permissive and non-permissive cell lines, respectively, for subsequent experimentation. These were chosen on the basis that the HEK-293T cell line expresses both Artemis and EGFP well,

grows rapidly, is easily transfected, and does not appear to be negatively affected by the over-expression of Artemis over a 48 hour time span. The HCT116 cell line was used as the representative non-permissive cell line as these cells most closely parallel the HEK-293T cell line with respect to growth rate, ease of transfection and EGFP expression levels.

The detection of EGFP in the non-permissive cell lines indicates that the ectopic expression of Artemis is not being regulated at the level of transcription. However, in order to rule out the possibility of Artemis-specific mRNA degradation or processing, Northern blot analysis of total RNA extracted from HEK-293T and HCT116 cells transiently transfected with the bicistronic EGFP construct (+/- Artemis sequence) was conducted. In this experiment, both bicistronic transcripts (EGFP +/- Artemis) were detected in the HEK-293T cell line (Figure 17Aii). Interestingly, neither transcript was detected in the HCT116 cell line. This observation was contradictory to western blot and immunofluorescence data, where a strong EGFP signal could be consistently detected via both methods (refer to Figure16). As comparable 28S and 18S rRNA levels were observed between both cell lines, the absence of transcripts in the HCT116 cell line could not be attributed to poor quality or low yield total RNA extracted (Figure 17Ai). Under the conditions used during probe hybridization, the 18S rRNA band is visible as a background signal on both blots. This band co-migrates with the EGFP transcript and may be sufficient to interfere with a weak EGFP signal in the HCT116 samples (refer to Figure 17Aii; HEK-293T samples). To address this issue, RT-PCR of total RNA extracted from HEK-293T and HCT116 cells transiently transfected with the bicistronic EGFP constructs (+/- Artemis sequence) was conducted. In this experiment, both

transcripts (EGFP +/- Artemis) were detected in both cell lines, thus confirming that Artemis is not being selectively degraded at the mRNA level. Although this method confirms the transcription of ectopic Artemis in the non-permissive cell line, it does not address why the EGFP/Artemis transcript was not observed via Northern analysis. This discrepancy may be due to a lower rate of ectopic Artemis transcription in the HCT116 cells compared with to HEK-293T cells. Although similar levels of both transcripts were detected between the two cell lines via RT-PCR, this method is only semi-quantitative. To truly identify differences in transcriptional efficiency, QRT- (quantitative reverse transcription) PCR would need to be employed.

In many instances, the turnover rate of a protein greatly influences its activity and accumulation within a cell (243-246). Cellular proteins have diverse turnover half-lives, ranging from a few minutes, to hundreds of hours (247-249). To investigate whether or not Artemis is being selectively targeted for post-translational degradation, inhibition of two separate protein-degradation pathways, proteasomal-mediated and lysosomal-mediated protein degradation, was conducted. Post-translational degradation appears to be a good candidate in the regulation of the ectopic expression of Artemis, as sequence analysis indicates that approximately one third of Artemis' sequence is comprised of PEST residues (Appendix III). PEST-rich proteins often display shorter half-lives than other cellular proteins (250-252). Additionally, four potential PEST sequences (aa383-402, aa495-520, aa610-629, and aa634-663) were identified within the β-CASP and C-terminal domains of Artemis (253). MCF-7 cells were used as the non-permissive cell line during the protein degradation inhibition assays, as these cells over-express the insulin-like growth factor receptor 1 (IGFR1). IGFR1 has been shown to be selectively

targeted for lysosomal-mediated protein degradation; a process that can be blocked via pre-treatment of these cells with a neutralizing antibody against IGFR1 and chloroquine (221). In this sense, MCF-7 cells contain an internal control for the efficacy of the chloroquine-dependent inhibition of lysosomal-mediated protein degradation. To control for inhibition of proteasomal-mediated protein degradation, MCF-7 cells were also transiently transfected with myc-tagged GR; a steroid receptor whose proteasome-dependent degradation can be blocked via treatment of cells with MG132 (222). Although moderate stabilization of IGFR1 and myc-GR was observed subsequent to prolonged chloroquine and MG132 treatment, respectively, neither EGFP stabilization nor Artemis protein were detected (Figure 18), indicating that Artemis is not being selectively targeted for protein degradation by either of these two pathways.

The ectopic expression of Artemis does not appear to be regulated at the levels of transcription, selective post-transcriptional degradation, or post-translational proteasomal- or lysosomal-mediated protein degradation. To observe whether or not the mode of translation influences the ectopic expression of Artemis, a new bicistronic EGFP/Artemis construct was generated, in which EGFP would be translated in a cap-dependent manner from a CMV promoter, and Artemis would be translated from an IRES in a cap-independent manner. The expression of Artemis and EGFP from both constructs in both the HEK-293T and HCT116 cell lines was examined via western blot and immunofluorescence analyses (Figure 19). It was observed that following IRES-mediated, but not cap-dependent translation, Artemis protein levels could be detected via western blot analysis in the HCT116 cell line. Studies using mono- and bicistronic vector systems have demonstrated that the ECMV IRES can increase the translation of its

downstream gene at levels of 8-10 fold higher than those observed for the cap-dependent translation of the same protein (254). Indeed, this event was observed, as both EGFP and Artemis expression levels increased post-IRES translation relative to CMV-mediated translation (Figure 19B). This observation may indicate that ectopic Artemis is poorly translated in "non-permissive cell lines," and that this event can be circumvented via cap-independent translation. The use of a coupled *in vitro* transcription/translation assay to monitor the ectopic expression of Artemis subsequent to cap-dependent versus IRES-mediated translation in both cell lines would have been a useful tool in quantifying these differences.

Indirect immunofluorescence in HEK-293T cell lines transiently transfected with the new Artemis/EGFP construct revealed the normal subcellular localization of both proteins. In the "non-permissive" HCT116 cell lines, however, Artemis appeared to be inconsistently mislocalized. Within some cells, Artemis appeared to be pan-cellular, with a slight enrichment within the nucleus, whereas in others, Artemis appeared to be excluded from the nucleus (refer to Figure 19 C, panels ii and iii). It is difficult to speculate what these collective observations mean within the context of the ectopic expression of Artemis. What does appear, however, is that the cap-independent, forced over-expression of Artemis in a cell line that cannot ectopically express Artemis under "normal" conditions (HCT116) results in the cytosolic accumulation of the protein. Literature describes only one other known instance of the cytosolic accumulation of Artemis, and that was observed in a subset of astrocytes within demyelinated plaques of PML (progressive multifocal leukoencephalopathy). Unfortunately, the nature of this mislocalization was not examined further (255).

The mislocalization of a protein following overexpression is a characteristic not unique to Artemis (256-257). For example, a similar phenotype has been described in the forced overexpression of the oncogene *rgr*. This recently identified GEF (guanine nucleotide exchange factor), like Artemis, is expressed physiologically at extremely low levels (217). However, when high level expression of RGR is forced (via the removal of a long 5'UTR with multiple AUGs), the normally Golgi-associated protein becomes localized to the plasma membrane, where it is involved in the activation of RAS (258). This closely parallels the behaviour of Artemis in HCT116 cells subsequent to IRES-mediated translation, where the normally nuclear Artemis becomes cytosolic. What is perhaps more interesting is that endogenously, the overexpression of RGR can be triggered in a cell-cycle dependent manner via an IRES present within its sequence. Interestingly, sequence analysis of Artemis using the RegRNA program (259) indicates the presence of a potential IRES within its 5'UTR (see appendix IV). Additionally, the overexpression of Artemis in the HCT116 cells could be achieved via EMCV IRES-mediated translation. Although Artemis has been implicated in the regulation of cell cycle progression (134, 260), it has not been shown to be regulated in a cell-cycle dependent manner. Interestingly, a related member of the metallo-β-lactamase family of proteins, hSNM1, has been shown to contain an IRES within its 5'UTR (261). hSNM1 shares homology with Artemis through an approximately 300aa region which includes the β-lactamase and β-CASP domains (130, 261). Endogenously, hSNM1 transcripts are ubiquitously expressed and readily detected, however like Artemis, its protein levels are extremely low (261). It was shown that the hSNM1 IRES could repress the expression of a downstream reporter gene by as much as 8-fold. Additionally, the IRES-mediated

expression of hSNM1 was shown to increase protein expression levels from late prophase to metaphase, followed by a decline in late telophase (261). Together, it appears that the hSNM1 IRES generally represses protein expression, except during mitosis, where it is responsible for increased translation. To elucidate the potential role of this regulatory element in the ectopic expression of Artemis, it would be interesting to observe the expression of an Artemis construct containing the full 5'UTR in cell-cycle synchronization studies. The potential IRES can be verified in a reporter gene assay with the use of a bicistronic dual luciferase construct (261b). This type of assays uses a reporter gene vector containing the ORFs of the *Renilla* (upstream) and firefly (downstream) luciferases separated by a short linker sequence. To test the presence of an IRES, the 5'UTR of Artemis would be inserted between the *Renilla* and firefly luciferase cistrons in lieu of the linker sequence. Following transfection of each construct into an appropriate cell line, the subsequent ratio of *Renilla* to firefly luciferase activity can be determined and quantified. An increase in firefly production would indicate the presence of an IRES. After confirming the presence of an IRES, its activity under different cellular conditions can be examined (cellular stress, post-DNA damage, cell-cycle dependence, etc). This may identify a novel means of regulating the expression of Artemis during periods of increased cellular stress.

Section III: Identification of octamer-binding transcription factor-1 interactors

The octamer-binding transcription factor-1 (Oct-1) has recently been described as a stress sensor, and has been shown to contribute to cell survival post-irradiation (65). In line with this, Oct-1 displays increased stabilization and hyper-phosphorylation following

DNA damage; a phenotype that is coincident with the down-regulation of numerous Oct-1 responsive genes (58). The hyperphosphorylation of Oct-1 has been mapped to its glutamine-rich transactivation domain, and is dependent on DNA-PKcs kinase activity (58). Blocking DNA-PKcs dependent phosphorylation of Oct-1 via site-directed mutagenesis abolishes the contribution of Oct-1 to cellular survival post-irradiation (58). The identification of Oct-1 interacting factors with potential regulatory significance will be paramount in investigating the role of Oct-1 in post-DNA damage survival. A modified TAP method was chosen to facilitate this as it allows for the efficient purification of factors to near homogeneity from crude lysates (224). Additionally, the purification and elution processes are performed under exceptionally mild conditions, such that retention of the functional activity of purified factors can be achieved (224, 267-269).

To differentiate between basal Oct-1 interactors and those eliciting regulatory functions, a series of different conditions must be set up prior to the purification. Initially, it is important to identify Oct-1 interactors specific to the DNA-damage response. This can be achieved by comparing interactors purified from untreated HCT116 cells with those purified from cells treated with DNA-damaging agents. Even within this initial setup, there are numerous facets of the response to examine. For example, purifying factors from cell lysates generated immediately post-damage versus those collected at different recovery points is likely to yield different interactors. Additionally, the DNA-damaging agent itself, as well as the administered does and duration of damage may all influence the dynamics of purified Oct-1 interacting complexes or factors.

In addition to identifying interactors specific to the DNA damage response, it is important to investigate the contribution of Oct-1 hyperphosphorylation in the association of factors with potential regulatory significance. As previously noted, the DNA-PKcs dependent hyperphosphorylation of Oct-1 is essential for post-DNA damage survival. One could reasonably speculate that hyperphosphorylated Oct-1 would interact with a different pool of factors than basally or un-phosphorylated Oct-1. Since blocking the hyperphosphorylation of Oct-1 eliminates post-DNA damage survival, these interactors may be eliciting regulatory functions in the contribution of Oct-1 to this survival. To identify this subset of interactors, wild-type TAP-tagged Oct-1 as well as TAP-tagged Oct-1 with mutated DNA-PKcs phosphorylation sites would be used as bait. Tandem affinity purification could then be used to purify TAP-tagged Oct-1 and its associated interacting factors from cells stably expressing either bait protein (+/- DNA damage). In this sense, interactors (i) specific to the DNA damage response, and (ii) with potential regulatory significance can be identified.

The first step in setting up this system is to select a suitable cell line. HCT116 cells were selected as they grow quickly, are easily infected and their endogenous Oct-1 demonstrates a reproducible post-DNA-damage phenotype following treatment with bleomycin, zeocin and etoposide. Interestingly, Oct-1 stabilization could not be observed following irradiation.

HCT116 cells stably expressing an N-terminally TAP-tagged Oct-1 (NTAP-Oct-1) were generated using a retroviral gene delivery system which results in the incorporation of NTAP-Oct-1 into the host cells genome. The pCeMM expression vector does not contain an antibiotic resistance marker for the selection of cell stably expressing

NTAP-Oct-1. Instead, selection can be achieved via FACS due to the co-expression of EGFP within these cells from an IRES. Unfortunately, although EGFP expression could be readily detected in the Phoenix-293T packaging cell line, it could not be observed in the HCT116 stables. Indirect immunofluorescence indicated that only approximately 20% of the HCT116 cells within the mixed population were stably expressing NTAP-Oct-1. Quantification of western blot data reveals that, within this mixed population of cells, NTAP-Oct-1 is expressed at levels approximately 3-fold higher than endogenous Oct-1 (Appendix V). This means that the per-cell expression of NTAP-Oct-1 is in the order of 16-fold higher than endogenous Oct-1. As the expression of the bait protein at levels as close to endogenous as possible is extremely important in identifying non-spurious interactors, it was clear that the pCeMM system would not be suitable for identifying Oct-1 interactors via TAP. Instead, the entire GS-TAP cassette (+/- Oct-1) was subcloned into the pBABE retroviral vector. Stable expression of NTAP-Oct-1 could be selected via puromycin treatment and would be driven by a much weaker promoter, the Malonely murine leukemia virus (MMLV) 5'LTR. Approximately 3-4 days into puromycin selection, the control uninfected HCT116 cells died whereas those stably expressing NTAP-Oct-1 (and the puromycin resistance gene) survived. Western blot analysis shows NTAP-Oct-1 to be stably expressed at levels approximately 5-fold higher than endogenous Oct-1 (Appendix V). As the stable expression of NTAP-Oct-1 has been continually selected for, it can be reasonable inferred that these cells represent a uniform population. Therefore, the expression levels determined via western analysis can be used approximate the per-cell expression levels of NTAP-Oct-1. Although pBABE-NTAP-Oct-1 is overexpressed relative to endogenous Oct-1, on a per-cell basis, these

levels are much lower than those observed in the previous system, and are suitable for identifying potential Oct-1 interactors via TAP. Unfortunately, indirect immunofluorescence using an α-Oct-1 polyclonal antibody was unable to detect differences in NTAP-Oct-1 expression levels over endogenous Oct-1 levels in a control cell line. This may reflect a limitation in the sensitivity of the antibody used for the detection of the Oct-1 expression level differences via indirect immunofluorescence. The use of Cy2-conjugated streptavidin to selectively identify the SBP portion of the GS-TAP tag via immunofluorescence also proved unsuccessful as low level, diffuse, pan-cellular staining was observed in both the stable and control HCT116 cell lines. Regardless of the lack of immunofluorescence data, by continuously selecting the infected cells with puromycin, thus ensuring that selective pressure on the stable expression of NTAP-Oct-1 is achieved, one can reasonably assert that all cells within this population are expressing NTAP-Oct-1. In concert with this selection, the reduced expression levels of NTAP-Oct-1 in these cells (relative to the first system) provide confidence that this system will be suitable for TAP analysis.

Several small- to mid-scale TAP analyses from HCT116 cells either transiently transfected with pCeMM-NTAP-Oct-1 or stably expressing pBABE-NTAP-Oct-1 were performed. In each of these cases, several trends were observed. Firstly, binding of TAP-tagged Oct-1 to the IgG resin appears to be fairly efficient. By comparing the amount of NTAP-Oct-1 in the cell lysate (input) versus the amount remaining unbound post IgG resin binding (SN1) it could be estimated that greater than 70% of the bait protein can be purified from the crude lysate. Secondly, in the case of pCeMM-NTAP-Oct-1, it appears that although TEV protease cleavage of the TAP-tagged protein appears

efficient (compare full-length NTAP-Oct-1 remaining on the IgG beads following TEV cleavage, Figure 23), recovery of the cleaved bait protein is poor. Figure 24 shows a significant amount of TEV-cleaved NTAP-Oct-1 remaining associated with the IgG resin following TEV cleavage, removal of the supernatant, and washing of the resin (compare lanes 4 to 6). Additionally, although this cleavage product can be observed in the TEV-cleavage supernatant via western blot analysis, it is not visible in the same fraction on a silver-stained gel (Figure 26). Together these results indicate that the amount of TEV-cleaved NTAP-Oct-1 recovered from the IgG resin is low, and that perhaps the resulting cleavage product has a high affinity for the IgG resin. An option is to scale-up the reaction such that sufficient amounts of TEV-cleaved NTAP-Oct-1 are recovered for use in the second step of purification. In the case of pBABE-NTAP-Oct-1, however, recovery of the TEV protease cleaved NTAP-Oct-1 appears much greater. During these sets of experiments, TEV cleavage was allowed to proceed for 1 hour at 30°C instead of overnight at 4°C. The optimization of this cleavage and recovery step allowed for detectable amounts of TEV cleaved NTAP-Oct-1 in all subsequent fractions, including in the final eluate (Figure 27).

The final elution of NTAP-Oct-1 and co-purifying interactors form the immobilized streptavidin resin is achieved through incubation of the resin with a 1mM biotin buffer. The high affinity of streptavidin for biotin (Ka ~ 10^{13} M^{-1}) should be sufficient to displace the SBP-containing TAP-tagged proteins from the resin. Silver stain analysis of the final eluates of six small- and mid-scale tandem affinity purifications of pCeMM-NTAP-Oct-1 (transient expression) from HCT116 cell lysates indicates a factor migrating at approximately 55kDa. This factor is not present in the final eluates

from control HCT116 cell lysates (Figure 24). The band containing the unknown factor was carefully excised from the gel and sent for analysis. In-gel tryptic digest, followed by MS (mass spectrometry) analysis of the factor resulted in the identification of 33 distinct m/z (mass-to-charge) peaks. Parallel analysis of a piece of gel excised from the control lane at the same migration (~55kDa) resulted in the identification of 11 distinct m/z peaks. The peaks on a mass spectrum represent the masses of the various peptides generated by the tryptic digest of the unknown factor. This form of mass spectrometry is known as peptide mass fingerprinting (PMF). Trypsin cleaves peptides on the carboxyl side of the amino acids lysine and arginine (except when followed by proline). As the amino acid sequence of each protein is unique, the resulting number of tryptic-peptides, as well as the mass of these peptides will be unique to each protein as well. The theoretical number and mass of the tryptic-peptides of a myriad of proteins has been determined and are available in PMF databases. By using analytical software to compare the number and masses of experimentally generated tryptic-peptides of an unknown factor with those compiled in databases, the identity of the unknown factor can be determined. Database searches using both the Aldente (262) and Mascot (263) programs revealed that the unknown 55kDa factor was human keratin (keratin type II; Hb6). Keratin is a common contaminating protein abundant on skin, hair and dust particles (264, 265). It is not surprising to observe keratin contamination in MS data of proteins excised from gels. What is surprising is that the contaminating keratin band is specific to the NTAP-Oct-1 samples. Additionally curious is the lack of TEV-cleaved NTAP-Oct-1 in the final eluates, which cannot be detected via western blot analysis or silver staining. This could perhaps be attributed to insufficient elution of the bait protein from the

streptavidin resin. Dissociation of the "interacting" keratin from resin-bound NTAP-Oct-1 may have been facilitated by changes in the salt and pH conditions of the elution buffer (100 mM Tris-Cl (pH7.4), 2.5 mM biotin, 1 mM EDTA) relative to the binding buffer (50 mM Tris-HCl (pH8.0), and 0.5 mM EDTA). This could also explain why additional, perhaps more tightly-associated factors are not observed in the final eluate.

The HCT116 cell line is derived from human colorectal cancers cells and naturally express endogenous keratin K5, K14 (HaCaT), K8, K18, and K19 (266). It is therefore conceivable that the keratin observed in the NTAP-Oct-1 containing eluate may be a bona fide interactor of Oct-1 and not merely a contaminating factor. It is perhaps more likely, however, that this interaction is spurious and merely a consequence of the endogenous overexpression of keratin within these cells coupled with the overexpression of NTAP-Oct-1 within these cells.

The final elution of pBABE-NTAP-Oct-1 and interacting factors from the streptavidin resin yielded significantly different results. Although identical stocks of elution buffer were used for the pCeMM and pBABE samples, elution was allowed to proceed overnight at 4°C as opposed to 2 hours at 4°C. In conjunction with the increased cleavage and recovery of TEV-cleaved NTAP-Oct-1, optimization of the biotin elution process resulted in the identification of four factors specific to NTAP-Oct-1 (Figure 26). These factors were not present in any of the other control eluates (NTAP-TAG or un-infected), nor were they visible in the NTAP-Oct-1 (+ bleomycin) final eluate. Following the in-gel tryptic digest of the samples, MS analysis resulted in the identification of 45 distinct m/z (mass-to-charge) peaks for sample 1 (100kDa factor), 11 m/z peaks for sample 2 (97kDa factor), 35 m/z peaks for sample 3 (65kDa factor), and 17 m/z peaks for

sample 4 (55kDa factor). Database searches using both the Aldente (262) and Mascot (263) programs allowed for the identification of only sample 1; the remaining three samples did not contain enough specific peptides for confident identifications.

Sample 1 appears to be zinc finger protein 295 (Znf295). Znf295 is a ubiquitously expressed transcription factor belonging to the POK family of transcription factors containing both the BTB/POZ (Broad Complex, Tramtrack, and Bric à Brac/Pox virus and Zinc finger) and *krüppel* type (C_2H_2) zinc finger domains (270). The BTB/POZ domain has been shown to mediate homomeric and heteromeric protein-protein interactions, can target proteins to distinct nuclear substructures, and is involved in DNA binding, transcriptional repression/activation, and chromatin remodelling (270-272). These effects are elicited primarily through the association of members of the POK family of transcription factors with transcriptional co-factors (SIN3A (SIN3 homolog A), SMRT (silencing mediator for retinoid and thyroid hormone receptor) and NCOR1 (nuclear receptor co-repressor 1) co-repressors, which in turn recruit HDACs (histone deacetylases)) (272b). Znf295 is expressed as two distinct isoforms, Znf295L and Znf295S, (119kDa and 96kDa, respectively) both of which have been shown to act in a selective manner on different promoters as transcriptional repressors (270). Due to the shared subcellular localization and parallel functionality of Znf295 with Oct-1, this potential interactor is a particularly exciting find. Additionally, as a differential interaction between Oct-1 and Znf295 was observed pre- and post-DNA damage, it is tempting to speculate that the nature of their interaction may be involved in the regulation of (a) gene(s) in response to DNA damageFollowing *in vivo* confirmation of the

interaction between these two factors, it will be interesting to examine which promoters are occupied by these factors both in the presence and absence of DNA damage.

It is evident that the optimization of two key steps within the tandem affinity purification of NTAP-Oct-1 (the TEV cleavage and biotin elution steps) significantly altered the detection of interacting factors in the final eluate. Additional optimization and variation of this system ranging from the method of the cell lysate preparation, to the choice of DNA damaging agent, duration of treatment, and length of recovery times may all influence the interaction of Oct-1 with different factors. Furthermore, the use of Oct-1 TAP constructs with mutated DNA-PKcs phosphorylation target sites will add a further dimension in the identification of Oct-1 interactors. In conjunction with treating the stably-expressing cells with DNA damaging agents, these constructs will be instrumental in the identification of Oct-1 interacting factors with potential regulatory significance. Overall, the tandem affinity purification of Oct-1 resulted in the identification of two factors using the TAP method (keratin with the pCeMM system, and Znf295 with the pBABE system). It is necessary, however, to confirm the interaction of each of these factors with Oct-1 *in vivo.* Co-immunoprecipitation of these potential interactors with endogenous Oct-1 would circumvent potential artefacts associated with the TAP procedure and bait overexpression. Overall, an early stage system in which the bait protein is expressed at suitable levels has been achieved. This system is also sensitive to DSB-inducing agents and displays a functional endogenous Oct-1 DNA-damage response phenotype. With the proper modifications and planning, the dynamic association of different interactors following the induction of DNA DSBs could be mapped throughout

the repair process across different recovery times, as well as in response to the different damaging agents and doses.

Conclusions

Although DNA DSBs represent a continuous threat to the genomic integrity of our cells, they are also essential aspects of our immune system development. The pathways and coordination of the factors involved in regulating the repair of these lesions are as diverse as the types of DNA DSBs themselves. By examining three factors from the V(D)J recombination and NHEJ pathways, new insight into the regulation, activity, and expression of these factors has been achieved. Through the use of association assays, it was concluded that the region of Rag-1 spanning amino acids 660-763 is sufficient, but not required for binding Ku70. Additionally, we have found that ectopic Artemis is transcribed in the non-permissive HCT116 cell line, and does not appear to be regulated at the level of post-transcriptional degradation of the mRNA, or via proteasomal- or lysosomal-mediated protein degradation. However, we did observe that forcing the ectopic expression of Artemis in a non-permissive cell line via cap-independent translation can result in the mislocalization of Artemis. Lastly, an early-stage tandem affinity purification system was established in which the stable expression of NTAP-Oct-1 was achieved at levels approximately 5-fold over endogenous Oct-1 levels. The identification of two Oct-1 interacting factors (keratin and Znf295) were identified via mass spectrometry, and await *in vivo* confirmation via coimmunoprecipitation experiments.

References

1. Lukas, C., J. Bartek, and J. Lukas. 2005. Imaging of protein movement induced by chromosomal breakage: tiny 'local' lesions pose great 'global' challenges. *Chromosoma.* 114(3): 146-154.

2. McKinnon, J.P., and K.W. Caldecott. 2007. DNA strand break repair and human genetic disease. *Annu. Rev. Genomics Hum. Genet.* 8: 37-55.

3. Bonner, W.M. 2003. Low-dose radiation: Thresholds, bystander effects, and adaptive responses. *Proc. Nat. Acad. Sci. U.S.A.* 100(9): 4973-7975.

4. Benitez-Bribiesca, L., and P. Sanchez-Suarez. 1999. Oxidative damage, bleomycin, and gamma radiation induce different types of DNA strand breaks in normal lymphocytes and thymocytes. A comet assay study. *Ann. NY. Acad. Sci.* 887: 133-149.

5. Sutherland, B. M., P. V. Bennett, H. Schenk, 0. Sidorkina., J. Laval, J. Trunk, D. Monteleone, and J. C. Sutherland. 2001. Clustered DNA damages induced by high and low LET radiation, including heavy ions. *Physica Medica.* 17: 204-206.

6. Fry, R.C., T.J. Begley, and L.D. Samson. 2004. Genome-wide responses to DNA-damaging agents. *Annu Rev Microbiol.* 59: 357–377.

7. Maroni, P.D, S. Koul, R.B. Meacham, and H.K. Koul .2004. Mitogen Activated Protein kinase signal transduction pathways in the prostate. *Cell Commun. Signal.* 2: 5-18.

8. Czarnecka, A.M., C. Campanella, G. Zummo, and F. Cappello. 2006. Heat shock protein 10 and signal transduction: a "capsula eburnean" of carcinogenesis? *Cell Stress Chaperones.* 11(4): 287-294.

9. Hafizi, S., Ibraimi, F., and Dahlbäck, B. 2005. C1-TEN is a negative regulator of the Akt/PKB signal transduction pathway and inhibits cell survival, proliferation, and migration. *FASEB J.* 19: 971-990.

10. Wahl,G.M., and Carr,A.M. 2001. The evolution of diverse biological responses to DNA damage: insights from yeast and p53. *Nat Cell Biol.* 3: 227-286.

11. Suzuki, K., Kodama, S., and Watanabe, M. 1999. Recruitment of ATM Protein to Double Strand DNA Irradiated with Ionizing Radiation. *J. Biol. Chem.* 274(36): 25571-25575.

12. Smith, G. C. R.B. Cary, N.D. Lakin, B.C. Hann, S. Teo, D.J. Chen, S.P. Jackson. 1999. Purification and DNA binding properties of the ataxia-telangiectasia gene product ATM. *Proc. Nat. Acad. Sci. U.S.A.* 96: 11134-11139.

13. Abraham, R.T., and R.S. Tibbetts. 2005. Guiding ATM to broken DNA. *Science*. 308: 510-511.

14. Yang, J., Y. Yu, H.E. Hamrick, J.P. Duerksen-Hughes. 2003. ATM, ATR and DNA-PK: initiators of the cellular genotoxic stress responses. *Carcinogenesis*. 24(10): 1571-1580.

15. Uziel T., Y. Lerenthal, L. Moyal, Y. Andegeko, L. Mittelman, and Y. Shiloh. 2003. Requirement of the MRN complex for ATM activation by DNA damage. *EMBO J.* 22(20): 5612-21.

16. Carson C.T., R.A. Schwartz, T.H. Stracker, C.E. Lilley, D.V. Lee, and M.D. Weitzman. 2003. The Mre11 complex is required for ATM activation and the G2/M checkpoint. *EMBO J.* 22(24): 6610-20.

17. Kurz E.U., and S.P. Lees-Miller. 2004. DNA damage-induced activation of ATM and ATM-dependent signaling pathways. *DNA Repair*. 3(8-9): 889-900.

18. Paul, T.T., E.P. Rogakou, V. Yamazaki, C.U. Kirchgessner, M. Gellert, and W.M. Bonner. 2000. A critical role for histone H2AX in recruitment of repair factors to nuclear foci after DNA damage. *Curr. Biol.* 10(15): 886-895.

19. Shiloh, Y. 2006. The ATM-mediated DNA-damage response: taking shape. *Trends Biochem. Sci.* 31(7): 402-410.

20. Lukas C. F. Melander , M. Stucki, J. Falck, S. Bekker-Jensen , M. Goldberg, Y. Lerenthal , S.P. Jackson, J. Bartek, and J. Lukas. 2004. Mdc1 couples DNA double-strand break recognition by Nbs1 with its H2AX-dependent chromatin retention. *EMBO J.* 23(13): 2674-83.

21. Bekker-Jensen S., C. Lukas, R. Kitagawa, F. Melander, M.B. Kastan, J. Bartek, J. Lukas. 2006. Spatial organization of the mammalian genome surveillance machinery in response to DNA strand breaks. *J Cell Biol.* 173(2): 195-206.

22. Yasui, L.S. 2006. Imaging Radiation-Induced gamma H2AX
Foci. Microsc Microanal 12(Supp 2): 248-249.

23. Löbrich, M., and P.A. Jeggo. 2005. Harmonising the response to DSBs: a new string in the ATM bow. *DNA Repair*. 4: 749–759.

23. Shiloh, Y. 2003. ATM and related protein kinases: safeguarding genome integrity. *Nat. Rev. Cancer*. 3: 155-168.

24. Cuadrado, M., B. Martinez-Pastor, and O. Fernandez-Capetillo. 2006. ATR activation in response to ionizing radiation: still ATM territory. *Cell Div.* 1(1): 7.

25. Zhou, J., C. Lim, J. Li, L. Cai, and Y. Zhang. 2006. The role of NBS1 in the modulation of PIKK family proteins ATM and ATR in the cellular response to DNA damage. *Cancer Lett.* 243(1): 9-15.

26. Cliby, W.A., C.J Roberts, K.A. Cimprich, C.M. Stringer, J.R. Lamb, S.L. Schreiber, and S.H. Friend. 1998. Overexpression of a kinase-inactive ATR protein causes sensitivity to DNA-damaging agents and defects in cell cycle checkpoints. *EMBO J.* 17(1): 159-69.

27. Stiff, T., S.A. Walker, K. Cerosaletti, A.A. Goodarzi, E. Petermann, P. Concannon, M. O'Driscoll, P.A. Jeggo. 2006. ATR-dependent phosphorylation and activation of ATM in response to UV treatment or replication fork stalling. *EMBO J.* 25: 5775–5782.

28. Jeggo. 2006. ATR-dependent phosphorylation and activation of ATM in response to UV treatment or replication fork stalling. *EMBO J.* 25(24): 5775-82.

29. Tembe, V., and B.R. Henderson. 2007. Protein trafficking in response to DNA damage. *Cellular Signalling.* 9(6): 1113-1120.

30. Latonen, L. and M. Laiho. 2005. Cellular UV damage responses-Functions of tumor suppressor p53 Biochim. Biophys. *Acta, Rev. Cancer.* 1755(2): 71-89.

31. Bradbury, J. M. and Jackson, S. P. 2003 The complex matter of DNA double-strand break detection. *Biochem. Soc. Trans* 31:40-44.

31b. Chuikov, S., J.K. Kurash, J.R. Wilson, B. Xiao, N. Justin, G.S. Ivanov, K. McKinney, P. Tempst, C. Prives, S.J. Gamblin, *et al.* 2004. Regulation of p53 activity through lysine methylation. *Nature.* 432: 353-360.

32. Soubeyrand, S., C. Schild-Poulter, and R.J. Haché. 2004. Structured DNA promotes phosphorylation of p53 by DNA-dependent protein kinase at serine 9 and threonine 18. *Eur. J. Biochem.* 271(18): 3776-84.

33. Hammond, E.M., M.J. Dorie, and A.J. Giaccia. 2003. ATR/ATM Targets Are Phosphorylated by ATR in Response to Hypoxia and ATM in Response to Reoxygenation. *J. Biol. Chem.* 278(14): 12207-12213.

34. Yajima, H., K. Lee, and B. P.C. Chen. 2006. ATR-Dependent Phosphorylation of DNA-Dependent Protein Kinase Catalytic Subunit in Response to UV-Induced Replication Stress. *Mol Cell Biol.* 20: 7520–7528.

35. Jeggo P.A., and M. Löbrich M. 2006. Contribution of DNA repair and cell cycle checkpoint arrest to the maintenance of genomic stability. *DNA Repair.* 5(9): 1192-1198.

36. Lavin M.F., and N. Gueven. 2006. The complexity of p53 stabilization and activation. *Cell Death Differ.* 13(6): 941-50.

37. Hirose Y., M.S. Berger, and R.O. Pieper. 2001. Abrogation of the Chk1-mediated G(2) checkpoint pathway potentiates temozolomide-induced toxicity in a p53-independent manner in human glioblastoma cells. *Cancer Res.* 61: 5843-5849.

38. Curman D., B. Cinel, D.E. Williams, N. Rundle, W.D. Block, A.A. Goodarzi, J.R. Hutchins, P.R. Clarke, B.B. Zhou, S.P. Lees-Miller, *et al.* 2001. Inhibition of the G2 DNA damage checkpoint and of protein kinases Chk1 and Chk2 by the marine sponge alkaloid debromohymenialdisine. *J. Biol. Chem.* 276: 17914-17919.

39. Hashiba, M., T. Kasahara, S.Y. Kim, S. Shibutani, and M. Degawa. 2006. DNA damage and altered gene expression of enzymes for metabolism and DNA repair by tamoxifen and toremifene in the female rat liver. *Cancer Sci.* 97(6): 468-477.

40. Kowara, R., A. Karaczyn, R.Y.S. Cheng, K. Salnikow, and K.S. Kasprzak. 2005. Microarray analysis of altered gene expression in murine fibroblasts transformed by nickel(II) to nickel(II)-resistant malignant phenotype. *Toxicol. Appl. Pharmacol.* 205(1): 1-10.

41. Herrera, R.E., V.P. Sah, B.O. Williams, T.P. Makela, R.A. Weinberg and T. Jacks. 1996. Altered cell cycle kinetics, gene expression, and G1 restriction point regulation in Rb-deficient fibroblasts. *Mol. Cell. Biol.* 16(5): 2402-2407.

42. Kote-Jarai, Z., R.D. Williams, N. Cattini, M. Copeland, I. Giddings, R. Wooster, R.H. tePoele, P. Workman, B. Gusterson, J. Peacock, *et al.* 2004. Gene Expression Profiling after Radiation-Induced DNA Damage Is Strongly Predictive of *BRCA1* Mutation Carrier Status. *Clin. Cancer Res.* 10: 958-963.

43. Zhao H., S. Jin, F. Fan, W. Fan, T. Tong, and Q. Zhan. 2000. Activation of the transcription factor Oct-1 in response to DNA damage. *Cancer Res.* 60(22): 6276-6280.

44. Sadowska, B., R. Barrucco, K. Khalili, and M. Safak. 2003. Regulation of Human Polyomavirus JC Virus Gene Transcription by AP-1 in Glial Cells. *J Virol.* 77(1): 665–672.

45. Wilkinson, D.E, and S.K. Weller. 2006. Herpes simplex virus type I disrupts the ATR-dependent DNA-damage response during lytic infection. *J. Cell Sci.* 119: 2695-2703.

46. Sturm R., T. Baumruker, B.R. Franza Jr., and W. Herr. 1987. A 100-kD HeLa cell octamer binding protein (OBP100) interacts differently with two separate octamer-related sequences within the SV40 enhancer. *Genes Dev.* 1(10): 1147-60.

47. Sive, H.L., and R.G. Roeder. 1986. Interaction of a Common Factor with Conserved Promoter and Enhancer Sequences in Histone H2B, Immunoglobulin, and U2 Small Nuclear RNA (snRNA) Genes. *Proc. Nat. Acad. Sci. U.S.A.* 83(17): 6382-6386.

48. Fletcher, C., N. Heintz, and R.G. Roeder. 1987. Purification and characterization of OTF-1, a transcription factor regulating cell cycle expression of a human histone H2b gene. *Cell.* 51(5): 773-781.

49. Das, G., and W. Herr. 1993. Enhanced activation of the human histone H2B promoter by an Oct-1 variant generated by alternative splicing. *J. Biol. Chem.* 268(33): 25026-25032.

50. Rave-Harel, N., M.L. Givens, S.B. Nelson, H.A. Duong, D. Coss, M.E. Clark, S.B. Hall, M.P. Kamps, and P.L. Mellona. 2004. TALE Homeodomain Proteins Regulate Gonadotropin-releasing Hormone Gene Expression Independently and via Interactions with Oct-1. *J. Biol. Chem.* 279(29): 30287-30297.

51. Cheng, C.K., C.M. Yeung, R.L. Hoo, B.K. Chow, and P.C. Leung. 2002. Oct-1 is involved in the transcriptional repression of the gonadotropin-releasing hormone receptor gene. *Endocrinology.* 143(12): 4693-701.

52. Dong, B., and F.Q. Zhao. 2007. Involvement of the ubiquitous Oct-1 transcription factor in hormonal induction of beta-casein gene expression. *Biochem J.* 1(1): 57-64.

53. Nogueira, M.L., V.E. Wang, D. Tantin, P.A. Sharp, and T.M. Kristie. 2004. Herpes simplex virus infections are arrested in Oct-1-deficient cells. *Proc Natl Acad Sci U S A.* 101(6): 1473-8.

54. van Leeuwen, H.C., M. Rensen, and P.C. van der Vliet. 1997. The Oct-1 POU homeodomain stabilizes the adenovirus preinitiation complex via a direct interaction with the priming protein and is displaced when the replication fork passes. *J Biol Chem.* 272(6): 3398-405.

55. Coenjaerts, F.E., J.A. van Oosterhout, P.C. van der Vliet. 1994. The Oct-1 POU domain stimulates adenovirus DNA replication by a direct interaction between the viral precursor terminal protein-DNA polymerase complex and the POU homeodomain. *EMBO J.* 13(22): 5401-9.

56. Mesplède T., M.L. Island, N. Christeff, F. Petek, J. Doly, and S. Navarro. 2005. The POU transcription factor Oct-1 represses virus-induced interferon A gene expression. *Mol Cell Biol.* 25(19): 8717-31.

57. Schwachtgen, J.L., J.E. Remacle, N. Janel, R. Brys, D. Huylebroeck, D. Meyer, and D. Kerbiriou-Nabias. 1998. Oct-1 is involved in the transcriptional repression of the von willebrand factor gene promoter. *Blood.* 92(4): 1247-58.

58. Schild-Poulter, C., A. Shih, D. Tantin, N.C. Yarymowich, S. Soubeyrand, P.A. Sharp, and R.J. Haché. 2007. DNA-PK phosphorylation sites on Oct-1 promote cell survival following DNA damage. *Oncogene.* 26(27): 3980-8.

59. Rosenfeld, M.G. 1991. POU-domain transcription factors: pou-er-ful developmental regulators. *Genes & Dev.* 5: 897-907.

60. Klemm, J.D., M.A. Rould, R. Aurora, W. Herr, and C.O. Pabo. 1994. Crystal structure of the Oct-1 POU domain bound to an octamer site: DNA recognition with tethered DNA-binding modules. *Cell.* 77(1): 21-32.

61. Dekker, N., M. Cox, R. Boelens, C.P. Verrijzer, P.C. van der Vliet, and R. Kaptein. 1993. Solution structure of the POU-specific DNA-binding domain of Oct-1. *Nature.* 362(6423): 852-5.

62. Cox, M., J.P. van Tilborg, W. de Laat, R. Boelens, H.C. van Leeuwen, P.C. van der Vliet, and R. Kaptein. 1995. Solution structure of the Oct-1 POU homeodomain determined by NMR and restrained molecular dynamics. *J Biomol NMR.* 6(1): 23-32.

63. Wang, V.E., T. Schmidt, J. Chen, P.A. Sharp, and D. Tantin. 2004. Embryonic lethality, decreased erythropoiesis, and defective octamer-dependent promoter activation in Oct-1-deficient mice. *Mol Cell Bio*l. 24(3): 1022-32.

64. Meighan-Mantha, R.L., A.T. Riegel, S. Suy, V. Harris, F.H. Wang, C. Lozano, T.L. Whiteside, and U. Kasid. 1999. Ionizing radiation stimulates octamer factor DNA binding activity in human carcinoma cells. *Mol Cell Biochem* 199: 209–215.

65. Tantin, D., C. Schild-Poulter, V. Wang, R.J. Haché, and P.A. Sharp. 2005. The octamer binding transcription factor Oct-1 is a stress sensor. *Cancer Res.* 65(23): 10750-8.

66. Magné, S., S. Caron, M. Charon, M.C. Rouyez, and I. Dusanter-Fourt. 2003. STAT5 and Oct-1 form a stable complex that modulates cyclin D1 expression. *Mol Cell Biol.* 23(24): 8934-45.

67. Kakizawa, T., T. Miyamoto, K. Ichikawa, A. Kaneko, S. Suzuki, M. Hara, T. Nagasawa, T. Takeda, J. Mori, M. Kumagai, *et al.* 1999. Functional interaction between Oct-1 and retinoid X receptor. *J Biol Chem.* 274(27): 19103-8.

68. Kim, J.S., T.B. Krasieva, H. Kurumizaka, D.J. Chen, A.M. Taylor, and K. Yokomori. 2005. Independent and sequential recruitment of NHEJ and HR factors to DNA damage sites in mammalian cells. *J Cell Biol.* 170(3): 341-7.

69. Zierhut, C., and J.F. Diffley. 2008. Break dosage, cell cycle stage and DNA replication influence DNA double strand break response. *EMBO J.* 27: 1875 -1885.

70. Delacôte, F., and B.S. Lopez. 2008. Importance of the cell cycle phase for the choice of the appropriate DSB repair pathway, for genome stability maintenance: the trans-S double-strand break repair model. *Cell Cycle*. 7(1): 33-38.

71. Shrivastav, M., L.P. De Haro, and J.A. Nickoloff. 2008. Regulation of DNA double-strand break repair pathway choice. *Cell Res*. 18(1): 134-147.

72. Michel, B., M. Flores, E. Viguera, G. Grompone, M. Seigneur, and V. Bidnenko. 2001. Rescue of arrested replication forks by homologous recombination. *Proc. Nat. Acad. Sci. U.S.A.* 98(15): 8181–8188.

72b. Weterings, E., and D.J. Chen. 2008. The endless tale of non-homologous end-joining. *Cell Res.* 18: 114–124.

73. Schwartz, M., E. Zlotorynski, M.Goldberg, E. Ozeri, A. Rahat, C. le Sage, B.P.C. Chen, D.J. Chen, R. Agami, and B. Kerem. 2005. Homologous recombination and nonhomologous end-joining repair pathways regulate fragile site stability. *Genes Dev.* 19(22): 2715–2726.

74. Kuhfittig-Kulle, S., E. Feldmann, A. Odersky, A. Kuliczkowska, W. Goedecke, A. Eggert, and P. Pfeiffer. 2007. The mutagenic potential of non-homologous end joining in the absence of the NHEJ core factors Ku70/80, DNA-PKcs and XRCC4-LigIV. *Mutagenesis*. 22(3): 217-233.

75. Pierce, A.J., and M. Jasin. 2001. NHEJ deficiency and disease. *Mol Cell*. 8(6): 1160-1161.

76. Collis, S.J., T.L. DeWeese, P.A. Jeggo, and A.R. Parker. 2005. The life and death of DNA-PK. *Oncogene*. 24(6): 949-961.

77. Ma, Y., and M.R. Lieber. 2006. In vitro nonhomologous DNA end joining system. *Methods Enzymol*. 408: 502-510.

78. Pastwa, E., and J. Błasiak. 2003. Non-homologous DNA end joining. *Acta Biochim Pol*. 50(4): 891-908.

79. Zhang, Z., L. Zhu, D. Lin, F. Chen, D.J. Chen, and Y. Chen. 2001. The three-dimensional structure of the C-terminal DNA-binding domain of human Ku70. *J Biol Chem*. 276(41): 38231-38236.

80. Rivera-Calzada A., L. Spagnolo, L.H. Pearl, and O. Llorca. 2007. Structural model of full-length human Ku70-Ku80 heterodimer and its recognition of DNA and DNA-PKcs. *EMBO Rep*. 8(1): 56-62.

81. Walker, J.R., R.A. Corpina, and J. Goldberg. 2001. Structure of the Ku heterodimer bound to DNA and its implications for double-strand break repair. *Nature*. 412(6847): 607-614.

82. Lehman, J.A., D.J. Hoelz, and J.J. Turchi. 2008. DNA-dependent conformational changes in the Ku heterodimer. *Biochemistry*. 47(15): 4359-4368.

83. Spagnolo, L., A. Rivera-Calzada, L.H. Pearl, and O. Llorca. 2006. Three-dimensional structure of the human DNA-PKcs/Ku70/Ku80 complex assembled on DNA and its implications for DNA DSB repair. *Mol Cell*. 22(4): 511-519.

84. Singleton, B.K., M.I. Torres-Arzayus, S.T. Rottinghaus, G.E. Taccioli, and P.A. Jeggo. 1999. The C terminus of Ku80 activates the DNA-dependent protein kinase catalytic subunit. *Mol Cell Biol*. 19(5): 3267-3277.

85. Featherstone, C., and S.P. Jackson. 1999. Ku, a DNA repair protein with multiple cellular functions? *Mutat Res*. 434(1): 3-15.

86. Raval, P., A.N. Kriatchko, S. Kumar, and P.C. Swanson. 2008. Evidence for Ku70/Ku80 association with full-length RAG1. *Nucleic Acids Res*. 36(6): 2060-2072.

87. Monferran, S., J. Paupert, S. Dauvillier, B. Salles, and C. Muller. 2004. The membrane form of the DNA repair protein Ku interacts at the cell surface with metalloproteinase 9. *EMBO J*. 23(19): 3758-3768.

88. Zhang, Z., W. Hu, L. Cano, T.D. Lee, D.J. Chen, and Y. Chen. 2004. Solution structure of the C-terminal domain of Ku80 suggests important sites for protein-protein interactions. *Structure*. 12(3): 495-502.

89. Matheos, D., M.T. Ruiz, G.B. Price, and M. Zannis-Hadjopoulos. 2002. Ku antigen, an origin-specific binding protein that associates with replication proteins, is required for mammalian DNA replication. *Biochim Biophys Acta*. 1578(1-3):59-72.

90. Li, B., and L. Comai. 2001. Requirements for the nucleolytic processing of DNA ends by the Werner syndrome protein-Ku70/80 complex. *J Biol Chem*. 276(13): 9896-9902.

91. Song, K., Y. Jung, D. Jung, and I. Lee. 2000. Human Ku70 interacts with heterochromatin protein 1alpha. *J Biol Chem*. 276(11): 8321-8327.

92. Ribes-Zamora, A., I. Mihalek, O. Lichtarge, and A.A. Bertuch. 2007. Distinct faces of the Ku heterodimer mediate DNA repair and telomeric functions. *Nat Struct Mol Biol*. 14(4): 301-307.

93. Celli, G.B., E.L. Denchi, and T. de Lange. 2006. Ku70 stimulates fusion of dysfunctional telomeres yet protects chromosome ends from homologous recombination. *Nat Cell Biol*. 8(8): 885-890.

94. Bailey, S.M., and E.H. Goodwin. 2004. DNA and telomeres: beginnings and endings. *Cytogenet Genome Res.* 104(1-4): 109-115.

95. Li, H., H. Vogel, V.B. Holcomb, Y. Gu, and P. Hasty. 2007. Deletion of Ku70, Ku80, or both causes early aging without substantially increased cancer. *Mol Cell Biol.* 27(23): 8205-8214.

96. Leong, T., M. Chao, S. Bassal, and M. McKay. 2003. Radiation-hypersensitive cancer patients do not manifest protein expression abnormalities in components of the nonhomologous end-joining (NHEJ) pathway. *Brit. J. Cancer.* 88: 1251-1255.

97. Nussenzweig, A., K. Sokol, P. Burgman, L. Li, and G.C. Li. 1997. Hypersensitivity of Ku80-deficient cell lines and mice to DNA damage: The effects of ionizing radiation on growth, survival, and development. *Proc. Natl. Acad. Sci.* 94: 13588-13593.

98. Myung, K., G. Ghosh, F.J. Fattah, G. Li, H. Kim, A. Dutia, E. Pak, S. Smith, and E.A. Hendrickson. 2004. Regulation of Telomere Length and Suppression of Genomic Instability in Human Somatic Cells by Ku86. *Mol Cell Biol.* 24(11): 5050-5059.

99. Fattah, K.R., B.L. Ruis, and E.A. Hendrickson. 2008. Mutations to Ku reveal differences in human somatic cell lines. *DNA Repair (Amst).* 7(5):762-74.

100. Walker, J.R, R.A. Corpina, and J. Goldberg. 2001. Structure of the Ku heterodimer bound to DNA and its implications for double-strand break repair. *Nature.* 412(6847): 607-614.

101. Kurimasa, A., S. Kumano, N.V. Boubnov, M.D. Story, C.S. Tung, S.R. Peterson, and D.J. Chen. 1999. Requirement for the kinase activity of human DNA-dependent protein kinase catalytic subunit in DNA strand break rejoining. *Mol Cell Biol.* 19(5): 3877-3884.

102. Daniel, R., R.A. Katz, and A.M. Skalka. 1999. A role for DNA-PK in retroviral DNA integration. *Science.* 284(5414):644-647.

103. Zhang, Y., J. Zhou, X. Cao, Q. Zhang, C.U. Lim, R.L. Ullrich, S.M. Bailey, and H.L. Liber. 2007. Partial deficiency of DNA-PKcs increases ionizing radiation-induced mutagenesis and telomere instability in human cells. *Cancer Lett.* 250(1): 63-73.

104. Taccioli, G.E., A.G. Amatucci, H.J. Beamish, D. Gell, X.H. Xiang, M.I. Torres Arzayus, A. Priestley, S.P. Jackson, A. Marshak Rothstein, P.A. Jeggo, *et al.* 1998. Targeted disruption of the catalytic subunit of the DNA-PK gene in mice confers severe combined immunodeficiency and radiosensitivity. *Immunity.* 9(3): 355-366.

Targeted disruption of the catalytic subunit of the DNA-PK gene in mice confers severe combined immunodeficiency and radiosensitivity. *Immunity*. 9(3): 355-366.

105. Tomkinson, A.E., and Z.B. Mackey. 1998. Structure and function of mammalian DNA ligases. *Mutat. Res-DNA Repair*. 407(1): 1-9.

106. Karanjawala, Z.E., N. Adachi, R.A. Irvine, E.K. Oh, D. Shibata, K. Schwarz, C.L. Hsieh, and M.R. Lieber. 2002. The embryonic lethality in DNA ligase IV-deficient mice is rescued by deletion of Ku: implications for unifying the heterogeneous phenotypes of NHEJ mutants. *DNA Repair (Amst)*. 1(12): 1017-1026.

107. Nijnik, A, L. Woodbine, C. Marchetti, S. Dawson, T. Lambe, C. Liu, N.P. Rodrigues, T.L. Crockford, E. Cabuy, A. Vindigni, *et al.* 2007. DNA repair is limiting for haematopoietic stem cells during ageing. *Nature*. Vol 447: 686-691.

108. Toita, N., N. Hatano, S. Ono, M. Yamada, R. Kobayashi, I. Kobayashi, N. Kawamura, M. Okano, A. Satoh, A. Nakagawa, *et al.* 2007. Epstein-Barr virus-associated B-cell lymphoma in a patient with DNA ligase IV (LIG4) syndrome. *Am J Med Genet A*. 143(7): 742-745.

109. Girard, P.M., B. Kysela, C.J. Härer, A.J. Doherty, and P.A. Jeggo. 2004. Analysis of DNA ligase IV mutations found in LIG4 syndrome patients: the impact of two linked polymorphisms. *Hum Mol Genet*. 13(20): 2369-2376.

110. O'Driscoll, M., A.R. Gennery, J. Seidel, P. Concannon, and P.A. Jeggo. 2004. An overview of three new disorders associated with genetic instability: LIG4 syndrome, RS-SCID and ATR-Seckel syndrome. *DNA Repair (Amst)*. 3(8-9):1227-1235.

111. Mori, M., H. Itsukaichi, A. Nakamura, and K. Sato. 2001. Molecular characterization of ionizing radiation-hypersensitive mutant M10 cells. *Mutat Res-DNA Repari.* 487(3-4): 85-92.

112. Mizuta, R., H. Cheng, Y. Gao, and W. Frederick. 1997. Molecular genetic characterization of XRCC4 function. *Int. Immunol.* 9(10): 1607-1613.

113. Drouet, J., C. Delteil, J. Lefrancois, P. Concannon, B. Salles and P. Calsou. 2005. DNA-dependent protein kinase and XRCC4-DNA ligase IV mobilization in the cell in response to DNA double strand breaks, *J. Biol. Chem.* 280(8): 7060–7069.

114. Calsou, P., C. Delteil, P. Frit, J. Drouet and B. Salles. 2003. Coordinated Assembly of Ku and p460 Subunits of the DNA-dependent Protein Kinase on DNA Ends is Necessary for XRCC4-ligase IV Recruitment, *J. Mol. Biol.* 326(1): 93–103.

115. Buck, D., L. Malivert, R. de Chasseval, A. Barraud, M. Fondanèche, O. Sanal, A. Plebani, J. Stéphan, M. Hufnagel, F. le Deist, *et al.* 2006. Cernunnos, a Novel

Nonhomologous End-Joining Factor, Is Mutated in Human Immunodeficiency with Microcephaly. *Cell.* 124(2): 287-299.

116. Ahnesorg, P., P. Smith, and S.P. Jackson. 2006. XLF interacts with the XRCC4-DNA ligase IV complex to promote DNA nonhomologous end-joining. *Cell.* 124(2):301-313.

117. Dai, Y., B. Kysela, L. A. Hanakahi, K. Manolis, E. Riballo, M. Stumm, T. O. Harville, S. C. West, M. A. Oettinger, and P. A. Jeggo. 2003. Nonhomologous end joining and V(D)J recombination require an additional factor. *Proc. Nat. Acad. Sci. U.S.A.* 100: 2462-2467.

118. Sekiguchi, J.M., and D.O. Ferguson. 2006. DNA double-strand break repair: a relentless hunt uncovers new prey. *Cell.* 124(2): 260-262.

119. Wu, P.Y., P. Frit, L. Malivert, P. Revy, D. Biard, B. Salles, P. Calsou. 2007. Interplay between Cernunnos-XLF and nonhomologous end-joining proteins at DNA ends in the cell. *J Biol Chem.* 282(44): 31937-13943.

120. Li, Y., D.Y. Chirgadze, V.M. Bolanos-Garcia, B.L. Sibanda, O.R. Davies, P. Ahnesorg, S.P. Jackson, and T.L. Blundell. 2007. Crystal structure of human LF/Cernunnos reveals unexpected differences from XRCC4 with implications for NHEJ. *EMBO J.* 27(1): 290-300.

121. Yano, K., and D.J. Chen. 2008. Live cell imaging of XLF and XRCC4 reveals a novel view of protein assembly in the non-homologous end-joining pathway. *Cell Cycle.* 7(10): 1321-1325.

122. Yano, K., K. Morotomi-Yano, S. Wang, N. Uematsu, K. Lee, A. Asaithamby, E. Weterings, and D.J Chen. 2008. Ku recruits XLF to DNA double-strand breaks. *EMBO reports.* 9: 91-96.

123. Dahm K. 2008. Role and regulation of human XRCC4-like factor/cernunnos. *J Cell Biochem.* 104(5): 1534-1540.

124. Le Deist, F., C. Poinsignon, D. Moshous, A. Fischer, and J.P. de Villartay. 2004. Artemis sheds new light on V(D)J recombination. *Immunol Rev.* 200: 142-155.

125. Mansilla-Soto, J., and P. Cortes. 2003. VDJ recombination: Artemis and its in vivo role in hairpin opening. *J Exp Med.* 197(5): 543-547.

126. Moshous, D., I. Callebaut, R. de Chasseval, C. Poinsignon, I. Villey, A. Fische, and J.P. de Villartay. 2003. The V(D)J recombination/DNA repair factor artemis belongs to the metallo-beta-lactamase family and constitutes a critical developmental checkpoint of the lymphoid system. *Ann N Y Acad Sci.* 987: 150-157.

127. Touvrey, C., C. Couedel, P. Soulas, R. Couderc, M. Jasin, J.P. de Villartay, P.N. Marche, E. Jouvin-Marche, and S.M. Candéias. 2008. Distinct effects of DNA-PKcs and Artemis inactivation on signal joint formation in vivo. *Mol Immunol.* 45(12): 3383-3391.

128. Kurosawa, A., H. Koyama, S. Takayama, K. Miki, D. Ayusawa, M. Fujii, S. Iiizumi, and N. Adachi. 2008. The requirement of Artemis in double-strand break repair depends on the type of DNA damage. *DNA Cell Biol.* 27(1): 55-61.

129. Rooney, S., J. Sekiguchi, C. Zhu, H.L. Cheng, J. Manis, S. Whitlow, J. DeVido, D. Foy, J. Chaudhuri, D. Lombard, *et al.* 2002. Leaky Scid phenotype associated with defective V(D)J coding end processing in Artemis-deficient mice. *Mol Cell.* 10(6): 1379-1390.

130. Poinsignon, C., D. Moshous, I. Callebaut, R. de Chasseval, I. Villey, J.P. de Villartay. 2004. The metallo-beta-lactamase/beta-CASP domain of Artemis constitutes the catalytic core for V(D)J recombination. *J Exp Med.* 199(3): 315-321.

131. Heinz, U., and H.W. Adolph. 2004. Metallo-b-lactamases: two binding sites for one catalytic metal ion? *Cell. Mol. Life Sci.* 61: 2827–2839.

132. Pannicke, U., Y. Ma, K.P. Hopfner, D. Niewolik, M.R. Lieber, and K. Schwarz. 2004. Functional and biochemical dissection of the structure-specific nuclease ARTEMIS. *EMBO J.* 23(9): 1987-1997.

133. Poinsignon, C., R. de Chasseval, S. Soubeyrand, D. Moshous, A. Fischer, R.J. Haché, and J.P. de Villartay. 2004. Phosphorylation of Artemis following irradiation-induced DNA damage. *Eur J Immunol.* 34(11): 3146-3155.

134. Zhang, X., J. Succi, Z. Feng, S. Prithivirajsingh, M.D. Story, and R.J. Legerski. 2004. Artemis is a phosphorylation target of ATM and ATR and is involved in the G2/M DNA damage checkpoint response. *Mol Cell Biol.* 24(20): 9207-9220.

135. Chen, L., T. Morio, Y. Minegishi, S. Nakada, M. Nagasawa, K. Komatsum, L. Chessa, A. Villa, D. Lecis, D. Delia, *et al.* 2005. Ataxia-telangiectasia-mutated dependent phosphorylation of Artemis in response to DNA damage. *Cancer Sci.* 96(2): 134-141.

136. Ma, Y., U. Pannicke, H. Lu, D. Niewolik, K. Schwarz, and M.R. Lieber. 2005. The DNA-dependent protein kinase catalytic subunit phosphorylation sites in human Artemis. *J Biol Chem.* 280(40): 33839-33846.

137. Ma, Y., K. Schwarz, and M.R. Lieber. 2005. The Artemis:DNA-PKcs endonuclease cleaves DNA loops, flaps, and gaps. *DNA Repair (Amst).* 4(7): 845-851.

138. Goodarzi, A.A., Y. Yu, E. Riballo, P. Douglas, S.A. Walker, R. Ye, C. Härer, C. Marchetti, N. Morrice, P.A. Jeggo, and S.P. Lees-Miller. 2006. DNA-PK autophosphorylation facilitates Artemis endonuclease activity. *EMBO J.* 25(16): 3880-3889.

139. Soubeyrand, S., L. Pope, R. De Chasseval, D. Gosselin, F. Dong, J.P. de Villartay, and R.J. Haché. 2006. Artemis phosphorylated by DNA-dependent protein kinase associates preferentially with discrete regions of chromatin. *J Mol Biol.* 358(5): 1200-1211.

140. Yannone, S.M., I.S. Khan, R.Z. Zhou, T. Zhou, K. Valerie, and L.F. Povirk. 2008. Coordinate 5' and 3' endonucleolytic trimming of terminally blocked blunt DNA double-strand break ends by Artemis nuclease and DNA-dependent protein kinase. *Nucleic Acids Res.* 36(10): 3354-3365.

141. Inagaki, K., C. Ma, T.A. Storm, M.A. Kay, and H. Nakai. 2007. The role of DNA-PKcs and artemis in opening viral DNA hairpin termini in various tissues in mice. *J Virol.* 81(20): 11304-11321.

142. Niewolik, D., U. Pannicke, H. Lu, Y. Ma, L.C. Wang, P. Kulesza, E. Zandi, M.R. Lieber, and K. Schwarz. 2006. DNA-PKcs dependence of Artemis endonucleolytic activity, differences between hairpins and 5' or 3' overhangs. *J Biol Chem.* 281(45): 33900-33909.

143. Drouet, J., P. Frit, C. Delteil, J.P. de Villartay, B. Salles, and P. Calsou. 2006. Interplay between Ku, Artemis, and the DNA-dependent protein kinase catalytic subunit at DNA ends. *J Biol Chem.* 281(38): 27784-27793.

144. Darroudi, F., W. Wiegant, M. Meijers, A.A. Friedl, M van der Burg, J. Fomina, J.J. van Dongen, D.C. van Gent, and M.Z. Zdzienicka. 2007. Role of Artemis in DSB repair and guarding chromosomal stability following exposure to ionizing radiation at different stages of cell cycle. *Mutat Res.* 615(1-2): 111-124.

145. Jeggo, P., and P. O'Neill. 2002. The Greek Goddess, Artemis, reveals the secrets of her cleavage. *DNA Repair (Amst).* 1(9): 771-777.

146. Schlissel, M.S. 2002. Does artemis end the hunt for the hairpin-opening activity in V(D)J recombination? *Cell.* 109(1): 1-4.

147. Ma, Y., U. Pannicke, K. Schwarz, and M.R. Lieber. 2002. Hairpin opening and overhang processing by an Artemis/DNA-dependent protein kinase complex in nonhomologous end joining and V(D)J recombination. *Cell.* 108(6): 781-794.

148. Lu, H., K. Schwarz, and M.R. Lieber. 2007. Extent to which hairpin opening by the Artemis:DNA-PKcs complex can contribute to junctional diversity in V(D)J recombination. *Nucleic Acids Res.* 35(20): 6917-6923.

149. Wang, J., J.M. Pluth, P.K. Cooper, M.J. Cowan, D.J. Chen, and S.M. Yannone. 2005. Artemis deficiency confers a DNA double-strand break repair defect and Artemis phosphorylation status is altered by DNA damage and cell cycle progression. *DNA Repair (Amst).* 4(5): 556-570.

150. Li, L., D. Moshous, Y. Zhou, J. Wang, G. Xie, E. Salido, D. Hu, J.P. de Villartay, and M.J. Cowan. 2002. A founder mutation in Artemis, an SNM1-like protein, causes SCID in Athabascan-speaking Native Americans. *J Immunol.* 168(12): 6323-6329.

151. Ege, M., Y. Ma, B. Manfras, K. Kalwak, H. Lu, M.R. Lieber, K. Schwarz, and U. Pannicke. 2005. Omenn syndrome due to ARTEMIS mutations. *Blood.* 105(11): 4179-4186.

152. Evans, P.M., L. Woodbine, E. Riballo, A.R. Gennery, M. Hubank, and P.A. Jeggo. 2006. Radiation-induced delayed cell death in a hypomorphic Artemis cell line. *Hum Mol Genet.* 15(8): 1303-1311.

153. Kobayashi, N., K. Agematsu, K. Sugita, M. Sako, S. Nonoyama, A. Yachie, S. Kumaki, S. Tsuchiya, H.D. Ochs, K. Sugita, *et al.* 2003. Novel Artemis gene mutations of radiosensitive severe combined immunodeficiency in Japanese families. *Hum Genet.* 112(4): 348-352.

154. Papavasiliou, F.N., and D.G. Schatz. 2000. Cell-cycle-regulated DNA double-stranded breaks in somatic hypermutation of immunoglobulin genes. *Nature.* 408(6809): 216-221.

155. Shrivastav, M., L.P. De Haro, and J.A. Nickoloff. 2008. Regulation of DNA double-strand break repair pathway choice. *Cell Res.* 18(1): 134-147.

156. Higuchi, Y. 2003. Chromosomal DNA fragmentation in apoptosis and necrosis induced by oxidative stress. *Biochem Pharmacol.* 66(8): 1527-1535.

157. Market, E., and F.N. Papavasiliou. 2003. V(D)J recombination and the evolution of the adaptive immune system. *PLoS Biol.* 1(1): E16.

158. Lieber, M.R., Y. Ma, U. Pannicke, and K. Schwarz. 2004. The mechanism of vertebrate nonhomologous DNA end joining and its role in V(D)J recombination. *DNA Repair (Amst).* 3(8-9): 817-826.

159. Lu, C.P., J.E. Posey, and D.B. Roth. 2008. Understanding how the V(D)J recombinase catalyzes transesterification: distinctions between DNA cleavage and transposition. *Nucleic Acids Res.* 36(9): 2864-2873.

160. Gellert, M. 2002. V(D)J recombination: RAG proteins, repair factors, and regulation. *Annu Rev Biochem.* 71: 101-132.

161. Lin, J.M., M.A. Landree, and D.B. Roth. 1999. V(D)J recombination catalyzed by mutant RAG proteins lacking consensus DNA-PK phosphorylation sites. *Mol Immunol.* 36(18): 1263-1269.

162. Rivera-Munoz, P., L. Malivert, S. Derdouch, C. Azerrad, V. Abramowski, P. Revy, and J.P. Villartay. 2007. DNA repair and the immune system: From V(D)J recombination to aging lymphocytes. *Eur J Immunol.* 37 Suppl 1: S71-S82.

163. Rolff J. 2007. Why did the acquired immune system of vertebrates evolve? *Dev Comp Immunol.* 31(5): 476-482.

164. Hsu, E., N. Pulham, L.L. Rumfelt, and M.F. Flajnik. 2006. The plasticity of immunoglobulin gene systems in evolution. *Immunol Rev.* 210: 8-26.

165. Burnet, F.M. 1969. The evolution of adaptive immunity in vertebrates. *Acta Pathol Microbiol Scand.* 76(1): 1-11.

166. Davis, M.M., D.S. Lyons, J.D. Altman, M. McHeyzer-Williams, J. Hampl, J.J. Boniface, and Y. Chien. 1997. T cell receptor biochemistry, repertoire selection and general features of TCR and Ig structure. *Ciba Found Symp.* 204: 94-104.

167. Mareeva, T., T. Lebedeva, N. Anikeeva, T. Manser, and Y. Sykulev. 2004. Antibody specific for the peptide.major histocompatibility complex. Is it T cell receptor-like? *J Biol Chem.* 279(43): 44243-4429.

168. Varani, L., A.J. Bankovich, C.W. Liu, L.A. Colf, L.L. Jones, D.M. Kranz, J.D. Puglisi, and K.C. Garcia. 2007. Solution mapping of T cell receptor docking footprints on peptide-MHC. *Proc Natl Acad Sci U S A.* 104(32): 13080-13085.

169. Almagro, J.C., E. Vargas-Madrazo, F. Lara-Ochoa, and E. Horjales. 1995. Molecular modeling of a T-cell receptor bound to a major histocompatibility complex molecule: implications for T-cell recognition. *Protein Sci.* 4(9): 1708-1717.

170. Wang, F., T. Ono, A.M. Kalergis, W. Zhang, T.P. DiLorenzo, K. Lim, and S.G. Nathenson. 1998. On defining the rules for interactions between the T cell receptor and its ligand: a critical role for a specific amino acid residue of the T cell receptor beta chain. *Proc Natl Acad Sci U S A.* 95(9): 5217-5222.

171. Barclay, A.N. 1999. Ig-like domains: evolution from simple interaction molecules to sophisticated antigen recognition. *Proc Natl Acad Sci U S A.* 96(26): 14672-14674.

172. Marchalonis, J.J., I. Jensen, and S.F. Schluter. 2002. Structural, antigenic and evolutionary analyses of immunoglobulins and T cell receptors. *J Mol Recognit.* 15(5): 260-271.

173. Sadofsky, M.J. 2001. The RAG proteins in V(D)J recombination: more than just a nuclease. *Nucleic Acids Res.* 29(7): 1399-1409.

174. Akamatsu, Y., N. Tsurushita, F. Nagawa, M. Matsuoka, K. Okazaki, M. Imai, and H. Sakano. 1994. Essential residues in V(D)J recombination signals. *J Immunol.* 153(10): 4520-4529.

175. Oettinger, M.A. 1992. Activation of V(D)J recombination by RAG1 and RAG2. *Trends Genet.* 8(12): 413-416.

176. Rodgers, K.K., I.J. Villey, L. Ptaszek, E. Corbett, D.G. Schatz, and J.E. Coleman. 1999. A dimer of the lymphoid protein RAG1 recognizes the recombination signal sequence and the complex stably incorporates the high mobility group protein HMG2. *Nucleic Acids Res.* 27(14): 2938-2946.

177. Gallo, M.L., F. Pergola, G.A. Daniels, and M.R. Lieber. 1994. Distinct roles for RAG-1 in the initiation of V(D)J recombination and in the resolution of coding ends. *J Biol Chem.* 269(35): 22188-22192.

178. Difilippantonio, M.J., C.J. McMahan, Q.M. Eastman, E. Spanopoulou, and D.G. Schatz. 1996. RAG1 mediates signal sequence recognition and recruitment of RAG2 in V(D)J recombination. *Cell.* 87(2): 253-262.

179. Mo, X., T. Bailin, S. Noggle, and M.J. Sadofsky. 2000. A highly ordered structure in V(D)J recombination cleavage complexes is facilitated by HMG1. *Nucleic Acids Res.* 28(5): 1228-1236.

180. Hagmann, M. 1997. RAGged repair: what's new in V(D)J recombination. *Biol Chem.* 378(8): 815-819.

181. Swanson, P.C. 2002. Fine structure and activity of discrete RAG-HMG complexes on V(D)J recombination signals. *Mol Cell Biol.* 22(5): 1340-1351.

182. West, R.B., and M.R. Lieber. 1998. The RAG-HMG1 complex enforces the 12/23 rule of V(D)J recombination specifically at the double-hairpin formation step. *Mol Cell Biol.* 18(11): 6408-6415.

183. Yu, K., and M.R. Lieber. 2000. The nicking step in V(D)J recombination is independent of synapsis: implications for the immune repertoire. *Mol Cell Biol.* 20(21): 7914-7921.

184. Yu, K., A. Taghva, Y. Ma, and M.R. Lieber. 2004. Kinetic analysis of the nicking and hairpin formation steps in V(D)J recombination. *DNA Repair (Amst)*. 3(1): 67-75.

185. De, P., M.M. Peak, and K.K. Rodgers. 2004. DNA cleavage activity of the V(D)J recombination protein RAG1 is autoregulated. *Mol Cell Biol*. 24(15): 6850-6860.

186. Drejer-Teel, A.H., S.D. Fugmann, and D.G. Schatz. 2007. The beyond 12/23 restriction is imposed at the nicking and pairing steps of DNA cleavage during V(D)J recombination. *Mol Cell Biol*. 27(18): 6288-6299.

187. Schlissel, M., A. Constantinescu, T. Morrow, M. Baxter, and A. Peng. 1993. Double-strand signal sequence breaks in V(D)J recombination are blunt, 5'-phosphorylated, RAG-dependent, and cell cycle regulated. *Genes Dev*. 7(12B): 2520-2532.

188. Roth, D.B., P.B. Nakajima, J.P. Menetski, M.J. Bosma, and M. Gellert. 1992. V(D)J recombination in mouse thymocytes: Double-strand breaks near T cell receptor δ rearrangement signals. *Cell*. 69: 41-53.

189. Ramsden, D.A., and M. Gellert. 1995. Formation and resolution of double-strand break intermediates in V(D)J rearrangement. *Genes Dev*. 9: 2409-2420.

190. Kim, D.R., S.J. Park, and M.A. Oettinger. V(D)J recombination: site-specific cleavage and repair. *Mol Cells*. 10(4): 367-374.

191. Bassing, C.H., W. Swat, and F.W. Alt. 2002. The mechanism and regulation of chromosomal V(D)J recombination. *Cell*. 109 Suppl: S45-S55.

192. Fanning, L., A. Connor, K. Baetz, D. Ramsden, and G.E. Wu. 1996. Mouse RSS spacer sequences affect the rate of V(D)J recombination. *Immunogenetics*. 44(2): 146-150.

193. van Gent, D.C.,D.A. Ramsden, and M. Gellert. 1996. The RAG1 and RAG2 proteins establish the 12/23 rule in V(D)J recombination. *Cell*. 85(1): 107-113.

194. Lewis, S.M., J.E. Hesse, K. Mizuuchi, and M. Gellert. 1988. Novel strand exchanges in V(D)J recombination. *Cell*. 55: 1099-1107.

195. Swanson, P.C. 2003. A RAG-1/RAG-2 tetramer supports 12/23-regulated synapsis, cleavage, and transposition of V(D)J recombination signals. *Mol Cell Biol*. 22(22): 7790-7801.

196. Lee, A.I., S.D. Fugmann, L.G. Cowell, L.M. Ptaszek, G. Kelsoe, and D.G. Schatz. 2003. A functional analysis of the spacer of V(D)J recombination signal sequences. *PLoS Biol*. (1): E1.

197. Montalbano, A., K.M. Ogwaro, A. Tang, A.G. Matthews, M. Larijani, M.A. Oettinger, and A.J. Feeney. 2003. V(D)J recombination frequencies can be profoundly affected by changes in the spacer sequence. *J Immunol.* 171(10): 5296-5304.

198. Alt, F.W., G. Rathbun, E. Oltz, G. Taccioli, and Y. Shinkai. 1992. Function and control of recombination-activating gene activity. *Ann N Y Acad Sci.* 651: 277-294.

199. Landree, M.A., J.A. Wibbenmeyer, and D.B. Roth. 1999. Mutational analysis of RAG1 and RAG2 identifies three catalytic amino acids in RAG1 critical for both cleavage steps of V(D)J recombination. *Genes Dev.* 13(23): 3059-3069.

200. Swanson, P.C. 2001. The DDE motif in RAG-1 is contributed in trans to a single active site that catalyzes the nicking and transesterification steps of V(D)J recombination. *Mol Cell Biol.* 21(2): 449-458.

201. Furusawa, T., M. Hosoe, K. Ohkoshi, S. Takahashi, N. Kiyokawa, J. Fujimoto, H. Amemiya, S. Suzuki, and T. Tokunaga. 2003. Catalytic RAG1 mutants obstruct V(D)J recombination in vitro and in vivo. *Mol Immunol.* 39(14): 871-878.

202. Sadofsky, M.J., J.E. Hesse, and M. Gellert. 1994. Definition of a core region of RAG-2 that is functional in V(D)J recombination. *Nucleic Acids Res.* 22(10): 1805-1809.

203. Kirch, S.A., P. Sudarsanam, and M.A. Oettinger. 1996. Regions of RAG1 protein critical for V(D)J recombination. *Eur J Immunol.* 26(4): 886-891.

204. Callebaut, I., and J.P. Mornon. 1998. The V(D)J recombination activating protein RAG2 consists of a six-bladed propeller and a PHD fingerlike domain, as revealed by sequence analysis. *Cell Mol Life Sci.* 54(8): 880-891.

205. McMahan, C.J., M.J. Difilippantonio, N. Rao, E. Spanopoulou, and D.G. Schatz. 1997. A basic motif in the N-terminal region of RAG1 enhances V(D)J recombination activity. *Mol Cell Biol.* 17(8): 4544-4552.

206. Steen, S.B., J.O. Han, C. Mundy, M.A. Oettinger, and D.B. Roth DB. 1999. Roles of the "dispensable" portions of RAG-1 and RAG-2 in V(D)J recombination. *Mol Cell Biol.* 19(4): 3010-3017.

207. Arbuckle, J.L., L.A. Fauss, R. Simpson, L.M. Ptaszek, and K.K. Rodgers. 2001. Identification of two topologically independent domains in RAG1 and their role in macromolecular interactions relevant to V(D)J recombination. *J Biol Chem.* 276(40): 37093-37101.

208. De, P., and K.K. Rodgers. 2004. Putting the pieces together: identification and characterization of structural domains in the V(D)J recombination protein RAG1. *Immunol Rev.* 200: 70-82.

209. Moshous, D., I. Callebaut, R. de Chasseval, C. Poinsignon, I. Villey, A. Fischer, and J.P. de Villartay. 2003. The V(D)J recombination/DNA repair factor artemis belongs to the metallo-beta-lactamase family and constitutes a critical developmental checkpoint of the lymphoid system. *Ann N Y Acad Sci.* 987: 150-157.

210. Lu, H., K. Schwarz, and M.R. Lieber. 2007. Extent to which hairpin opening by the Artemis:DNA-PKcs complex can contribute to junctional diversity in V(D)J recombination. *Nucleic Acids Res.* 35(20): 6917-6923.

211. Sekiguchi, J.M., Y. Gao, Y. Gu, K. Frank, Y. Sun, J. Chaudhuri, C. Zhu, H.L. Cheng, J. Manis, D. Ferguson, *et al.* 1999. Nonhomologous end-joining proteins are required for V(D)J recombination, normal growth, and neurogenesis. *Cold Spring Harb Symp Quant Biol.* 64: 169-181.

212. Meier, J.T., and S.M. Lewis. 1993. P nucleotides in V(D)J recombination: a fine-structure analysis. *Mol Cell Biol.* 13(2): 1078-1092.

213. Nadel, B., and A.J. Feeney. 1997. Nucleotide deletion and P addition in V(D)J recombination: a determinant role of the coding-end sequence. *Mol Cell Biol.* 17(7): 3768-3778.

214. Lieber, M.R. 2006. The polymerases for V(D)J recombination. *Immunity.* 25(1): 7-9.

215. Gangi-Peterson, L., D.H. Sorscher, J.W. Reynolds, T.B. Kepler, and B.S. Mitchell. 1999. Nucleotide pool imbalance and adenosine deaminase deficiency induce alterations of N-region insertions during V(D)J recombination. *J Clin Invest.* 103(6): 833-841.

216. Bertocci, B., A. De Smet, J.C. Weill, and C.A. Reynaud. 2006. Nonoverlapping functions of DNA polymerases mu, lambda, and terminal deoxynucleotidyltransferase during immunoglobulin V(D)J recombination in vivo. *Immunity.* 25(1): 31-41.

216b. Zheng, X. 2005. Definition of Ku-interacting domains in RAG1 and RAG2 proteins in V(D)J recombination. University of Ottawa (M.Sc. thesis).

217. Moshous, D., I. Callebaut, R. de Chasseval, B. Corneo, M. Cavazzana-Calvo, F. Le Deist, I. Tezcan, O. Sanal, Y. Bertrand, N. Philippe N, *et al.* 2001. Artemis, a novel DNA double-strand break repair/V(D)J recombination protein, is mutated in human severe combined immune deficiency. *Cell.* 105(2): 177-186.

218. Kuroda, S., C. Tokunaga, Y. Kiyohara, O. Higuchi, H. Konishi, K. Mizuno, G.N. Gill, and U. Kikkawa. 1996. Protein-protein interaction of zinc finger LIM domains with protein kinase C. *J. Biol. Chem.* 271(49): 31029-31032.

218b. Fox, J.D., and D.S. Waugh. 2003. Maltose-binding protein as a solubility enhancer. *Methods Mol. Biol.* 205: 99-117.

219. Clontech. 2007. TALON® Metal Affinity Resins User Manual. Protocol No. PT1320-1. Version No. PR7Y2405.

219b. Parker, R.C., R.M. Watson, and B. Vinograd. 1977. Mapping of closed circular DNAs by cleavage with restriction endonucleases and calibration by agarose gel electrophoresis. *Proc. Natl. Acad. Sci. U. S. A.* 74: 851-855.

219c. Schroter, H., G. Maier, H. Ponstingl, and A. Nordheim. 1985. DNA intercalators induce specific release of HMG 14, HMG 17 and other DNA-binding proteins from chicken erythrocyte chromatin. *EMBO J.* 4: 3867-3872.

219d. Lai, J.S., and W. Herr. 1992. Ethidium bromide provides a simple tool for identifying genuine DNA-independent protein associations *Proc. Natl. Acad. Sci. U. S. A.* 89: 6958-6962.

220. Trevigen®, Inc. 2008. Technical Support Inquiry (number CN00003429). (Personal e-mail).

221. Hailey, J., E. Maxwell, K. Koukouras, W.R. Bishop, J.A. Pachter, and Y.Wang. 2002. Neutralizing Anti-Insulin-like Growth Factor Receptor 1 Antibodies Inhibit Receptor Function and Induce Receptor Degradation in Tumor Cells. *Mol Cancer Ther.* 1: 1349-1353.

222. Deroo, B.J., C. Rentsch, S. Sampath, J, Young, D.B. DeFranco, and T.K. Archer. 2002. Proteasomal inhibition enhances glucocorticoid receptor transactivation and alters its subnuclear trafficking. *Mol Cell Biol.* 22(12): 4113-4123.

223. Rigat, G., A. Shevchenko, B. Rutz, M. Wilm, M. Mann, and B. Séraphin. 1999. A generic protein purification method for protein complex characterization and proteome exploration. *Nat Biotechnol.* 17(10): 1030-1032.

224. Puig, O., F. Caspary, G. Rigaut, B. Rutz, E. Bouveret, E. Bragado-Nilsson, M. Wilm, and B. Séraphin. 2001. The tandem affinity purification (TAP) method: a general procedure of protein complex purification. *Methods.* 24(3): 218-229.

225. Bürckstümmer, T., K.L. Bennett, A. Preradovic, G. Schütze, O. Hantschel, G. Superti-Furga, and A. Bauch. 2006. An efficient tandem affinity purification procedure for interaction proteomics in mammalian cells. *Nat Methods.* 3(12): 1013-1019.

226. Stratagene®. Adenoviral Delivery and InterPlay™ TAP Maximize Protein Discovery. *Strategies.* 19(3): 84-85.

226b. Stonely, M., T. Subkhankulova, J.P.C. Le Quesne, M.J. Coldwell, C.L. Jopling, G.J. Belsham, and A.E. Willis. 2000. Analysis of the c-*myc* IRES: a potential role for cell-type specific trans-acting factors and the nuclear compartment. *Nucleic Acids Res.* 28(3): 687–694.

227. Weinstock, D. M., and M. Jasin,. 2006. Alternative Pathways for the Repair of RAG-Induced DNA Breaks. *Mol. Cell. Biol.* 26: 131-139.

228. Lee, G.S. M B. Neiditch, S.S. Salus, and D.B. Roth. 2004. RAG Proteins Shepherd Double-Strand Breaks to a Specific Pathway, Suppressing Error-Prone Repair, but RAG Nicking Initiates Homologous Recombination. *Cell.* 117:171-184.

229. Cui, X., Meek, K. 2007. Linking double-stranded DNA breaks to the recombination activating gene complex directs repair to the nonhomologous end-joining pathway. *Proc. Natl. Acad. Sci. USA* 104: 17046-17051.

230. Corneo, B., R.L. Wendland, L. Deriano, X. Cui, I.A. Klein, S.Y. Wong, S. Arnal, A.J. Holub, G.R. Weller, B.A. Pancake, *et al.* 2007. Rag mutations reveal robust alternative end joining. *Nature*. 449(7161): 483-486.

231. Sawchuk, D.J. J. Mansilla-Soto, C. Alarcon, N. C. Singha, H. Langen, M. E. Bianchi, S. P. Lees-Miller, M. C. Nussenzweig, and P. Cortes. 2004. Ku70/Ku80 and DNA-dependent Protein Kinase Catalytic Subunit Modulate RAG-mediated Cleavage: IMPLICATIONS FOR THE ENFORCEMENT OF THE 12/23 RULE. *J. Biol. Chem.* 279: 29821-29831.

232. Izsvák, Z., E.E. Stüwe, D. Fiedler, A. Katzer, P.A. Jeggo, and Z. Ivics. 2004. Healing the wounds inflicted by sleeping beauty transposition by double-strand break repair in mammalian somatic cells. *Mol Cell.* 13(2): 279-290.

233. Agrawal, A. and D.G. Schatz. 1997. RAG1 and RAG2 form a stable postcleavage synaptic complex with DNA containing signal ends in V(D)J recombination, *Cell.* 89: 43-53.

234. Zhu, C., M.A. Bogue, D.S. Lim, P. Hasty, and D.B. Roth. 1996. Ku86-deficient mice exhibit severe combined immunodeficiency and defective processing of V(D)J recombination intermediates. *Cell.* 86: 379-389.

235. Gao, Y., J. Chaudhuri, C. Zhu, L. Davidson, D.T. Weaver, and F.W. Alt. 1998. A Targeted DNA-PKcs-Null Mutation Reveals DNA-PK-Independent Functions for KU in V(D)J Recombination. *Immunity.* 9(3): 367-376.

236. Lieber, M.R., J.E. Hesse, S. Lewis, G.C. Bosma, N. Rosenberg, K. Mizuuchi, M.J. Bosma, and M. Gellert. 1988. The defect in murine severe combined immune deficiency: joining of signal sequences but not coding segments in V(D)J recombination. *Cell.* 55(1): 7-16.

237. Bogue, M.A., C. Wang, C. Zhu, and D.B Roth. 1997. V(D)J recombination in Ku86-deficient mice: distinct effects on coding, signal, and hybrid joint formation. *Immunity.* 7(1): 37-47.

238. Lieber, M.R. 1998. Pathological and physiological double-strand breaks: roles in cancer, aging, and the immune system. *Am J Pathol.* 153(5): 1323-1332.

239. Raina, J., Y. Simpson, E.D. Cram, R. Czolij, J.M. Matthews, M. Crossley, and J.P. Mackay. 2003. CCHX Zinc Finger Derivatives Retain the Ability to Bind Zn(II) and Mediate Protein-DNA Interactions. *J. Biol. Chem.* 278(30): 28011-28018.

240. Trainor, C.D., R. Ghirlando, and M.A. Simpson. 2000. GATA Zinc Finger Interactions Modulate DNA Binding and Transactivation. *J. Biol. Chem.* 275(36): 28157-28166.

241. Hanakahi, L.A. 2007. 2-step purification of the Ku DNA repair protein expressed in *Escherichia coli. Protein Expr Purif.* 52(1): 139–145.

242. Dronkert, M.L, J. de Wit, M. Boeve, M.L. Vasconcelos, H. van Steeg, T.L. Tan, J.H. Hoeijmakers, and R. Kanaar. 2000. Disruption of mouse SNM1 causes increased sensitivity to the DNA interstrand cross-linking agent mitomycin C. *Mol. Cell Biol.* 20: 4553-4561.

243. Ju, H.J., C.M. Ye, and J. Verchot-Lubicz. 2008. Mutational analysis of PVX TGBp3 links subcellular accumulation and protein turnover. *Virology.* 375(1): 103-117.

244. Bayot, A., N. Basse, I. Lee, M. Gareil, B. Pirotte, A.L. Bulteau, B. Friguet, and M. Reboud-Ravaux. 2008. Towards the control of intracellular protein turnover: mitochondrial Lon protease inhibitors versus proteasome inhibitors. *Biochimie.* 90(2): 260-269.

245. Sadoul, K., C. Boyault, M. Pabion, and S. Khochbin. 2008. Regulation of protein turnover by acetyltransferases and deacetylases. *Biochimie.* 90(2): 306-312.

246. Ohsumi, Y. 2006. Protein turnover. *IUBMB Life.* 58(5-6): 363-369.

247. Bachmair, A., D. Finley, and A. Varshavsky. 1986. In vivo half-life of a protein is a function of its amino-terminal residue. *Science.* 234(4773): 179-186.

248. Zhou, P. 2004. Determining protein half-lives. *Methods Mol Biol.* 284: 67-77.

249. Dice, J.F. 1987. Molecular determinants of protein half-lives in eukaryotic cells. *FASEB J.* 1(5): 349-357.

250. Belizario, J.E., J. Alves, M. Garay-Malpartida, and J.M. Occhiucci. 2008. Coupling caspase cleavage and proteasomal degradation of proteins carrying PEST motif. *Curr Protein Pept Sci.* 9(3): 210-220.

251. Martinez, L.O., B. Agerholm-Larsen, N. Wang, W. Chen, and A.R. Tall. 2003. Phosphorylation of a pest sequence in ABCA1 promotes calpain degradation and is reversed by ApoA-I. *J Biol Chem.* 278(39): 37368-37374.

252. Wang, N., W. Chen, P. Linsel-Nitschke, L.O. Martinez, B. Agerholm-Larsen, D.L. Silver, and A.R. Tall. 2003. A PEST sequence in ABCA1 regulates degradation by calpain protease and stabilization of ABCA1 by apoA-I. *J Clin Invest.* 111(1): 99-107.

253. Savas S., M. Shariff, I.W. Taylor, and H. Ozcelik. (2007). Human non-synonymous single nucleotide polymorphisms can influence ubiquitin-mediated protein degradation. *OMICS.* 11(2):200-8.

254. Bochkov, Y.A., and A.C. Palmenberg. 2006. Translational efficiency of EMCV IRES in bicistronic vectors is dependent upon IRES sequence and gene location. *BioTechniques®.* 41(3): 283-292.

255. Darbinyan, A., M.K. White, S. Akan, S. Radhakrishnan, L. Del Valle, S. Amini, and K. Khalili. 2007. Alterations of DNA damage repair pathways resulting from JCV infection. *Virology.* 364(1): 73-86.

256. Heun, P., S. Erhardt, M.D. Blower, S. Weiss, A.D. Skora, and G.H. Karpen. 2006. Mislocalization of the Drosophila Centromere-Specific Histone CID Promotes Formation of Functional Ectopic Kinetochores. *Dev. Cell.* 10(3): 303-315.

257. Yoshino, A., B.M. Bieler, D.C. Harper, D.A. Cowan, S. Sutterwala, D.M. Gay, N.B. Cole, J.M. McCaffery, and M.S. Marks. 2003. A role for GRIP domain proteins and/or their ligands in structure and function of the trans Golgi network. *J. Cell Sci.* 116: 4441-4454.

258. Hernandez-Munoz, I., M. Benet, M. Calero, M. Jimenez, R. Diaz, and A. Pellicer. 2003. rgr Oncogene: Activation by Elimination of Translational Controls and Mislocalization. *Cancer Res.* 63(14): 4188-4195.

259. Huang, H.Y., C.H. Chien, K.H. Jen, and H.D. Huang. (2006). RegRNA: an integrated web server for identifying regulatory RNA motifs and elements. *Nucleic Acids Res.* 34(Web Server issue):W429-34.

260. Geng, L., X. Zhang, S. Zheng, and R.J. Legerski. 2007. Artemis links ATM to G2/M checkpoint recovery via regulation of Cdk1-cyclin B. *Mol Cell Biol.* 27(7): 2625-2635.

261. Zhang, X., C. Richie, and R.J. Legerski. 2002. Translation of hSNM1 is mediated by an internal ribosome entry site that upregulates expression during mitosis. *DNA Repair (Amst).* 1(5): 379-390.

261b. Bert, A.G., R. Grépin, M.A. Vadas, and G.J. Goodall. 2006. Assessing IRES activity in the HIF-1a and other cellular 5'UTRs. *RNA.* 2(6): 1074-1083.

262. Lebon, A., D. Seyer, P. Cosette, L. Coquet, T. Jouenne, P. Chan, J. Leprince, A. Fournier, H Vaudry, B.J. Gonzalez, *et al* (2006). Identification of proteins regulated by PACAP in PC12 cells by 2D gel electrophoresis coupled to mass spectrometry. *Ann N Y Acad Sci.* 1070: 380-387.

263. Ramos-Fernández A., A. Paradela, R. Navajas, and J.P. Albar. (2008). Generalized Method for Probability-based Peptide and Protein Identification from Tandem Mass Spectrometry Data and Sequence Database Searching. *Mol Cell Proteomics.* 7(9): 1748-1754.

264. Hoffmann, H.J., L.M. Tabaksblat, J.J. Enghild, and R. Dahl. 2008. Human skin keratins are the major proteins in exhaled breath condensate. *Eur Respir J.* 31(2): 380-384.

265. Fox, K., E. Castanha, A. Fox, C. Feigley, and D. Salzberg. 2008. Human K10 epithelial keratin is the most abundant protein in airborne dust of both occupied and unoccupied school rooms. *J Environ Monit.* 10(1): 55-59.

266. Werner, N.S., R. Windoffer, P. Strnad, C. Grund, R. E. Leube, and T. M. Magin. 2004. Epidermolysis Bullosa Simplex-Type Mutations Alter the Dynamics of the Keratin Cytoskeleton and Reveal a Contribution of Actin to the Transport of Keratin Subunits. *Mol. Biol. Cell.* 15(3): 990-1002.

267. Kaiser, P., D. Meierhofer, X. Wang, and L. Huang. 2008. Tandem affinity purification combined with mass spectrometry to identify components of protein complexes. *Methods Mol Biol.* 439: 309-326.

268. Gregan, J., C.G. Riedel, M. Petronczki, L. Cipak, C. Rumpf, I. Poser, F. Buchholz, K. Mechtler, and K. Nasmyth. 2007. Tandem affinity purification of functional TAP-tagged proteins from human cells. *Nat Protoc.* 2(5): 1145-1151.

269. Gould, K.L., L. Ren, A.S. Feoktistova, J.L. Jennings, and A.J. Link. 2004. Tandem affinity purification and identification of protein complex components. *Methods.* 33(3): 239-244.

270. Wang, J., J. Kudoh, A. Takayanagi, and N. Shimizu. 2004. Novel human BTB/POZ domain-containing zinc finger protein ZNF295 is directly associated with ZFP161. *Biochem. Biophys. Res. Commun.* 327(2): 615-627.

271. Collins, T., J.R. Stone, and A.J. Williams. 2001. All in the family: the BTB/POZ, KRAB, and SCAN domains, *Mol. Cell. Biol.* 21: 3609-3615.

272. Albagli, O., P. Dhordain, C. Deweindt, G. Lecocq and D. Leprince, 1995. The BTB/POZ domain: a new protein-protein interaction motif common to DNA- and actin-binding proteins, *Cell Growth Differ.* 6: 1193-1198.

272b. Costoya, J.A. 2007. Functional analysis of the role of POK transcriptional repressors. *Brief Funct Genomic Proteomic.* 6(1): 8-18.

273. Huang, H.D. 2006. RegRNA: A Regulatory RNA Motifs and Elements Finder. Department of Biological Science and Technology, Institute of Bioinformatics, National Chiao Tung University, Taiwan. http://regrna.mbc.nctu.edu.tw/

274. Kimura, S. and T. Iyanagi. High-level expression of porcine liver cytochrome P-450 reductase catalytic domain in Escherichia coli by modulating the predicted local secondary structure of mRNA. *J. Biochem.* 134(3): 403-413.

Contributions of Collaborators

I would like to thank Fumin Dong for his assistance in analyzing my rough mass spectrometry data, as well as conducting database searches and determining the identification of the unknown factors.

Appendices

Appendix I. Table of primers and probes.

Primer name	Sequence
CoreRag-1 primer I	5'-ggacacattcttcagtggggg-3'
CoreRag-1 primer II	5'-aatccgtatcatgagtccgtggaag-3'
CoreRag-1 primer III	5'-gcttctggctcagtctacatctgtac-3'
CoreRag-1 primer IV	5'-cataagacacaacggcttgcaacac-3'
MCS top	5'-atggcagatctggatccgtcgactcccgagtgc-3'
MCS bottom	5'-ggccgcactcgggagtcgacggatccagatctgccatggt-3'
EGFP forward	5'-gatatagctagcatggtgagcaaggcgaggagctg-3'
EGFP reverse	5'-gatataccgcggttacttgtacagctcgtccatgcc-3'
Artemis antisense (1st strand cDNA)	5'-agtttttgttcgaagggccctctagaggta-3'
EGFP antisense (1st strand cDNA)	5'-ttacttgtacagctcgtccatgcc-3'
Artemis forward (nested PCR)	5'- gatctgggctctgtacttcacctgcaaaag -3'
Artemis reverse (nested PCR)	5'-atttagcaaacttttttcctcgggtatatg-3'
EGFP forward (nested PCR)	5'-aagttcatctgcaccaccggcaagc-3'
EGFP reverse (nested PCR)	5'-cagcacggggccgtcgccgatggg-3'
^{32}P-Artemis probe	5'-cagtttttcaggctgcttttctgatactgc-3'
^{32}P-EGFP probe	5'-gatataccgcggttacttgtacagctggtccatgcc-3'
Oct-1 forward (NTAP; pCeMM)	5'-ggcggccggagatctatgaacaatccgtcagaaacc-3'
Oct-1 reverse (NTAP; pCeMM)	5'-gcttttggccggcctctgtgccttggaggcggt-3'
Oct-1 forward (NTAP; pBABE)	5'- ctatgaggatccatgggcacccccgcagtc-3'
Oct-1 reverse (NTAP; pBABE)	5'-attattgtcgactcacggctcgcgctgcccctgggg-3'
NTAP cassette reverse (pBABE)	5'-attattgtcgactcacggctcgcgctgcccctgggg-3'

Appendix II. Identifying the Ku70-binding domain of coreRag-1.

Peptide mapping of the Ku70-binding domain of coreRag-1 using direct binding assays. MBP-coreRag-1 deletion products were expressed in bacteria and purified via the MBP moiety with an amylose resin. Following elution from the resin, purified proteins were incubated with 60μg Jurkat T cell nuclear extracts. Ku immunoprecipitation was performed on the incubation reaction with a Ku70 antibody. Ethidium bromide (200mg /ml) was included throughout the binding reactions. The presence of MBP-coreRag-1 constructs was detected with an anti-MBP antibody. The binding with Ku was compared with 10% of the input MBP fusion RAG1 proteins. Immunoprecipitated Ku was detected with an anti-Ku70 antibody. The smallest deletion identified that abrogated Ku binding was MBP-coreRag-1(Δ660-763). Adapted from the thesis "Definition of Ku-interacting domains in RAG1 and RAG2 proteins in V(D)J recombination" by Xiuzhong Zheng (July 2005).

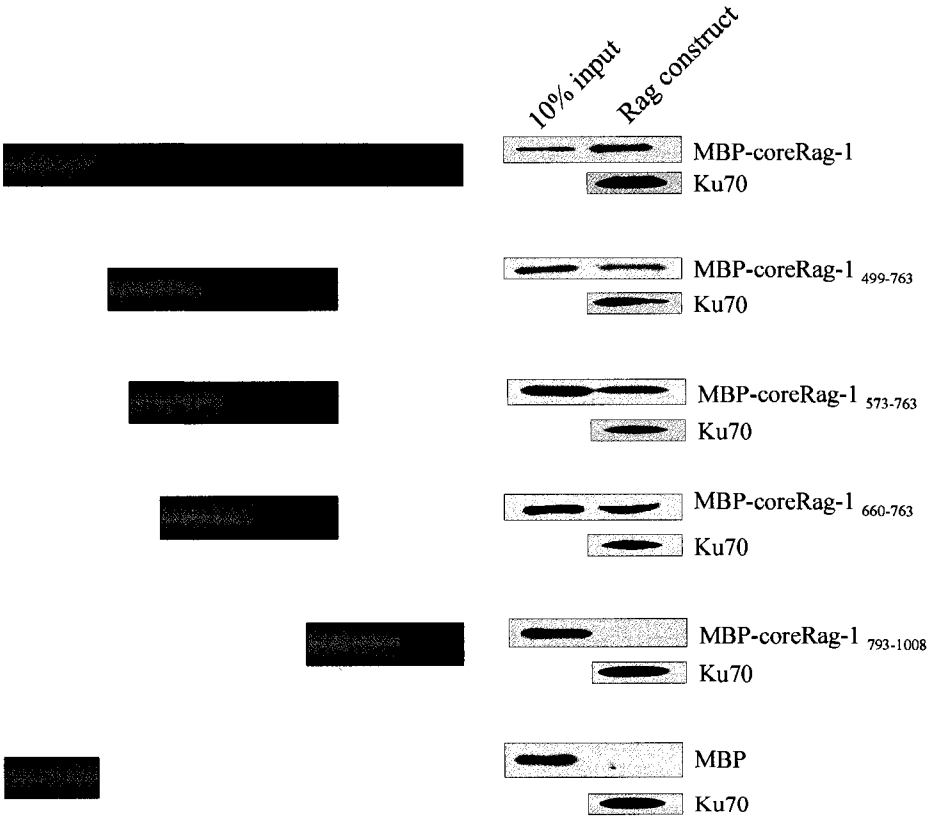

Appendix III. Artemis PEST residues.

The amino acid sequence of Artemis is depicted below. Green residues represent the β-lactamase domain (aa1-155), orange residues represent the β-CASP domain (aa156-385) and black residues represent the C-terminal domain (aa386-692). PEST residues are represented by bold type. The four potential PEST sequences (aa383-102, aa495-520, aa610-629 and aa634-663), as determined by PESTfind Analysis (253), are underlined.

MSSFEGQMAEYPTISIDRFDRENLRARAYFLSHCHKDHMKGLRAPTLKRRLECS
LKVYLYCSPVTKELLLTSPKYRFWKKRIISIEIETPTQISLVDEASGEKEEIVVTL
LPAGHCPGSVMFLFQGNNGTVLYTGDFRLAQGEAARMELLHSGGRVKDIQSVY
LDTTFCDPRFYQIPSREECLSGVLELVRSWITRSPYHVVWLNCKAAYGYEYLFT
NLSEELGVQVHVNKLDMFRNMPEILHHLTTDRNTQIHACRHPKAEEYFQWSKL
PCGITSRNRIPLHIISIKPSTMWFGERSRKTNVIVRTGESSYRACFSFHSSYSEIKDF
LSYLCPVNAYPNVIPVGTTMDKVVEILKPLCRSSQSTEPKYKPLGKLKRARTVH
RDSEEEDDYLFDDPLPIPLRHKVPYPETFHPEVFSMTAVSEKQPEKLRQTPGCC
RAECMQSSRFTNFVDCEESNSESEEEVGIPASLQGDLGSVLHLQKADGDVPQW
EVFFKRNDEITDESLENFPSSTVAGGSQSPKLFSDSDGESTHISSQNSSQSTHITE
QGSQGWDSQSDTVLLSSQERNSGDITSLDKADYRPTIKENIPASLMEQNVICPKD
TYSDLKSRDKDVTIVPSTGEPTTLSSETHIPEEKSLLNLSTNADSQSSSDFEVPST
PEAELPKREHLQYLYEKLATGESIAVKKRKCSLLDT

Appendix IV. A potential IRES is found within the 5'UTR of Artemis.

A putative IRES was found in the 5'UTR of the Artemis nuclease using the RegRNA program (259). A potential structure of this IRES was determined using free energy calculations (total free energy -13.6kcal/mol) with a RNA secondary structure prediction web program (274).

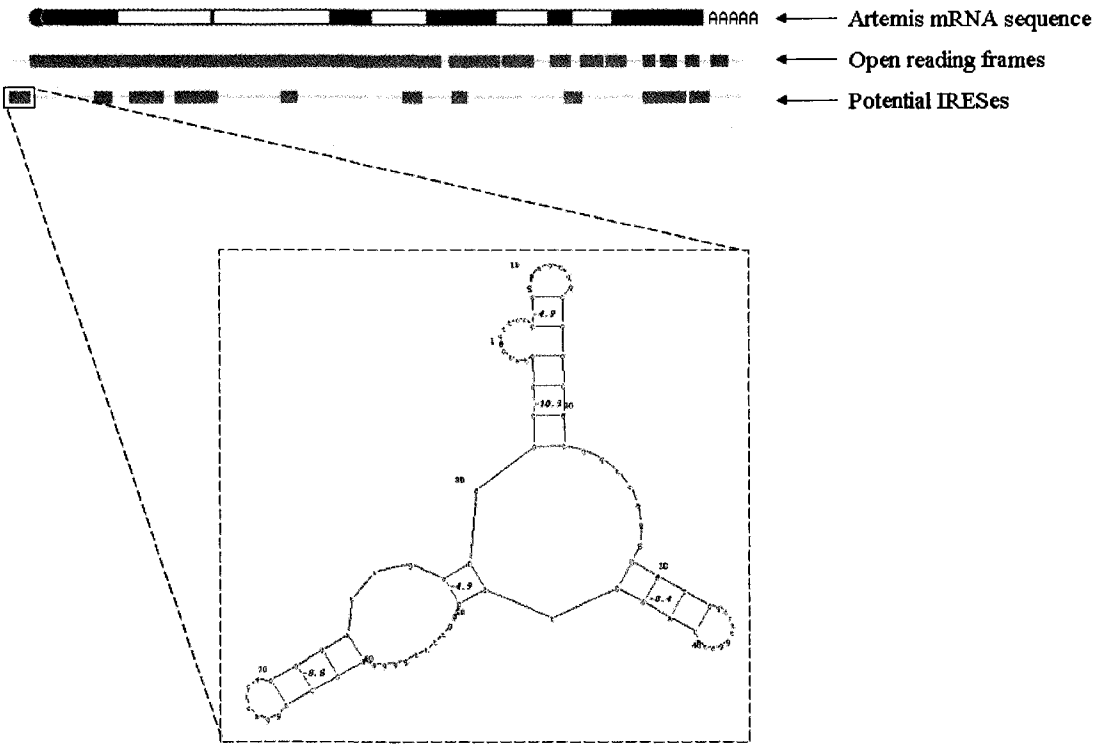

Appendix V: Determining the per-cell expression levels of pCeMM-NTAP-Oct-1 and pBABE-NTAP-Oct-1.

The GeneTools application (Syngene) was used for band quantification of NTAP-Oct-1 and endogenous Oct-1 from the western blots shown in Figures 19 and 20.

	TAP system	
	pCeMM	pBABE
	Band intensity[1]	
NTAP-Oct-1	2275700	287133
Endogenous Oct-1	1338145	219890
Background	891250	202084
Corrected NTAP-Oct-1[2]	1384450	85049
Corrected endogenous Oct-1[2]	446895	17806
Fold increase[3]	3.1	4.8

1 values indicate band intensities in random units

2 band intensity minus background

3 ratio of corrected NTAP-Oct-1 over corrected endogenous Oct-1

For pCeMM:

- Approximately 20% of cells in a mixed population express NTAP-Oct-1 (based on IF data).
- Western blot analysis of the mixed pool of cells shows a 3.1-fold overexpression of NTAP-Oct-1.
- Therefore:

  $(20/100)(\mathbf{X}) = 3.1$

  where **X** represents the per-cell expression level of NTAP-Oct-1.

  $\mathbf{X} = 3.1\ (100/20)$
  $= 15.5$

  Therefore, the per-cell expression of NTAP-Oct-1 is approximately 16-fold higher than endogenous Oct-1.

For pBABE:

- Conservatively approximate 95% of cells to express NTAP-Oct-1 (based on continuous puromycin selection).
- Western blot analysis of the mixed pool of cells shows a 4.8-fold overexpression of NTAP-Oct-1.
- Therefore:

  $(95/100)(\mathbf{X}) = 4.8$

where **X** represents the per-cell expression level of NTAP-Oct-1.

$\mathbf{X} = 4.8\ (100/95)$
$= 5.1$

Therefore, the per-cell expression of NTAP-Oct-1 is approximately 5-fold higher than endogenous Oct-1.

Appendix VI. Amino acid sequences of Rag-1, Ku70, Artemis and Oct-1.

Rag1 amino acid sequence

```
  1 maasfpptlg lssapdeiqh phikfsewkf klfrvrsfek tpeeaqkekk dsfegkpsle
 61 qspavldkad gqkpvptqpl lkahpkfskk fhdnekargk aihqanlrhl cricgnsfra
121 dehnrrypvh gpvdgktlgl lrkkekrats wpdliakvfr idvkadvdsi hptefchncw
181 simhrkfssa pcevyfprnv tmewhphtps cdicntarrg lkrkslqpnl qlskklktvl
241 dqarqarqrk rraqarissk dvmkkiancs kihlstklla vdfpehfvks iscqicehil
301 adpvetnckh vfcrvcilrc lkvmgsycps crypcfptdl espvksflsv lnslmvkcpa
361 kecneevsle kynhhisshk eskeifvhin kggrprqhll sltrraqkhr lrelklqvka
421 fadkeeggdv ksvcmtlfll alrarnehrq adeleaimqg kgsglqpavc lairvntfls
481 csqyhkmyrt vkaitgrqif qplhalrnae kvllpgyhhf ewqpplknvs sstdvgiidg
541 lsglsssvdd ypvdtiakrf rydsalvsal mdmeedileg mrsqdlddyl ngpftvvvke
601 scdgmgdvse khgsgpvvpe kavrfsftim kitiahssqn vkvfeeakpn selcckplcl
661 mladesdhet ltailsplia ereamkssel mlelggilrt fkfifrgtgy deklvreveg
721 leasgsvyic tlcdatrlea sqnlvfhsit rshaenlery evwrsnpyhe sveelrdrvk
781 gvsakpfiet vpsidalhcd ignaaefyki fqleigevyk npnaskeerk rwqatldkhl
841 rkkmnlkpim rmngnfarkl mtketvdavc elipseerhe alrelmdlyl kmkpvwrssc
901 pakecpeslc qysfnsqrfa ellstkfkyr n
```

Ku70 amino acid sequence

```
  1 msgwesyykt egdeeaeeeq eenleasgdy kysgrdslif lvdaskamfe sqsedeltpf
 61 dmsiqciqsv yiskiissdr dllavvfygt ekdknsvnfk niyvlqeldn pgakrileld
121 qfkgqqgqkr fqdmmghgsd yslsevlwvc anlfsdvqfk mshkrimlft nednphgnds
181 akasrartka gdlrdtgifl dlmhlkkpgg fdislfyrdi isiaededlr vhfeesskle
241 dllrkvrake trkralsrlk lklnkdivis vgiynlvqka lkpppiklyr etnepvktkt
301 rtfntstggl llpsdtkrsq iygsrqiile keeteelkrf ddpglmlmgf kplvllkkhh
361 ylrpslfvyp eeslvigsst lfsallikcl ekevaalcry tprrnippyf valvpqeeel
421 ddqkiqvtpp gfqlvflpfa ddkrkmpfte kimatpeqvg kmkaiveklr ftyrsdsfen
481 pvlqqhfrnl ealaldlmep eqavdltlpk veamnkrlgs lvdefkelvy ppdynpegkv
541 tkrkhdnegs gskrpkveys eeelkthisk gtlgkftvpm lkeacraygl ksglkkqell
601 ealtkhfqd
```

Artemis amino acid sequence

```
  1 mssfegqmae yptisidrfd renlrarayf lshchkdhmk glraptlkrr lecslkvyly
 61 cspvtkelll tspkyrfwkk riisieietp tqislvdeas gekeeivvtl lpaghcpgsv
121 mflfqgnngt vlytgdfrla qgeaarmell hsggrvkdiq svyldttfcd prfyqipsre
181 eclsgvlelv rswitrspyh vvwlnckaay gyeylftnls eelgvqvhvn kldmfrnmpe
```

241 ilhhlttdrn tqihacrhpk aeeyfqwskl pcgitsrnri plhiisikps tmwfgersrk
301 tnvivrtges syracfsfhs syseikdfls ylcpvnaypn vipvgttmdk vveilkplcr
361 ssqstepkyk plgklkrart vhrdseeedd ylfddplpip lrhkvpypet fhpevfsmta
421 vsekqpeklr qtpgccraec mqssrftnfv dceesnsese eevgipaslq gdlgsvlhlq
481 kadgdvpqwe vffkrndeit deslenfpss tvaggsqspk lfsdsdgest hissqnssqs
541 thiteqgsqg wdsqsdtvll ssqernsgdi tsldkadyrp tikenipasl meqnvicpkd
601 tysdlksrdk dvtivpstge pttlssethi peeksllnls tnadsqsssd fevpstpeae
661 lpkrehlqyl yeklatgesi avkkrkcsll dt

Oct-1 amino acid sequence

1 mnnpsetskp smesgdgntg tqtngldfqk qpvpvggais taqaqaflgh lhqvqlagts
61 lqaaaqslnv qsksneesgd sqqpsqpsqq psvqaaipqt qlmlaggqit gltltpaqqq
121 lllqqaqaqa qllaaavqqh sasqqhsaag atisasaatp mtqiplsqpi qiaqdlqqlq
181 qlqqqnlnlq qfvlvhpttn lqpaqfiisq tpqgqqgllq aqnlltqlpq qsqanllqsq
241 psitltsqpa tptrtiaatp iqtlpqsqst pkridtpsle epsdleeleq faktfkqrri
301 klgftqgdvg lamgklygnd fsqttisrfe alnlsfknmc klkpllekwl ndaenlssds
361 slsspsalns pgieglsrrr kkrtsietni rvaleksfle nqkptseeit miadqlnmek
421 evirvwfcnr rqkekrinpp ssggtssspi kaifpsptsl vattpslvts saattltvsp
481 vlpltsaavt nlsvtgtsdt tsnntatvis tappassavt spslspspsa sastseassa
541 setsttqtts tplssplgts qvmvtasglq taaaaalqga aqlpanasla amaaaaglnp
601 slmapsqfaa ggallslnpg tlsgalspal msnstlatiq alasggslpi tsldatgnlv
661 fanaggapni vtaplflnpq nlslltsnpv slvsaaaasa gnsapvaslh atstsaesiq
721 nslftvasas gaasttttas kaq

Cirriculum Vitae

Kyna Mensch

EDUCATION

University of Ottawa
Faculty of Medicine
Department of Biochemistry, Microbiology and Immunology
Ottawa, Ontario

- M.Sc. candidate in Biochemistry with specialization in human and molecular genetics.

Thesis: A study of the dynamics of V(D)J recombination and DNA-damage response factors.

University of Ottawa
Faculty of Science
Departments of Biochemistry, Microbiology and Immunology
Ottawa, Ontario.

- B.Sc. with Honours in Biochemistry.
- Graduated June 2005, *cum laude* (DGPA of 8.1).

Thesis: Identification and characterization of the putative Serum Response Factor interactor, Crp-1.

ABSTRACTS AND POSTERS

- Mensch K, Soubeyrand S, and RJG Haché. (2007) Examining the regulation of ectopic Artemis expression and identifying Oct-1 interactors with potential regulatory significance via tandem affinity purification. University of Ottawa (Department of Biochemistry, Microbiology and Immunology, and the Ottawa Health Research Institute).
- Mensch K, Soubeyrand S, and RJG Haché. (2006) Examining the regulation of ectopic Artemis expression. University of Ottawa (Department of Biochemistry, Microbiology and Immunology, and the Ottawa Health Research Institute).
- Mensch K, and JW Copeland. (2005) Identification and characterization of the putative Serum Response Factor interactor, Crp-1. University of Ottawa (Departments of Biochemistry, Microbiology and Immunology, and Cellular and Molecular Medicine).

SCHOLARSHIPS AND AWARDS

- 3rd prize at the 2007 Annual University of Ottawa graduate student research symposium.
- University of Ottawa Admissions Scholarship (2001).

TEACHING AND RESEARCH EXPERIENCE

Sept. 2005 – present

Ottawa Health Research Institute
University of Ottawa
Ottawa, Ontario

Position: M.Sc. candidate

Duties: Investigation of the expression and interaction of factors involved in the processes of V(D)J recombination and non-homologous end-joining. This includes defining the Ku70 binding domain of Rag-1, examining the ectopic expression of the Artemis nuclease, and identifying octamer-binding transcription factor-1 (Oct-1) interactors with potential regulatory significance through a modified tandem affinity purification protocol.

Supervisor: Dr. Robert Haché

Sept. 2006 - Dec. 2006
Jan. 2007 - April 2007
Sept. 2007 - Dec. 2007
Jan. 2008 - April 2008

University of Ottawa
Department of Biochemistry, Microbiology and Immunology
Ottawa, Ontario

Position: Teaching/laboratory assistant for 2nd year biochemistry and 3rd year molecular biology laboratories.

Duties: Supervised undergraduate laboratory courses, marked lab reports and gave lectures on basic molecular biology and biochemistry techniques.

Supervisor: Drs. Gabriel Guillet and Miguel Rodriguez

May 2004 - April 2005

University of Ottawa
Departments of Biochemistry, Microbiology and Immunology & Cellular and Molecular Medicine
Ottawa, Ontario

Position: Honours student/ Summer Researcher

Duties: Verified and investigated the interaction of Serum Response Factor interacting proteins initially identified via yeast two hybrid.

Supervisor: Dr. John Copeland

References available upon request.